MECHANISTIC BASIS OF NMDA RECEPTOR CHANNEL PROPERTY VARIATION

by

Beth Siegler Retchless

Sc.B., Brown University, 1999

Submitted to the Graduate Faculty of

Arts and Sciences in partial fulfillment

of the requirements for the degree of

Doctor of Philosophy

University of Pittsburgh

2010

UNIVERSITY OF PITTSBURGH

FACULTY OF ARTS AND SCIENCES

This dissertation was presented

by

Beth Siegler Retchless

It was defended on

November 8, 2010

and approved by

Dr. Stephen Meriney, Associate Professor, Department of Neuroscience

Dr. Michael Cascio, Adjunct Associate Professor, Department of Microbiology and Molecular Genetics

Dr. Michael Grabe, Assistant Professor, Department of Biological Sciences

Dr. Pierre Paoletti, Professor, Laboratoire de Neurobiologie, École Normale Supérieure

Dr. David Wood, Emeritus Associate Professor, Department of Neuroscience

Dissertation Advisor: Dr. Jon Johnson, Professor, Department of Neuroscience

MECHANISTIC BASES OF NMDA RECEPTOR CHANNEL PROPERTY VARIATION

Beth Siegler Retchless, Ph.D.

University of Pittsburgh, 2010

Glutamate mediates the majority of fast excitatory neurotransmission in the vertebrate brain. Glutamate receptors (GluRs) transduce signals in two ways: metabotropic GluRs signal via intracellular G proteins, whereas ionotropic GluRs (iGluRs) open intrinsic ion channels in response to agonist binding.

NMDA receptors (NMDARs) are glutamate- and glycine-gated iGluRs that play critical roles in spatial learning, contextual fear memory acquisition, synapse elimination, and chronic pain. Their particularly high calcium (Ca^{2+}) permeability and strongly voltage-dependent channel block by external magnesium (Mg^{2+}) distinguish NMDARs from other iGluRs. Mg^{2+} channel block of NMDARs inhibits current influx through the majority of agonist-bound, open NMDARs at resting membrane potentials (V_ms), but this block is relieved by depolarization. Thus, significant current flow through NMDARs requires presynaptic activity (glutamate release) and postsynaptic activity (depolarization to relieve Mg^{2+} channel block), conferring on NMDARs a coincidence-detection capability that is central to their physiological importance. To mediate this and other important functions, NMDARs require tight regulation of the voltage-dependent Mg^{2+} block that provides crucial control of NMDAR-mediated current flow and Ca^{2+} influx.

NMDARs are typically composed of NR1 and NR2 subunits. The four NR2 subunits (NR2A-D) contribute to four diheteromeric NMDAR subtypes (NR1/2A-NR1/2D), which differ

in many respects, including the magnitudes of channel block by Mg^{2+}, Ca^{2+} permeability, and single-channel conductance. Previously-gathered data from our lab demonstrates that the subtype specificity of Mg^{2+} block is principally conferred by a single amino acid site in the third transmembrane region (M3) of NR2 subunits. This "NR2 S/L site" contains a serine in NR2A and NR2B subunits and a leucine in NR2C and NR2D subunits.

Surprisingly, the NR2 S/L site does not line the pore. I created several structural homology models of NMDARs to generate hypotheses regarding how the NR2 S/L site conveys its effects to the pore. I tested these hypotheses experimentally and found that the NR2 S/L site interacts with an NR1 subunit tryptophan in the pore-loop to regulate Mg^{2+} block properties. I further determined that the NR2 S/L site greatly contributes to the subtype variation in single-channel conductance, and likely plays a role in the subtype variation in Ca^{2+} permeability.

TABLE OF CONTENTS

LIST OF TABLES

LIST OF FIGURES

LIST OF EQUATIONS

PREFACE

Many people have enriched my years at Pitt. I am especially indebted to Dr. Jon Johnson, my wise and supportive dissertation advisor. If I leave Pitt with a fraction of his knowledge, careful attention to detail and compassion, I will be a better scientist and a better person.

Members of the dissertation committee that I was fortunate to convene have been immensely helpful to me. Dr. Steve Meriney, the chair of this committee, has been a source of invaluable advice on both my research and my progress through the Center for Neuroscience at the University of Pittsburgh (CNUP) graduate program. Dr. Mike Cascio provided critical insight into the biochemical aspects of my research, and was a fabulous labmate for a period of time that was, in my self-serving opinion, far too short. Dr. Michael Grabe has been a wonderful source of knowledge and direction, especially regarding the computational modeling that I performed. Dr. Grabe also strongly contributing to my understanding of fundamental ion channel properties, and even conditionally agreed to serve on this dissertation committee before he was hired by Pitt. Dr. Dave Wood helped me understand some basic electrophysiology concepts that I thought I already knew, and each of these committee members have endured countless presentations and meetings; I thank them all for generously donating their time. Finally, Dr. Pierre Paoletti was an ideal collaborator, and kindly lent to the Johnson lab Dr. Marc Gielen, his fabulous former graduate student with whom I immensely enjoyed performing experiments (Dr. Paoletti has also written some of my favorite papers in the glutamate receptor field.) I am especially grateful to Dr. Paoletti for extending his time in the United States so that he can serve as the external examiner in this great dissertation committee.

The directors and graduate program directors of the CNUP have been accommodating and supportive. I am grateful for their strong contributions to the warm and collaborative environment of the CNUP, as well as their personal encouragement. Drs. Pat Card and Alan Sved have been particularly generous with their time and support. The larger neuroscience community in Pittsburgh has also greatly enhanced my development as a scientist. I thank Dr. Jon Rubin for introducing me to computational neuroscience and Dr. Karl Kandler for introducing me to slice physiology and I also thank him for his guidance.

Members of the Johnson lab contributed to a stimulating and supportive environment that I greatly enjoyed and benefited from. I offer my abundant thanks to Dr. Wei Gao, whose research provided the foundation on which my dissertation research is based. Drs. Richard Clarke and Shawn Kotermanski were especially helpful in providing technical training and insight into the topics of our research, and Karen Bouch and Christen Shiber provided excellent technical assistance on which I have absolutely relied. Dr. Nadya Povysheva has been a strong source of broader contexts in which my work may be relevant.

Above all I thank my husband, Adam Retchless, the center of my life, whose intellectual stimulation and warm love sustains me.

1.0 OVERVIEW

The nervous system controls most biological processes in the body. The central nervous system (CNS), composed of the brain and spinal cord, is at the core of the nervous system; it integrates information from the body and administrates outgoing commands to the body. The cells that comprise the nervous system, neurons and glia, form circuits to coordinate nervous system activity.

Neurons consist of a cell body, or soma, plus neurites that extend out of the soma to contact other neurons. Dendrites are the primary locales of receiving information from other neurons, whereas axons convey information to other neurons. Throughout the neuron, a voltage gradient is maintained across the membrane. When neurons are at rest (inactive) this voltage is often between -85 and -60 mV, depending on cell type. Ion channels in the membrane can open to allow ions to flow in or out of the cell; this current flow can hyperpolarize the cell (making the voltage more negative), depolarize the cell (making the voltage more positive), or participate in maintaining the resting potential. When dendritic or somatic ion channels allow positively charged ions to enter the cell and neurons become sufficiently depolarized, an action potential is initiated. Starting near the junction of soma and axon, a self-propagating series of ion channel openings and closings send a strong depolarizing impulse down the axon. The electrical activity of the neuron is then communicated to other neurons at specialized structures called synapses.

The presynaptic cell conveys information about its activation to the postsynaptic cell in one of two ways. At electrical synapses, an electrical signal travels from the presynaptic cell into

the postsynaptic cell via small connecting pores. At chemical synapses, however, the presynaptic and postsynaptic cells are not physically connected; instead, presynaptic activation is signaled via a chemical signal released by the presynaptic cell and subsequently bound by molecules on the postsynaptic cell. Most vertebrate synapses in the central nervous system use the latter form of communication.

Neurotransmitters, a common class of chemical signal, are broadly categorized by their effect on the postsynaptic cell. Excitatory neurotransmitters cause postsynaptic depolarization, making the neuron more likely to become activated. Inhibitory neurotransmitters inhibit cell activity, often by causing postsynaptic hyperpolarization. The neurotransmitter glutamate mediates the majority of excitatory neurotransmission in the vertebrate brain. Glutamate receptors (GluRs) transduce signals in two different ways: metabotropic GluRs initiate intracellular signal cascades via G proteins, whereas ionotropic GluRs (iGluRs) open intrinsic ion channels in response to neurotransmitter binding.

IGluRs are nearly ubiquitous in the central nervous system, with subtype expression depending on many factors, including developmental stage and brain region. Regional and temporal variation in subtype expression suggests that the unique properties of each iGluR subtype confer to each subtype a unique physiological role. Indeed, several CNS disorders are known to involve improper regulation of specific iGluR subtypes (Bowie, 2008). Subtype-specific iGluR functional properties emerge from divergent aspects of iGluR structures. Understanding the ways in which functional properties arise from structural variation among iGluR subtypes will contribute to our conceptualization of human health and disease.

1.1 DIVERSITY OF IONOTROPIC GLUTAMATE RECEPTORS

Ionotropic glutamate receptors are commonly divided into three families: N-methyl-D-aspartate receptors (NMDARs), α -amino-3-hydroxy-5-methyl-4-isoxazolepropionate receptors (AMPARs), and kainate receptors (KARs). Delta glutamate receptor subunits (δGlus) are likely to form ionotropic glutamate receptors, as well, although no ligand that activates the putative δGlu receptor channel has been identified. Originally defined by the synthetic agonists that activate individual iGluR subtypes, each iGluR family is now known to comprise proteins that share many more properties.

1.1.1 NMDA Receptors

NMDA receptors (NMDARs) are unique among iGluRs in the co-requirement of both glutamate and glycine binding for activation (Johnson and Ascher, 1987; Kleckner and Dingledine, 1988). Strongly voltage-dependent channel block by external magnesium (Mg^{2+}) and particularly high Ca^{2+} permeability further distinguish NMDARs from other iGluRs (Dingledine et al., 1999). At resting membrane potentials, Mg^{2+} blocks the majority of open NMDAR channels and inhibits current influx. Mg^{2+} exits the channel to the extracellular solution more rapidly at depolarized potentials. Permeation of Mg^{2+} occurs at more hyperpolarized potentials, albeit with less frequency than unblock to the external milieu. The voltage-dependent nature of channel block by Mg^{2+} allows NMDARs to act as coincidence detectors, in which significant current flow through NMDARs requires presynaptic activity (glutamate release) and postsynaptic activity (depolarization to relieve Mg^{2+} channel block). The coincidence-detector function of NMDARs is central to their roles in processes such as NMDAR-dependent long-term potentiation (LTP), a

strengthening of synapses at which coincident pre- and postsynaptic activation occurs. NMDAR-dependent LTP relies on Ca^{2+} influx through NMDARs, and this influx is necessary for many types of learning and memory (Lynch, 2004). Hence, Mg^{2+} block and Ca^{2+} permeation play critical roles in healthy brain function.

NMDAR malfunction is implicated in a wide array of disorders, including epilepsy, Alzheimer's disease, and Huntington's disease (Muir, 2006). Due to their high degree of Ca^{2+} permeability, NMDARs are particularly likely to contribute to excitotoxic cell death during neurodegenerative processes. Furthermore, NMDAR subtype expression may be abnormal in several mental illnesses, including schizophrenia, major depressive disorder, and bipolar disorder (Machado-Vieira et al., 2009). NMDAR subtype expression is highly regulated and varies by brain region (Ishii et al., 1993), developmental stage (Chen et al., 2000), experience (Tongiorgi et al., 2003) and disease state (Clinton and Meador-Woodruff, 2004), suggesting that NMDAR subtypes play distinct physiological roles.

Most NMDARs are composed of two NR1 (or GluN1) and two NR2 (or GluN2) subunits. Both NR1 and NR2 subunits are necessary to form functional glutamate-gated NMDARs in mammalian systems (Fukaya et al., 2003). NR3 subunits can also participate in NMDAR complexes. Eight NR1 variants are produced by alternative splicing of a single mRNA transcript (Llansola et al., 2005), whereas the four NR2 subunits (NR2A-D) are encoded by four genes (Ishii et al., 1993; Monyer et al., 1992) and the two NR3 subunits (NR3A-B) are encoded by two genes (Ciabarra et al., 1995; Nishi et al., 2001). NR2 subunits share roughly 50% sequence identity, but are less homologous to NR1 subunits (Ishii et al., 1993) and NR3 subunits. Expression of the four principal NMDAR subtypes (NR1/2A – NR1/2D receptors) is highly regulated and varies by brain region (Ishii et al., 1993), developmental stage (Chen et al.,

2000), experience (Tongiorgi et al., 2003) and disease state (Clinton and Meador-Woodruff, 2004), suggesting that NMDAR subtypes play distinct physiological roles.

1.1.2 AMPA Receptors

AMPARs play a critical role in synaptic transmission at most glutamatergic synapses. The fast component of glutamate-induced synaptic current is mediated by AMPARs at these synapses, and AMPARs carry the majority of the total synaptic current near resting membrane potentials. Subtype-specific AMPAR expression and membrane insertion is particularly important for spatial working memory and the maintenance of potentiated synapses.

Proper AMPAR function is necessary for many processes in the healthy brain, and malfunctioning AMPARs contribute to wide-ranging disorders. For example, improper AMPAR regulation has been implicated in Amyotrophic Lateral Sclerosis, glioblastoma cell proliferation, and Fragile X mental retardation (Bowie, 2008). AMPARs also likely play a role in drug addiction (Kessels and Malinow, 2009).

The mammalian AMPAR family includes four genes that encode subunits GluA1, GluA2, GluA3, and GluA4 (also termed GluR1-4 or GluRA-D). These subunits share 54% sequence identity (Traynelis et al., 2010). AMPARs can be homo- or heterotetramic, although most AMPARs in the brain are heterotetramers. GluA1/GluA2, GluA2/GluA3, or GluA2/GluA4 appear to be the most common AMPAR heteromers (Conti et al., 1994; Lu et al., 2009). Like NMDARs, AMPAR subunit expression is regulated by both development and experience (Traynelis et al., 2010).

Most AMPARs in the adult brain are permeable to monovalent cations only, although some AMPARs are permeable to Ca^{2+}, as well. Ca^{2+}-permeable AMPARs in the cerebellum are

particularly important in Purkinje cell LTP, and those in the basal forebrain may play a key role in neurodegeneration at this locale (Weiss and Sensi, 2000).

1.1.3 Kainate Receptors

KARs are expressed throughout the brain, and high expression is observed in several areas, including the CA3 region of the hippocampus and the amygdala (Bailey et al., 2001). KARs mediate fast synaptic currents in some areas of the brain, though most KARs are likely to be presynaptic (Traynelis et al., 2010). Proper KAR function is critical to fear memory formation and LTP at hippocampal mossy fiber synapses (Bortolotto et al., 2003; Ko et al., 2005). Improper KAR function, however, is implicated in Huntington's disease, neuropathic pain disorders and temporal lobe epilepsy (Bowie, 2008).

The mammalian KAR family includes five genes that encode GluK1-5 subunits (also termed GluR5-7, KA1, and KA2). Whereas GluK1-3 subunits can form either homo- or heterotetrameric receptors, GluK4 and GluK5 subunits participate only in heteromeric complexes with GluK1-GluK3 subunits. GuK1-GluK3 subunits are highly homologous, with 70% sequence identity. The sequence identity of these subunits with GluK4 and GluK5 is lower at 29% (Traynelis et al., 2010).

Like AMPARs, KARs display a range of Ca^{2+}-permeabilities, depending on subunit composition and pre-mRNA editing (Kohler et al., 1993) (see Section 1.3.7). KAR subunit expression is both regionally and temporally specific (Bernard and Khrestchatisky, 1994; Lohrke and Friauf, 2002). Hippocampal CA1 and cerebellar KARs, for example, are composed of subunits that confer Ca^{2+}-impermeability (Lerma, 2006; Savidge and Bristow, 1998), whereas KARs in the CA3 region of the hippocampus are composed of subunits that permit Ca^{2+}

permeation (Perrais et al., 2009) (albeit to a much lesser extent than NMDARs). In the adult brain, Ca^{2+}-permeable KARs appear to be more common than Ca^{2+}-permeable AMPARs (Kohler et al., 1993).

1.2 IONOTROPIC GLUTAMATE RECEPTOR STRUCTURE

1.2.1 IGluR subunit transmembrane topology

Ionotropic glutamate receptors are tetrameric proteins consisting of one or more subunit subtypes surrounding a pore (Laube et al., 1998; Rosenmund et al., 1998). Each subunit is comprised of several components that act in a semi-modular fashion: an extracellular N-terminal domain (NTD), an extracellular agonist binding domain (ABD), a transmembrane domain, and an intracellular carboxy-terminal domain (CTD). The extracellular N-terminal sequence of each iGluR subunit forms the clamshell-shaped NTD, composed of upper (R1) and lower (R2) lobes (Figure 1). The NTD is followed by a sequence (S1) that forms much of the upper lobe (D1) of the similarly clamshell-shaped ABD. D1 links to the first of three transmembrane domains (M1, M3 and M4). A short intracellular linker connects M1 to a pore-lining reentrant loop (p-loop, or M2), which forms the selectivity filter toward the intracellular aspect of the channel. Another short linker connects the p-loop to M3. The longer sequence that connects M3 to M4 (S2) comprises most of the lower lobe of the ABD (D2). The CTD, likely to be in an extended conformation (Ryan et al., 2008), is formed by residues C-terminal to M4.

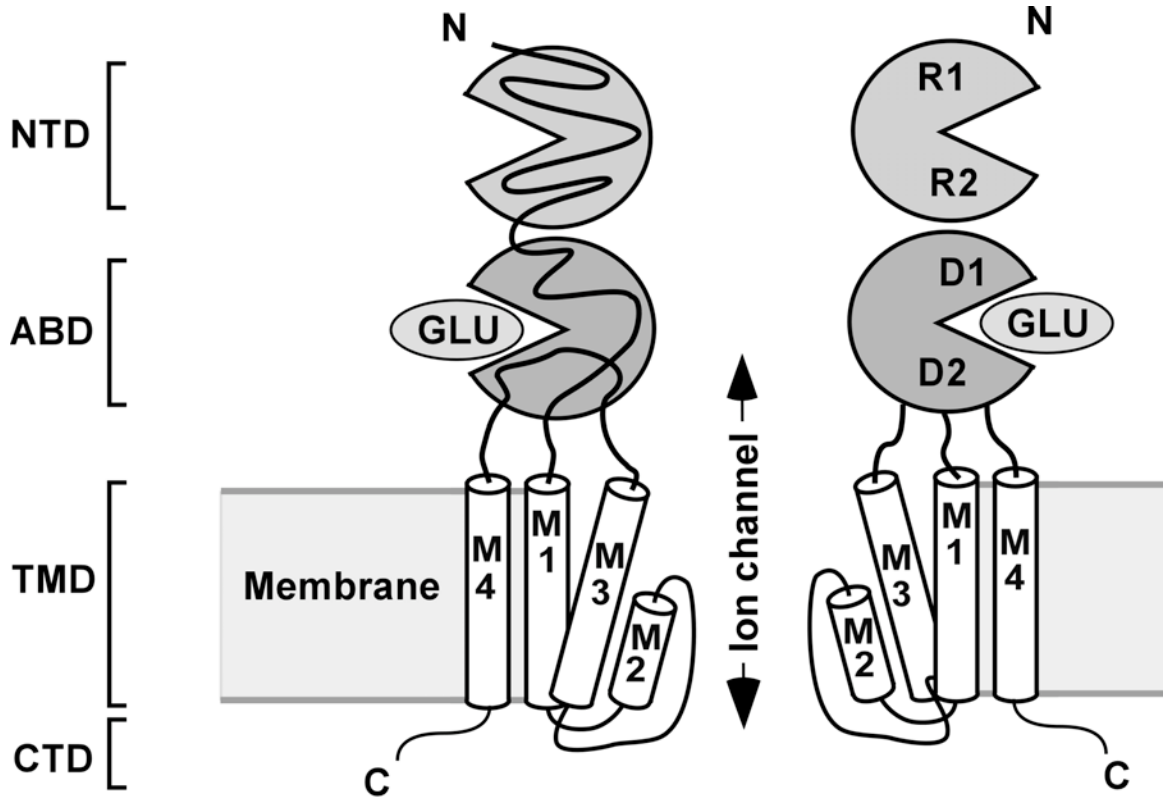

Figure 1 IGluR Topology

Cartoon diagram depicts an iGluR with front and back subunits removed for clarity. Each iGluR subunit contains an extracellular N-terminal domain (NTD) and agonist binding domain (ABD), three transmembrane domains (M1, M3, M4), a re-entrant loop (M2/p-loop) and an intracellular C-terminal domain. The NTD and ABD domains are clamshell-shaped, with upper lobes termed R1 and D1, respectively, and lower lobes termed R2 and D2, respectively.

1.2.2 Extracellular region of iGluRs

The current conceptualization of iGluR structure stems from inferences based on biochemical and electrophysiological studies, information provided by the many crystal structures of isolated iGluR ABDs (Armstrong et al., 1998; Furukawa and Gouaux, 2003; Plested and Mayer, 2007), and the recently-published crystal structure of the homomeric GluA2 glutamate receptor (Sobolevsky et al., 2009). The GluA2 receptor crystal structure verifies many of experimentally-based inferences about iGluR structure and provides further detailed information. As was predicted, the four GluA2 receptor NTDs are arranged as a dimer of dimers. Each two-NTD dimer is composed of side-to-side NTDs, with clamshell clefts facing the front and back of the receptor. The ABDs are also arranged in a dimer of dimers. ABD dimers, however, are arranged as back-to-back clamshells. The short linker sequence connecting the NTD and ABD of each subunit permits asymmetric dimerization of ABDs and NTDs, such that the NTDs of subunits A and B form a dimer, but the ABD of subunit A forms a dimer with the ABD of subunit D (Sobolevsky et al., 2009). Whereas the extracellular regions of KARs are likely to be arranged in a similar manner (Das et al., 2010; Kumar et al., 2009), mounting evidence indicates that NMDAR NTD arrangement is quite different (Karakas et al., 2009; Stroebel et al., 2010).

1.2.3 Transmembrane domain of iGluRs

Each iGluR subunit transmembrane domain contains three α-helical transmembrane regions (M1, M3, and M4) plus a p-loop; the p-loop contains an α-helical section followed by a pore-

lining segment (Figure 1). The GluA2 receptor further displays pre-M1 interfacial helices, which may be a common feature of iGluRs (Sobolevsky et al., 2009).

The open iGluR pore is shaped like an inverted tepee, with a wide external vestibule and a narrow selectivity filter that runs from roughly halfway through the pore to the intracellular aspect of the pore. M1, M3 and M4 residues participate in forming the external vestibule (Beck et al., 1999; Sobolevsky et al., 2009), and p-loop residues line the selectivity filter. In closed iGluRs, M3 domains cross to occlude the ion permeation pathway near the membrane-solvent junction (Chang and Kuo, 2008; Sobolevsky et al., 2009). This crossing occurs along the most highly-conserved motif among iGluRs, the SYTANLAAF motif (Chiu et al., 1999), and forms the narrowest part of the closed pore in the GluA2 receptor (Sobolevsky et al., 2009).

1.2.4 Accessory subunits of iGluRs

AMPARs and KARs can associate with accessory subunits, which drastically affect channel properties and likely impact iGluR structure (Kim et al., 2010; Tomita, 2010). The vast majority of investigations into iGluR structure and function, however, have focused on receptors that lack, or likely lack, accessory subunits. My dissertation research centers on NMDARs that do not incorporate accessory subunits, and therefore I will limit the discussion in this document to accessory subunit-lacking iGluRs.

1.3 STRUCTURAL BASES OF FUNCTIONAL CONSERVATION AND DIVERSITY AMONG IGLURS

1.3.1 Conservation of iGluR amino acid sequence

Sequence identity between iGluR subunits ranges from 5% to 81%. Some regions are more highly conserved than others: the transmembrane domain of GluR subunits share 14-87% sequence identity, whereas the sequence identity of iGluR subunit CTDs is between 0% and 9% (Gasic and Hollmann, 1992; Traynelis et al., 2010). Particularly in the transmembrane domains, iGluR subunits have few insertions or deletions relative to one another; the conservation of transmembrane residue sequence contributes to the structural similarities of iGluR transmembrane domains. Divergent iGluR properties often depend on regions of the protein with low sequence identity, such as the NTD and CTD (Herin and Aizenman, 2004; Tikhonov and Magazanik, 2009), whereas more conserved properties are found in regions with higher sequence identity, such as the ABD and transmembrane domain (Traynelis et al., 2010).

1.3.2 Agonist EC_{50} in iGluRs

Whereas the endogenous agonist for NR1 and NR3 subunits is glycine, all other iGluR subunits are agonized by glutamate. Several conserved residues in the ABD core play consistent roles in binding glutamate across iGluRs (Chen and Wyllie, 2006), but EC_{50}, the concentration of agonist that induces half of the maximum response (Erreger et al., 2007), varies widely according to iGluR subtype. Among the iGluR families, NMDARs display the lowest EC_{50}s (0.4 μM - 7.7 μM) , whereas AMPARs and KARs display higher EC_{50}s (19 μM - 5900 μM) (Traynelis et al.,

2010). The NR2 NTD is critical to the variation in EC_{50}s among NMDAR subtypes (Yuan et al., 2009); however, no such NTD control of EC_{50}s is known to occur in other iGluRs.

1.3.3 Mechanisms of iGluR gating

Gating kinetics determine the time course of iGluR responses to synaptic glutamate and regulate the total amount of current that passes through an iGluR under physiological conditions (Erreger et al., 2005). The fast, high-amplitude AMPAR current responses to synaptic glutamate, for instance, quickly decay as deactivation and desensitization set in, whereas the slower, smaller-amplitude responses of NMDARs are less hindered by desensitization and less quickly deactivated (Erreger et al., 2004).

The mechanisms by which agonist binding induces pore opening are not fully understood, although an understanding of several of the critical components of channel activation is emerging. Crystal structures of ABDs bound to agonists, partial agonists and antagonists have been invaluable in dissecting the structural mechanisms of channel gating. Combined with functional studies, these structures have led to the conclusion that agonists stabilize a closed-cleft conformation of the ABD, whereas antagonists stabilize an open-cleft conformation (Armstrong and Gouaux, 2000; Armstrong et al., 1998; Jin et al., 2002). Upon agonist binding, the lower lobe of the ABD clamshell (D2) moves toward the upper lobe (D1) to close the clamshell (Figure 1) (Armstrong and Gouaux, 2000). Many synthetic partial agonists of iGluRs have been created, and the degree of ABD cleft closure around each agonist is determined by the structure of the ligand (Jin et al., 2003). In AMPARs and some KARs, the degree of cleft closure correlates with extent of channel activation (Armstrong et al., 2003; Jin et al., 2003; Mayer, 2005; Nanao et al., 2005). This and other observations have led to the

hypothesis that D2 displacement creates strain on the activation gate, activating the channel to an extent that varies with the extent of D2 displacement. The activation gate of iGluRs has long been hypothesized to involve amino acid residues in M3 and those that connect M3 to D2 (Jones et al., 2002; Qian et al., 2002; Wollmuth et al., 2000). Thus, agonist binding and subsequent D2 movement might overcome the steric occlusion of the pore at crossed M3 domains by creating strain on the S2-M3 linker and promoting M3 domain rearrangements that open the pore (Erreger et al., 2004; Mayer, 2006; Sobolevsky et al., 2009). Hence, the extent of M3 rearrangement would depend on the degree of ABD cleft closure.

AMPARs can be activated by the binding of merely two agonist molecules and appear to ratchet open the pore in a stepwise fashion corresponding to the number of agonist molecules bound (2 - 4) (Laube et al., 1998; Rosenmund et al., 1998). In contrast, NMDA receptor activation requires that all four ABDs be occupied (Clements and Westbrook, 1991; Schorge et al., 2005)(see Section 1.3.7). Indeed, the extent of D2 displacement in crystallized NR1 subunits does not correlate with channel activation quantified with electrophysiology (Furukawa and Gouaux, 2003; Inanobe et al., 2005). Similarly, activation of KARs is likely to require the binding of four agonist molecules (Gebhardt and Cull-Candy, 2006; Smith and Howe, 2000) (but see Swanson et al., 2002).

The manner in which iGluR transmembrane domains rearrange to allow ion permeation has been proposed to be similar to that of a related group of channels, the voltage-gated K^+ channels. The bacterial KcsA K^+ channel, which has transmembrane regions similar in structure to the M2-M3 regions of iGluRs (Doyle et al., 1998; Sobolevsky et al., 2009; Wood et al., 1995), opens by M2 helix movement away from the center of the pore (Cuello et al., 2010a; Cuello et al., 2010b) (M2 in KcsA channel subunits is homologous to M3 in NMDAR subunits). The M2

helices of the KcsA channel splay apart to open the pore by bending at a hinge located roughly halfway through the M2 domain (Cuello et al., 2010b). Furthermore, electron paramagnetic resonance spectroscopy experiments suggest that M2 helices rotate counterclockwise (viewed from the extracellular aspect of the channel) during gating (Perozo et al., 1999). Based on electrophysiological studies, iGluR channel activation has been proposed to involve a similar transmembrane domain rotation and movement away from the center of the pore (Sobolevsky et al., 2009; Wollmuth and Sobolevsky, 2004). The M3 helices of iGluRs, however, are likely more rigid than the M2 helices of K^+ channels, and are unlikely to bend at a hinge homologous to the KcsA channel hinge (Sobolevsky et al., 2003). The GluA2 receptor has an interfacial pre-M1 helix that may play a role in regulating ion channel opening and closing, similar to slide helix regulation of the evolutionarily-related inward rectifier K^+ channels (Enkvetchakul et al., 2007; Sobolevsky et al., 2009).

IGluR desensitization, a process in which agonist remains bound but the pore closes, primarily stems from rearrangements of iGluR extracellular domains (Mayer and Armstrong, 2004; Traynelis et al., 2010). In AMPARs and KARs, desensitization involves disruption of the ABD dimer interface (Armstrong et al., 2006; Horning and Mayer, 2004; Sun et al., 2002; Weston et al., 2006b). This is proposed to decouple the activation gate from the open transmembrane regions by relaxing the S2-M3 linker, leading to channel closure. The manner in which ABD dimer stability in agonist-bound iGluRs is regulated varies by subtype. For instance, Na^+ and Cl^- ions bind and stabilize the ABD dimer interface to decrease the rate of desensitization in KARs, but not other iGluRs (Chaudhry et al., 2009; Vijayan et al., 2009). In contrast, the synthetic chemical cyclothiazide binds at the dimer interface of AMPARs, but no other iGluRs, to stabilize the dimer interface (Partin et al., 1995; Sun et al., 2002), thus

preventing desensitization. NMDAR desensitization is far less extensive than that of AMPARs and KARs, and structural mechanisms by which NMDARs desensitize are unclear.

IGluR deactivation occurs upon agonist unbinding and channel closure. Several structural features of iGluRs are known to regulate the variation in deactivation rates among subtypes, including interdomain interactions within an ABD (Weston et al., 2006a) and interactions between ABDs at the dimer interface (Jin et al., 2005). Differences in interdomain interactions are the predominant source of the variation in deactivation rates of GluA2 and GluK2 receptors (Traynelis et al., 2010; Weston et al., 2006a). In contrast, the vast differences between the slow deactivation rate of NMDARs and the faster deactivation rates observed in other iGluRs may be mediated in part by an NR1 tyrosine residue at the NR1-NR2A ABD dimer interface. This residue is proposed to slow agonist unbinding by stabilizing the ABD closed-cleft conformation in a manner similar to the way in which aniracetam stabilizes the GluA2 ABD (Furukawa et al., 2005; Jin et al., 2005).

1.3.4 Ca^{2+} permeability of iGluRs

The ion channel region of iGluR subunits is among the most highly conserved iGluR regions: 10% of the residues in the transmembrane domain are identical across all iGluR subunits (Traynelis et al., 2010). Several individual residues in the transmembrane domain are critical to imparting the channel properties that individuate iGluR families. The most prominent of these is the asparagine (N), glutamine (Q), or arginine (R), residue at the Q/R/N site of almost every iGluR subunit (Burnashev et al., 1992a; Burnashev et al., 1992b; Mori et al., 1992) (NR3 subunits, the sole exceptions, contain a glycine at this site). Located at the external tip of the selectivity filter, the Q/R/N-site is an essential regulator of Ca^{2+} permeability and Mg^{2+} block

(Burnashev et al., 1992b; Mishina et al., 1993; Mori et al., 1992; Sakurada et al., 1993; Wollmuth et al., 1996). The asparagine at the Q/R/N site of NMDARs (the "N-site") imparts a high selectivity for Ca^{2+} over monovalent cations, whereas the presence of an arginine in one or more subunits of an AMPAR confers Ca^{2+} impermeability to the channel (Burnashev et al., 1992a). Although all non-NMDAR iGluR subunit genes encode a glutamine at the Q/R/N site, pre-mRNA editing alters the codon to encode arginine in virtually all GluA2 subunits and many KAR subunits. Because the majority of AMPARs in the adult brain contain GluA2 subunits, most adult AMPARs are impermeable to Ca^{2+}. Even GluA2-lacking AMPARs, however, are 2-4 times less permeable to Ca^{2+} than are NMDARs (Burnashev, 1996; Burnashev et al., 1995; Jatzke et al., 2002; Schneggenburger, 1996).

Replacement of the NR1 N-site asparagine with the glutamine encoded in AMPAR and KAR subunits sharply attenuates Ca^{2+} permeability and slightly decreases channel block by Mg^{2+} (Burnashev et al., 1992b), and the converse mutation in GluA2 and GluA4 receptors increases Ca^{2+} permeability (Burnashev et al., 1992a) (Wollmuth and Sakmann, 1998).

The influence of Q/R editing on Ca^{2+} permeability of KARs is somewhat more complicated, as two independently-edited M1 sites also influence Ca^{2+} permeability (Dingledine et al., 1999; Puchalski et al., 1994). In GluK2 homomers with fully edited M1 domains, an arginine at the Q/R/N site increases Ca^{2+} permeability, though these KARs are less permeable to Ca^{2+} than NMDARs. In absence of pre-mRNA editing in the M1 region, however, the Q/R/N site is less influential; these KARs display low permeability to Ca^{2+}, regardless of Q/R editing. Thus, the identity of the residue at this site is important for, but not definitive of, iGluR Ca^{2+} permeability.

The M3 SYTANLAAF motif also plays an important role in Ca^{2+} permeation through iGluRs; mutation of the asparagine in this motif reduces Ca^{2+} permeability of both NMDARs and Ca^{2+}-permeable AMPARs (Jatzke et al., 2003; Watanabe et al., 2002). The nearby DRPEER motif of NR1 subunits, C-terminal to M3, also contributes to the high Ca^{2+} permeability of NMDARs (Watanabe et al., 2002). The homologous residues in Ca^{2+}-permeable GluA2 and GluK2 receptors, however, do not appear to influence Ca^{2+} permeability (Jatzke et al., 2003). Thus, Ca^{2+} permeability properties arise from both conserved and divergent features of iGluRs.

1.3.5 IGluR channel block by extracellular cations

Ca^{2+}-permeable iGluR channels are blocked by both extracellular Ca^{2+} and extracellular spermine, though block by extracellular spermine is quite weak (Bahring et al., 1997; McGurk et al., 1990; Ransom and Stec, 1988; Washburn and Dingledine, 1996). Ca^{2+} blocks these channels more strongly, affecting ion permeation under physiological conditions (Gu and Huang, 1991; Jatzke et al., 2002) This block is voltage-independent or weakly voltage-dependent in NMDARs, but strongly voltage-dependent in AMPARs and weakly voltage-dependent in KARs (Gu and Huang, 1991; Jatzke et al., 2002; Wollmuth and Sakmann, 1998{Premkumar, 1996 #125)}. Voltage dependence of ion interactions with pores often indicate that the interaction site is located within the transmembrane electric field. Hence, Ca^{2+} likely blocks AMPAR currents, but not NMDAR currents, at a transmembrane site in the extracellular vestibule.

Voltage-dependent channel block by extracellular Mg^{2+} is unique to NMDARs, and strongly influences NMDAR function (Dingledine et al., 1999). This block depends on the NR2 N-site and the neighboring N+1 site. Whereas mutation of the NR1 N-site to glutamine had essentially no effect on Mg^{2+} block, the same mutation at the NR2 N-site reduced Mg^{2+} block

and increased Mg^{2+} permeation. A similar but greater effect was observed upon mutation of the NR2 N+1 site (Wollmuth et al., 1998a). In AMPARs and KARs, however, the Q/R/N site does not account for the lack of channel block by Mg^{2+}; GluA2 and GluA4 receptors with Q-to-N mutations, for instance, exhibited no Mg^{2+} block (Burnashev et al., 1992a).

1.3.6 IGluR channel block by intracellular cations

NMDAR channels are further distinguished by voltage-dependent intracellular Mg^{2+} block (Bowie and Mayer, 1995; Johnson and Ascher, 1990). This block is regulated by the NR1 N-site and, to a lesser extent, the NR2A N+1 site (Wollmuth et al., 1998b). Polyamines are a more common source of channel block by intracellular cations; Ca^{2+}-permeable AMPARs and KARs both exhibit voltage-dependent block by intracellular polyamines. NMDARs are also blocked by intracellular polyamines, though to a much lesser extent than is observed in AMPARs and KARs (Benveniste and Mayer, 1993; Williams, 1997). Spermine likely mediates the majority of polyamine block *in vivo* (Bowie and Mayer, 1995; Kamboj et al., 1995), and can also permeate Ca^{2+}-permeable iGluRs; permeation rate increases as V_m becomes more positive (Bahring et al., 1997; Bowie and Mayer, 1995; Donevan and Rogawski, 1995). The Q/R/N site strongly contributes to iGluR sensitivity to channel block by polyamines; in AMPARs and KARs, only those receptors lacking an arginine at this site are blocked by intracellular polyamines (Perrais et al., 2010). Because polyamines affect NMDARs in multiple ways, and because polyamine block of NMDAR channels is quite weak, determining the structural mechanisms by which this block arises in NMDARs is more difficult (Jin et al., 2008; Kashiwagi et al., 1997).

1.3.7 Single-channel conductance of iGluRs

Single-channel conductance, a measure of the ease with which ions permeate the channel, varies among iGluR families. The single-channel conductances of Ca^{2+}-permeable AMPARs display the most variation, ranging from 7 pS to 45 pS. Ca^{2+}-permeable KAR single-channel conductances are between 5 pS and 25 pS, and those of NMDARs are between 17 and 50 pS. Not surprisingly, the Q/R/N site influences single-channel conductance in both AMPARs and KARs.: editing the glutamine to an arginine at this site dramatically decreases single-channel conductance, often to less than 1 pS (Swanson et al., 1996). Furthermore, replacement of the NMDAR N-site arginine with glutamine results in the appearance of a sub state conductance that is not observed in wild-type receptors (Premkumar and Auerbach, 1996; Premkumar et al., 1997).

Whereas AMPARs display two or three subconductance states (in addition to the main conductance state), KARs display two subconductance states and diheteromeric NMDARs display only one. AMPARs may be unique among iGluRs in that sub state occupancy depends on the number of bound agonist molecules. The four AMPAR conductance states are thought to reflect the number of bound glutamate molecules, with the lowest conductance state corresponding to receptors with one or two bound agonist molecules and the highest conductance state corresponding to receptors with four bound agonist molecules (Gebhardt and Cull-Candy, 2006; Prieto and Wollmuth, 2010; Rosenmund et al., 1998).

1.3.8 Allosteric modulation of iGluR channel properties

Numerous modulators of iGluR channel properties exert their effects through interactions with the extracellular regions of iGluRs. For instance, extracellular protons inhibit nearly all iGluRs in a voltage-independent manner (Mott et al., 2003; Traynelis et al., 1995). Several iGluR subtypes are likely to be under tonic proton inhibition; the proton IC_{50}s of NR1/2A, NR1/2B, NR1/2D, and GluK2 receptors are particularly close to physiological pH (Gielen et al., 2009; Traynelis et al., 1995; Traynelis et al., 2010). IGluR proton sensors are tightly coupled with iGluR gating machinery, with several residues that are key to proton sensitivity located at the ABD dimer interface (Gielen et al., 2008) and in the linker sequences that connect the ABD to M3 and M4 (Kashiwagi et al., 1996; Low et al., 2003).

Perturbation of the ABD dimer strongly affects proton inhibition of both AMPARs and NMDARs, and protons likely inhibit NR1/2A receptors by inducing rearrangement of the NR1-NR2A ABD heterodimer in a manner similar to that which AMPARs undergo during desensitization (Gielen et al., 2008; Sobolevsky et al., 2009; Sun et al., 2002). Although protons affect channel gating in many iGluRs, the manner in which protons alter channel gating are subtype-specific. For example, protons reduce channel open probability (P_{open}) and decrease mean open time in some NMDARs (Banke et al., 2005; Dravid et al., 2007; Traynelis and Cull-Candy, 1990). In contrast, AMPAR inhibition by protons is predominantly mediated by enhanced desensitization (but also involves a slight decrease in maximum P_{open}) (Ihle and Patneau, 2000; Lei et al., 2001).

Extracellular spermine interacts with the NTDs of several iGluRs to affect channel activity. For instance, spermine potentiation of NR1/2A and NR1/2B receptors is in part mediated by an increase in glycine affinity (Zhang et al., 1994). In contrast, studies indicate that

spermine binding to the GluK2 receptor NTD reduces proton inhibition (Masuko et al., 1999; Mott et al., 2003). Proton inhibition of NR1/2B receptors is also reduced by spermine binding (Masuko et al., 1999; Traynelis et al., 1995). The Q/R/N site plays a role in the conferring subtype specificity to spermine potentiation, but the structural mechanisms by which this site affects spermine potentiation are unknown (Kashiwagi et al., 1997; Panchenko et al., 1999).

1.4 STRUCTURAL BASES OF FUNCTIONAL CONSERVATION AND DIVERSITY AMONG NMDAR SUBTYPES

1.4.1 Agonist EC_{50}s of NMDARs

NMDAR glutamate EC_{50}s range from 0.35 μM in NR1/2D receptors to 3.3 μM in NR1/2A receptors (Erreger et al., 2007; Yuan et al., 2009). The NTD+L regions of NR2 subunits dramatically influence the NMDAR subunit specificity; NR1/2A receptors in which the NR2A receptor NTD has been replaced by the NR2D receptor NTD display a glutamate EC_{50} that is remarkably similar to that of wild-type NR1/2D receptors. A similar phenomenon is observed in NMDARs containing the converse chimera (NR2D subunits with the NR2A NTD). Redundant mechanisms of agonist potency regulation appear to have developed, however, as merely deleting the NTD does not strongly affect the EC_{50}s of NR1/2A and NR1/2D receptors, nor does this manipulation appear to affect NR1/2B or NR1/2C receptor EC_{50}s (Yuan et al., 2009). Indeed, the NR2 ABD strongly influences agonist potency, as well: in NR1/2A receptors, substituting the NR2D ABD for the NR2A ABD results in an EC_{50} equal to that of wild-type NR1/2D receptors (Erreger et al., 2007).

The NMDAR subtype specificity of glycine EC_{50} is also strongly affected by the NR2 NTD; in NMDARs with low glycine EC_{50}s (NR1/2B, NR1/2C and NR1/2D receptors), removal of the NR2 NTD markedly increases glycine EC_{50}. NR1/2A receptors maintain a high glycine EC_{50}, however, even without the NR2A NTD (Yuan et al., 2009). Further evidence indicates that the NR2 ABD is also involved regulating glycine EC_{50} among NMDAR subtypes (O'Leary and Wyllie, 2009) .

1.4.2 NMDAR gating

As described in 1.3.3, the M3 helices of iGluRs participate in the activation gate and form the narrowest part of the closed channel near the extracellular side of the membrane (Beck et al., 1999; Sobolevsky et al., 2002a; Sobolevsky et al., 2009). In the closed GluA2 receptor, the narrowest section of the M3 helix crossing has a diameter of less than 1 Å (Sobolevsky et al., 2009). In closed NMDAR channels, this region is likely to be wider (Sobolevsky et al., 2002a). Nevertheless, the activation gates move apart upon channel activation, opening to a diameter of about 11 Å (Sobolevsky et al., 1999).

NMDAR channel gating is strongly affected by the NR2 NTD (Krupp et al., 1998), and several modulators of channel activity bind to this domain (Fayyazuddin et al., 2000; Gallagher et al., 1996; Paoletti et al., 1995; Paoletti et al., 2000). This region is likely to be highly dynamic, with oscillations between closed- and open-cleft conformations impacting NMDAR channel behavior (Gielen et al., 2009). Closure of the NR2 NTD cleft (for example, due to Zn^{2+} binding), is proposed to destabilize the NR1-NR2 ABD heterodimer interface by placing strain on the NTD-to-ABD linker. (Figure 1). A destabilized NR1-NR2 ABD heterodimer may then induce or allow rearrangement of the extracellular region and channel closure, similar to the

rearrangement and channel closure that takes place during desensitization of AMPARs and KARs (Gielen et al., 2008; Mayer, 2006).

Yuan et al. (2009) and Gielen et al. (2009)[1] demonstrated that the NMDAR subtype dependence of several gating properties are principally conferred by the NTD and the NTD-to-ABD linker (the "NTD+L region"). Maximum P_{open}, channel open duration and deactivation rate are all strongly regulated by the NR2 NTD+L region. Furthermore, modulation of channel gating by protons and Zn^{2+} depends on the NTD+L region (Gielen et al., 2009) (see Section 1.4.6). These exciting discoveries demonstrate the highly modular nature of NMDARs, as well as further illuminate the surprising range of allosteric interactions within the protein.

1.4.3 Ca^{2+} permeability of NMDARs

Several structural features of NMDARs have been identified that promote or modulate Ca^{2+} permeability. As discussed in Section 1.3.4, Ca^{2+} permeability of iGluRs is regulated by the Q/R/N site (Burnashev et al., 1992b; Sakurada et al., 1993). NMDAR permeability to Ca^{2+} is further modulated by a concentration-dependent, voltage-independent channel block by Ca^{2+}. To account for this phenomenon, several groups have proposed that NMDARs contain one or more Ca^{2+} binding sites in or near the external vestibule of the channel, but outside or nearly outside the voltage field (Jahr and Stevens, 1993; Premkumar and Auerbach, 1996; Sharma and Stevens, 1996b).

The DRPEER peptide, C-terminal to the NR1 subunit M3 domain, may participate in an external Ca^{2+} binding site; substitution of any of the negatively charged DRPEER residues with a

[1] I contributed to this study (see Appendix A).

positively charged residue sharply decreases both relative Ca^{2+} permeability and fractional Ca^{2+} current. Furthermore, the negatively charged residues of the DRPEER motif are all accessible to modification by extracellular solvent reagents. Moreover, charge neutralization at these sites decreases Ca^{2+} permeability, but does not appear to affect Mg^{2+} block in absence of Ca^{2+} (Watanabe et al., 2002).

The extent of Ca^{2+} permeability of NMDARs is strongly influenced by NR2 subunit composition: NR1/2A and NR1/2B receptors allow a higher proportion of Ca^{2+} ions to permeate, compared to NR1/2C receptors (Burnashev et al., 1995; Schneggenburger, 1996). To my knowledge, the permeability of Ca^{2+} of NR1/2D receptors has not been reported. Structural mechanisms by which the variation in Ca^{2+} permeability among NMDAR subtypes arises are also unknown.

1.4.4 Mg^{2+} block of NMDAR channels

Mg^{2+} block of NMDARs is strongly dependent on membrane voltage. This voltage dependence stems from at least two mechanisms: (1) the Mg^{2+} binding site, located within the transmembrane electric field of the channel, allows Mg^{2+} ions to sense the membrane potential, and (2) Mg^{2+} ions interact with other ions that bind NMDARs, some of which also bind in a voltage-dependent manner. Two monovalent cation binding sites are present external to the selectivity filter (likely in the extracellular vestibule beyond the electric field), and one or two monovalent cation binding sites are present internal to the selectivity filter. Whereas the binding of extracellular ions to the external sites is not voltage-dependent, the binding of intracellular ions to these sites is heavily voltage-dependent (Antonov et al., 1998; Zhu and Auerbach, 2001a, b). When either or both of the external binding sites are occupied, Mg^{2+} occupying the channel

cannot exit to the external solution. Likewise, when a monovalent cation binds the internal site(s), Mg^{2+} cannot permeate. Furthermore, when any of the monovalent cation binding sites are occupied, Mg^{2+} cannot enter the channel (Antonov and Johnson, 1999; Zhu and Auerbach, 2001a, b).

NMDAR channel block by Mg^{2+} varies across subtypes: NR1/2A and NR1/2B receptors exhibit stronger block by Mg^{2+}, whereas NR1/2C and NR1/2D receptors exhibit weaker block. In NR1/2A receptors that are blocked by Mg^{2+}, the binding of a monovalent cation to an external site largely forces the Mg^{2+} ion to remain in the channel. In NR1/2D receptors, however, Mg^{2+} can permeate the channel; this ability provides an "escape route" for Mg^{2+} when one of the external monovalent cation sites is occupied. Indeed, the difference in Mg^{2+} permeabilities of NR1/2A and NR1/2D receptors is likely contributes to the subtype specificity of Mg^{2+} block strength (Qian et al., 2005; Qian and Johnson, 2006).

Several NMDAR regions have been proposed to contribute to the NR2 subunit dependence of Mg^{2+} block, including the M1-M3 region (Kuner and Schoepfer, 1996; Wrighton et al., 2008) and the ABD (Wrighton et al., 2008). Drs. Jon Johnson and Wei Gao recently identified a single NR2 residue in the M3 domain that strongly regulates the NR2 subunit-specificity of Mg^{2+} block (see Section 2.3). This discovery instigated many of the experiments I performed in my dissertation research.

1.4.5 Single-channel conductance of NMDARs

NMDAR single-channel conductance appears to primarily depend on residues in or near the transmembrane domain. Mutations in the DRPEER motif and at the N-site alter single-channel conductance, for example (Premkumar et al., 1997; Schneggenburger and Ascher, 1997;

Watanabe et al., 2002), whereas mutations in the NTD, ABD, and linkers to the transmembrane domain do not appear to affect this property (Krupp et al., 1998; O'Leary and Wyllie, 2009; Wyllie et al., 2006; Yuan et al., 2009).

The main state conductances of NMDARs ranges from roughly 35 pS in NR1/2C and NR1/2D receptors to 50 pS in NR1/2A and NR1/2B receptors. Subconductance states are similarly grouped: roughly 20 pS in NR1/2C and NR1/2D receptors, and 40 pS in NR1/2A and NR1/2B receptors (Stern et al., 1992; Stern et al., 1994; Wyllie et al., 1996). To my knowledge, no structural mechanisms have been proposed to explain the variation of single-channel conductance among NMDAR subtypes.

1.4.6 Allosteric regulation of NMDARs

A growing body of research provides insight into the critical role of the NR2 NTD in channel modulation by allosteric inhibitors (Gielen et al., 2008; Gielen et al., 2009; Krupp et al., 1998; Paoletti et al., 2000; Yuan et al., 2009). The NR2 subunit specificity of proton sensitivity, for instance, was recently found to be strongly regulated by the NR2 NTD+L (Gielen et al., 2009). Furthermore, the NR2 subunit NTD+L determines the NMDAR subtype specificity of allosteric inhibition by Zn^{2+} (Gielen et al., 2009). Zn^{2+} binding to the NR2A subunit NTD is proposed to induce NTD clamshell closure and subsequent destabilization of the ABD dimer interface, promoting ABD heterodimer rearrangement and channel closure (Karakas et al., 2009; Paoletti et al., 2000). This theory, and the observation that proton inhibition of NR1/2A receptors is enhanced by Zn^{2+} binding to the NR2A subunit NTD (Choi and Lipton, 1999; Erreger and Traynelis, 2008), has led to the hypothesis that Zn^{2+} NTD cleft closure around Zn^{2+} enhances proton accessibility to the proton sensor (Gielen et al., 2009). The NR1/2B receptor inhibitor

ifenprodil is proposed to affect proton inhibition in a similar manner (Mott et al., 1998; Pahk and Williams, 1997). Proton inhibition of NMDARs is likely further regulated by NTD interactions with extracellular Mg^{2+} and polyamines (Paoletti et al., 1995; Williams, 1993).

1.5 DISSERTATION CONTENTS

My dissertation research has focused on identifying structural determinants of NR2 subunit-specific open channel properties. I present the results of this research in three chapters. The initial chapter, *Section 2.0 : Structural Determinants of Channel Property Variation Among NMDAR Subtypes*, first details background regarding the discovery of the NR2 S/L site, a single residue in NR2 subunits that largely controls the subtype specificity of Mg^{2+} block. I then present my research, which identifies the NR2 S/L site as the principal determinant of the subtype specificity of single-channel main- and subconductance states. I further describe my research characterizing the variation of Ca^{2+} permeability among wild-type NMDARs, and present evidence suggesting that the NR2 S/L site strongly influences this property. In the second results chapter of my dissertation, *Section 3.0 : Structural Models of NMDARs*, I present three molecular homology models of the NMDAR ion channel. With these models, I generated predictions regarding the mechanism by which the NR2 S/L site, which is not part of the pore loop, conveys its effects to the pore. The third results chapter, *Section 4.0 : Mechanistic basis of NR2 S/L site effects*, describes my discovery of an intersubunit interaction in the NMDAR transmembrane domain. I identified a tryptophan residue in the NR1 subunit p-loop that interacts with the NR2 S/L site to form the subtype specificity of Mg^{2+} block that is described in Section 2.0 .

2.0 STRUCTURAL BASIS OF ION CHANNEL PROPERTY VARIATION AMONG NMDAR SUBTYPES

2.1 INTRODUCTION

NR2 subunit composition shapes numerous NMDAR properties, which therefore vary among NMDAR subtypes. Two recent studies (Gielen et al., 2009; Yuan et al., 2009) demonstrated that the NMDAR subtype-dependence of several properties, including channel open probability and agonist potency, are largely conferred by the NR2 subunit NTD+L. Less understood are the structural bases of the NMDAR subtype-dependence of properties of the open channel, including single-channel conductance, Mg^{2+} block, and Ca^{2+} permeability. Based on these properties, NMDARs can be divided into two groups with similar channels: NR1/2A and NR1/2B receptors exhibit similarly high single-channel conductances, Mg^{2+} affinities, and Ca^{2+} permeabilities, and NR1/2C or NR1/2D receptors exhibit similarly low single-channel conductances and Mg^{2+} affinities (Dingledine et al., 1999). Furthermore, NR1/2C receptors are less permeable to Ca^{2+} than NR1/2A and NR1/2B receptors (Burnashev et al., 1995; Schneggenburger, 1996) (to my knowledge, the Ca^{2+} permeability of NR1/2D receptors has not been assessed). The NMDAR subtype variation in Mg^{2+} block has been found to depend on three portions of the M1-M4 regions, as well as the agonist binding domain (Kuner and Schoepfer, 1996; Wrighton et al.,

2008). To my knowledge, there is no information on the structural origin of the NMDAR subtype dependence of single-channel conductance and Ca^{2+} permeability.

In the M1-M4 regions, NR2A and NR2B subunits have more sequence identity with each other than with NR2C or NR2D subunits; NR2C and NR2D subunits also share more sequence identity with each other than with the other NR2 subunits (Figure 1). Members of the Johnson lab took advantage of this difference in sequence identities to search for amino acid residues that influence subtype specific NMDAR channel properties. An M3 residue in NR2 subunits was found to regulate the subtype specificity of channel block by Mg^{2+}. My data indicate that this residue additionally principally underlies the NMDAR subtype dependence single-channel main state and sub state conductance. To determine whether the NR2 S/L site affects the NR2 subunit specificity of Ca^{2+} permeability and block, I quantified relative Ca^{2+} permeabilities of NR1/2A-2D receptors, as well as in NR1/2A(S632L) receptors. Initial results indicate that the NR1/2A(S632L) site does indeed regulate subtype-specific Ca^{2+} permeability. Furthermore, preliminary data suggest that the NR1/2D receptors may exhibit surprising variation in permeability to Ca^{2+}.

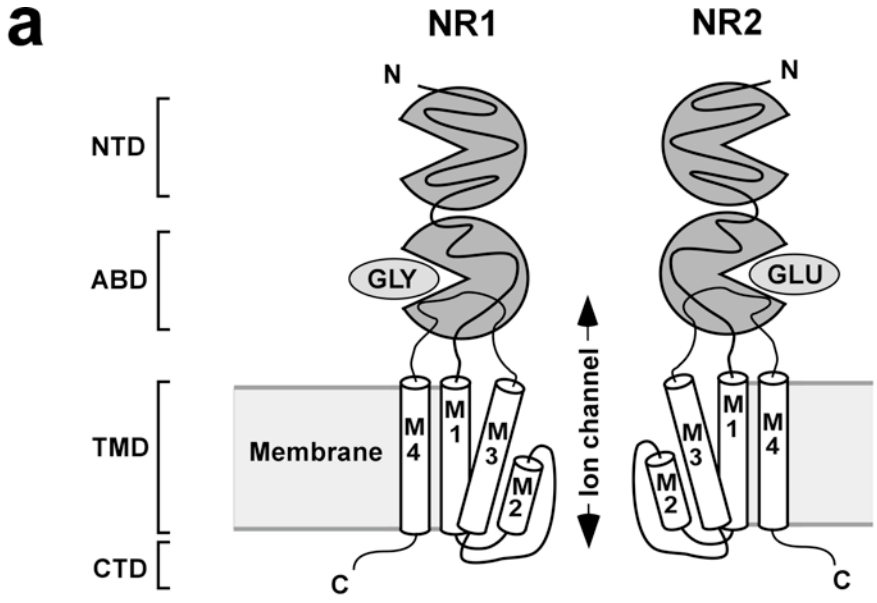

b

```
                    M1
NR2A   EPFSASVWVMMFVMLLIVSAIAVFVFEYFSPVGYNR  586
NR2B   EPFSADVWVMMFVMLLIVSAVAVFVFEYFSPVGYNR  587
NR2C   EPYSPAVWVMMFVMCLTVVAITVFMFEYFSPVSYNQ  597
NR2D   EPYSPAVWVMMFVMCLTVVAVTVFIFEYLSPVGYNR  611
         * *          *
                    M2
NR2A   NLAKGKAPHGPSFTIGKAIWLLWGLVFNNSVPVQNP  622
NR2B   CLADGREPGGPSFTIGKAIWLLWGLVFNNSVPVQNP  623
NR2C   NLTKGKKPGGPSFTIGKSVWLLWALVFNNSVPIENP  633
NR2D   SLATGKRPGGSTFTIGKSIWLLVALVFNNSVPVENP  647
                                        *
                    M3
NR2A   KGTTSKIMVSVWAFFAVIFLASYTANLAAFMIQEEF  658
NR2B   KGTTSKIMVSVWAFFAVIFLASYTANLAAFMIQEEY  659
NR2C   RGTTSKIMVLVWAFFAVIFLASYTANLAAFMIQEQY  669
NR2D   RGTTSKIMVLVWAFFAVIFLASYTANLAAFMIQEEY  683
       *       *
                    M4
NR2A   //SQLDIDNMAGVFYMLAAAMALSLITFIWEHLFYW  843
NR2B   //SQLDIDNMAGVFYMLGAAMALSLITFICEHLFYW  844
NR2C   //SKLDIDNMAGVFYMLLVAMGLALLVFAWEHLVYW  854
NR2D   //SKLDIDNMAGVFYMLLVAMGLSLLVFAWEHLVYW  868
         *
```

Figure 2 NMDAR transmembrane topology and NR2 subunit sequence alignment

(**a**) NMDAR transmembrane topology (see text for details). For clarity, only two of the four subunits are shown. This depiction does not indicate subunit arrangement around the pore.
(**b**) Alignment of the M1-M3 and M4 regions of NR2A-D subunits, with transmembrane regions labeled. Slashes indicate discontinuity in amino acid sequences. Asterisks mark residues examined in this study. Large asterisk marks the NR2 S/L site.

2.2 METHODS

Cell culture and transfection. HEK 293T cell (ATCC, whole-cell experiments) and HEK 293 cells (ATCC, single-channel experiments) were maintained as previously described (Qian et al., 2005). Calcium phosphate transfections or FuGENE transfections (Roche) were performed with a cDNA ratio of 1 eGFP:1 NR1:2 NR2. NMDA receptors were transiently expressed in HEK 293T cells after transfections using calcium phosphate (Clarke and Johnson, 2006), FuGENE (Siegler Retchless et al., submitted) or Lipofectamine (Qian and Johnson, 2006). Calcium phosphate and FuGENE transfections were performed with plasmids containing *rattus* NR1-1a cDNA in the pcDM8 vector and one NR2 subunit cDNA in the pcDNA 3.1 vector or the pcDNA 1 vector. EGFP in pcDM8 was co-transfected as a marker for probable NMDAR expression. For calcium phosphate transfections, the ratio of eGFP:NR1:NR2 subunit cDNA was 1:2:4. Most Lipofectamine transfections were performed with an eGFP:NR1:NR2 subunit cDNA ratio of 1:3:6, with each construct in a pcDM8 vector. For NR1/2C receptors, the cDNA ratio was 1:3:12.

Mutagenesis and cDNA preparation. cDNAs encoding *rattus* NR1-1a (GenBank accession number (ACCN) X63255), NR2A (ACCN M91563), and NR2D (ACCN L31612) NMDAR subunit genes in ampicillan resistance-encoding plasmids (pcDNA 3.1 or pcDNA 1) were mutagenized with the Stratagene Quik-Change XL sited-directed mutagenesis kit. Wizard MiniPrep kits and Qiagen MaxiPrep kits were used to amplify cDNAs. After mutagenesis, NMDAR subunit cDNAs from isolated colonies were sequenced from 100-200 bases upstream to 100-200 bases downstream of each mutation (University of Pittsburgh Genomics and Proteomics Core Laboratories). In most cases, mutant-containing plasmids from at least two colonies were expressed for electrophysiological experiments to ensure that experimental results

did not arise from unintended mutations. Furthermore, the entire coding sequence of the mutant subunit NR2A(S632L) from one colony was sequenced (GeneWIZ) to ensure that no unintended mutations had occurred.

Electrophysiology. Experiments was performed 12-48 hours after transfection initiation. Borosilicate micropipettes with resistances of 2-5 MΩ (whole-cell recordings) or 5-11 MΩ (single-channel recordings) were pulled on a Sutter Instruments P-97 electrode puller. Micropipettes used for single-channel experiments were coated with Sylgard 184.

Outside-out patch and whole-cell currents were amplified using an Axopatch 200B or Axopatch 200 patch-clamp amplifier (Molecular Devices) and recorded on video tape and/or a Dell computer in pClamp version 9 or 10 format (Molecular Devices). Currents were filtered at 1 kHz (whole-cell recordings) or 2.5 kHz (single-channel recordings) with a Warner Instruments low-pass bessel filter and sampled every 50 μs (whole-cell recordings) or 20 μs (single-channel recordings).

Mg^{2+} IC_{50} experiments. Mg^{2+} IC_{50} experiments were performed in the whole-cell recording configuration. Intracellular solution consisted of (in mM): CsCl (130), HEPES (10), EGTA (10). CsOH (~22 mM) was added to arrive at pH 7.2 ± .05 and 275 ± 5 mosmol. Extracellular solution ("Ringer's solution") consisted of (in mM): NaCl (140), KCl (2.8), $CaCl_2$ (1.0), HEPES (10). NMDAR responses were elicited by 30 μM glycine plus 10 μM NMDA whole-cell experiments, referred to as "agonists". Magnesium solutions were composed of the aforementioned extracellular solution, agonists, and $MgCl_2$; Mg^{2+} concentrations are specified in the text and figures. Because of their effects on Mg^{2+} channel block, no compensatory reductions in permeant ion concentrations were made in Mg^{2+}-containing solutions.

To facilitate efficient data collection for data presented in Figure 5, Figure 6 and Figure 19, we developed a method for rapid measurement of Mg^{2+} IC_{50}s at seven voltages. Mg^{2+}-free solution plus agonists was applied until a steady-state current was reached. Successively higher [Mg^{2+}]s (0-10 mM in Ringer's solution plus agonists) were applied to the cell for 5 seconds each via a gravity-fed 10-barrel fast perfusion system (Figure 4). During the last 1.5 s of each solution application, the command voltage was stepped from a holding potential of -65 mV (corrected for a junction potential of 4 mV) through a series of voltages ranging from -115 mV to -15 mV, in 20 mV increments. Each stepped command voltage was maintained for 210 ms. The current at each command voltage was averaged over a period of 150 msec, from 50 ms until 200 ms after the voltage was changed. Before and after application of agonists, baseline (0 agonists) current at each command voltage was measured; the baseline currents were averaged and subtracted from the agonist-activated currents in each [Mg^{2+}] at each command voltage to calculate the NMDAR-mediated current. Using this approach, current measurements in ten [Mg^{2+}]s at seven voltages each were made in 3-4 minutes. The ten [Mg^{2+}]s covered a wide concentration range so that an accurate estimate of Mg^{2+} IC_{50} could be made at each of the voltages used, despite the powerful voltage dependence of Mg^{2+} block. A complete data set for one cell was gathered by repeating this protocol at least 3 times and averaging the NMDAR-mediated current at each [Mg^{2+}] and command voltage across trials.

For each cell, at each voltage, fractional current ($I_{Mg}/I_{control}$) measured in each [Mg^{2+}] was plotted to create a [Mg^{2+}]-inhibition curve, which was fit with Equation 1:

$$\frac{I_{Mg}}{I_{Control}} = \frac{1}{1+\left(\frac{\left[Mg^{2+}\right]}{IC_{50}}\right)^{n}} \qquad \textbf{Equation 1}$$

where n is the Hill coefficient, I_{Mg} is the amplitude of agonist-induced current in $[Mg^{2+}]$, and $I_{control}$ is the amplitude of NMDAR-mediated current in the absence of Mg^{2+} (Figure 3b and Figure 4b).

I calculated the percent of the difference between NR1/2A and NR1/2D receptor Mg^{2+} IC_{50}s that was accounted for by the NR2 S/L site for the NR2A(S632L) mutation (88%; see Section 2.3) using Equation 2:

$$100 \times \frac{\left[\log\left\langle Mg^{2+}\ IC_{50}, NR1/2A(S632L)\right\rangle - \log\left\langle Mg^{2+}\ IC_{50}, NR1/2A\right\rangle\right]}{\log\left\langle Mg^{2+}\ IC_{50}, NR1/2D\right\rangle - \log\left\langle Mg^{2+}\ IC_{50}, NR1/2A\right\rangle} \qquad \textbf{Equation 2}$$

A related equation was used to calculate percent of the difference between NR1/2A and NR1/2D receptor Mg^{2+} IC_{50}s accounted for by the NR2D(L654S) mutation (57%). Although use of log-transformed IC_{50} data is the more appropriate (Colquhoun, 1998), similar calculations were performed arithmetically (without log-transformation), yielding 81% for the NR2A(S632L) mutation and 73% for the NR2D(L654L) mutation.

Single-channel experiments. Single-channel experiments were performed in extracellular Ringer's solution, with NMDAR-mediated currents elicited by 30 μ M glycine plus 30 μM NMDA. Intracellular composition for most single-channel experiments was (in mM): CsFl (115), CsCl (10), HEPES (10), EGTA (10). For some experiments included in the kinetic analyses, CsCl was substituted for CsF. CsOH (~ 40 mM) was added to both intracellular solutions to arrive at pH 7.2 ± .05 and 275 ± 5 mosmol.

Single-channel data analysis. Analyses of single-channel currents were performed using the DC analysis programs (http://www.ucl.ac.uk/Pharmacology/dcpr95.html). Conductances were calculated as the slope of the best-fit linear regression to an *i*-V graph containing data collected at four or more voltages. To determine single-channel current amplitude for each patch at each voltage, one or two binomial curves were fit to single-channel current amplitude event histograms using the maximum-likelihood method (Colquhoun and Sigworth, 1995). Kinetic analyses were also performed with the DC analysis programs, using the maximum likelihood method to fit multiple curves to shut time and open period distributions. For each distribution of events, fits were generated using two to four components.

Statistical Analysis. Most statistical tests were performed using Origin 7 software (OriginLab Corporation). T-tests for heterogeneity of slopes were performed in SAS 9.2 (SAS Institute Inc.) In Figure 19, Mg^{2+} IC_{50} data are presented as mean Mg^{2+} IC_{50} value (averaged across cells) ± s.e.m.

Ca^{2+} permeability experiments. Relative Ca^{2+} permeability (P_{Ca}/P_{Cs}) was assessed in biionic conditions, using an intracellular Cs^+ solution and and extracellular solution containing 1.8 mM Ca^{2+}, 10mM Ca^{2+}, or 146 mM Cs^+ as the sole permeant ions. Ca^{2+} solutions consisted of (in mM): 140 NMDG (an NMDAR-impermeant cation), 10 Hepes, 1.8 or 10 Ca^{2+}, pH adjusted to 7.2 ± 0.05 with HCl. Extracellular Cs^+ solution contained (in mM): 140 CsCl, 10 HEPES, pH adjusted to 7.2 ± 0.05 with CsOH. When necessary, sucrose was added to reach 290 ± 10 mosmol. The intracellular Cs^+ solution was the same as that for Mg^{2+} IC_{50} experiments. Voltage drift was measured at the end of each experiment; data from experiments in which the voltage drift exceeded 2 mV were excluded from analysis.

Before each recording, the pipette offset was zeroed in Ringer's solution. To minimize voltage drift, and to avoid errors due to junction potential changes at the ground electrode, a 3M KCl agarose cushion ground electrode was used. A stable whole-cell recording configuration was then achieved in Ringer's Solution. Extracellular solution containing a single permeant ion (Cs^+ or Ca^{2+}) was then bath-applied via a gravity-fed perfusion system for several minutes, to ensure complete solution exchange. 1 mM glutamate plus 50 μM glycine in the single permeant-ion solution were bath-applied for 30 - 60 s, until desensitization was complete. In continued presence of glutamate and glycine, the command voltage was stepped from a holding potential of -65 mV through a series of voltages ranging from -95 mV to -55 mV, in 10 mV increments, then stepped from -50 mV to 10 mV, in 2 mV increments, and finally from 15 mV to 55 mV, in 10 mV increments (see Figure 10). As with Mg^{2+} IC_{50} experiments, the stepped command voltages were maintained for 210 ms each. The current at each command voltage was averaged in the same manner as that described for Mg^{2+} IC_{50} determination. As with Mg^{2+} IC_{50} experiments, NMDAR-mediated current was calculated by subtracting the average of current recorded before and after agonist application from current recorded in the presence of agonists. The NMDAR-mediated current at each voltage was plotted as a function of voltage (corrected for a junction potential of 8 mV in Ringer's solution) , and V_{rev} was determined to be the voltage at which the plotted function crossed the x-axis. The plotted linear function connected the smallest inward current to the smallest outward current.

Inclusion criteria required that the whole-cell NMDAR-mediated Ca^{2+} current exceeded -6 pA at -65 mV, and that the baseline current at -65 mV (in absence of agonists) was no more than 2 times the agonist-induced Ca^{2+} current at that voltage. Experiments in which voltage drift

was greater than 2.5 mV were excluded from analysis, as were experiments in which the baseline current (in absence of agonists) changed by more than 10%.

Relative Ca^{2+} permeability was calculated with a modified Lewis equation (Lewis, 1979; Wollmuth and Sakmann, 1998)(Equation 3):

$$V_{rev(Ca)} - V_{rev(Cs)} = \frac{RT}{F} \ln \frac{4\frac{P_{Ca}}{P_{Cs}} \times [Ca^{2+}]_o}{[Cs]_o \times (1 + e^{\frac{V_{rev(Ca)}}{(RT)/F}})} \qquad \textbf{Equation 3}$$

Where $[Cs^+]_o$ and $[Ca^{2+}]_o$ are the extracellular concentrations of Cs^+ and Ca^{2+}, and P_{Ca}/P_{Cs} is the permeability ratio of Ca^{2+} to Cs^+. For results presented in Table 5.2, activity coefficients were included in P_{Ca}/P_{Cs} calculations: 0.72 (146 mM Cs^+), 0.30 (1.8 mM Ca^{2+}), and 0.31 (10 mM Ca^{2+}), as in Wollmuth & Sakmann (1998).

The percent decrease in P_{Ca}/P_{Cs} of NR1/2A(S632L) receptors, from the NR1/2A receptor P_{Ca}/P_{Cs} to the NR1/2C or NR1/2D receptor P_{Ca}/P_{Cs}, was calculated using the following equations:

$$100 \times \frac{(\frac{P_{Ca}}{P_{Cs}}, NR1/2A, [Ca^{2+}]) - (\frac{P_{Ca}}{P_{Cs}}, NR1/2A(S632L), [Ca^{2+}])}{(\frac{P_{Ca}}{P_{Cs}}, NR1/2A, [Ca^{2+}]) - (\frac{P_{Ca}}{P_{Cs}}, NR1/2C, [Ca^{2+}])} \qquad \textbf{Equation 4}$$

$$100 \times \frac{(\frac{P_{Ca}}{P_{Cs}}, NR1/2A, [Ca^{2+}]) - (\frac{P_{Ca}}{P_{Cs}}, NR1/2A(S632L), [Ca^{2+}])}{(\frac{P_{Ca}}{P_{Cs}}, NR1/2A, [Ca^{2+}]) - (\frac{P_{Ca}}{P_{Cs}}, NR1/2D, [Ca^{2+}])} \qquad \textbf{Equation 5}$$

where [Ca^{2+}] = 1.8 mM or 10 mM extracellular Ca^{2+}, and (P_{Ca}/P_{Cs}, NR1/2A, [Ca^{2+}]) is the P_{Ca}/P_{Cs} of NR1/2A receptors in the specified [Ca^{2+}].

The percent of P_{Ca}/P_{Cs} that was accounted for by the NR2 S/L site (78%; see Section 2.5.2) was calculated by averaging the four values that arose from inserting P_{Ca}/P_{Cs} values into Equation 4 and Equation 5.

2.3 FOUNDATIONAL STUDIES: STRUCTURAL DETERMINANTS OF VARIATION IN MG^{2+} IC_{50}

To identify a structural basis for the NR2 subunit dependence of Mg^{2+} block, members of the Johnson lab compared the aligned amino acid sequences of the four NR2 subunits in or near transmembrane domain. We took advantage of the pattern of variation in Mg^{2+} channel block properties among NMDAR subtypes: Mg^{2+} blocks the channels of NR1/2A and NR1/2B receptors with similarly high affinity, and the channels of NR1/2C and NR1/2D receptors with similar, lower affinity (Dingledine et al., 1999). Sites that were targeted reflect this clustering of NMDAR subtypes: sites at which NR2A and NR2B subunits contain the same residue, but at which NR2C and NR2D subunits share a different residue (Figure 2b). In NR2A subunits, the wild-type residue was replaced with the residue found in NR2C and NR2D subunits.

Dr. Wei Gao, a postdoctoral fellow in the Johnson lab, compared the Mg^{2+} block properties of receptors composed of NR1 combined with wild-type NR2A, wild-type NR2D, or mutant NR2A subunits. For each NMDAR subunit combination, he quantified the Mg^{2+} IC_{50}, the concentration of Mg^{2+} ([Mg^{2+}]) necessary to inhibit 50% of the NMDAR-mediated current

(Equation 1) (Figure 3a and b). Because Mg^{2+} block of NMDARs is strongly voltage-dependent, data were often gathered at several voltages. Consistent with previous data (Ishii et al., 1993; Kuner and Schoepfer, 1996; Monyer et al., 1992), NR1/2A receptors had higher Mg^{2+} IC_{50}s than did NR1/2D receptors at each voltage tested (Figure 3d).

The M1-M4 region sites that were targeted are identified in Figure 2 and Figure 3c. At one or more voltages, Dr. Gao measured the Mg^{2+} IC_{50}s of NMDARs with the NR2C and NR2D subunit residue substituted at the corresponding NR2A subunit site. For instance, the NR2A subunit glutamine (Q) at position 620 was replaced with aspartate (E), the residue at the homologous location in NR2C and NR2D subunits, creating NR2A(Q620E). Dr. Gao did not examine sites that were previously demonstrated to not affect channel block by Mg^{2+} (for example, Kuner and Schoepfer (1996) found that several M2 residues do not influence Mg^{2+} IC_{50} at -100 mV, nor did these residues influence $K_{0.5}(0)$, a value extrapolated from a linear fit of Mg^{2+} IC_{50}s between -75 mV and -35 mV). Because external and internal permeant ions bind near the extracellular and intracellular entrances of the pore to affect Mg^{2+} block (Antonov et al., 1998; Antonov and Johnson, 1999; Zhu and Auerbach, 2001a, b), residue sites near these entrances were of particular interest. Transmembrane region residue sites were of interest, as well. Seven NR1/2A receptors at which an NR2D subunit residue was substituted for the homologous NR2A subunit residue were examined. Most mutant receptors, however, had Mg^{2+} IC_{50}s that were similar to wild-type NR1/2A receptors (Figure 3e and f). When the NR2C and NR2D leucine (L) was substituted for the NR2A and NR2B serine (S) at NR2A(S632) in M3, however, we observed Mg^{2+} IC_{50}s that were strikingly similar to NR1/2D receptor Mg^{2+} IC_{50}s (Figure 3g).

To study the effects of mutations at NR2A(S632) more thoroughly and efficiently, a method of rapidly characterizing NMDAR Mg^{2+} IC_{50}s at seven voltages, ranging from -115 mV to -15 mV, was developed. This method is similar to that presented in Figure 3a, except that each Mg^{2+}-containing solution was applied for 5 s, and an I-V curve was measured quickly near the end of each solution application (see Section 2.2 and Figure 4). I found that this protocol yielded Mg^{2+} IC_{50} measurements that were similar to those made with the protocol illustrated in Figure 3 **(**Figure 5) With both protocols, Dr. Gao found that NR1/2A(S632L) receptor Mg^{2+} IC_{50}s are very close to those of NR1/2D receptors (Figure 3g and Figure 5a). I later determined that substitution of leucine for serine at this site (the "NR2 S/L site") accounted for 88% of the difference between NR1/2A and NR1/2D receptor Mg^{2+} IC_{50}s (averaged across voltages; see Experimental Procedures). Furthermore, substitution of the NR2A serine for the homologous NR2C and NR2D leucine at the NR2 S/L site resulted in NR1/2D(L654S) receptor Mg^{2+} IC_{50}s that were decreased toward those of NR1/2A receptors by an average of 57% (Figure 5b).

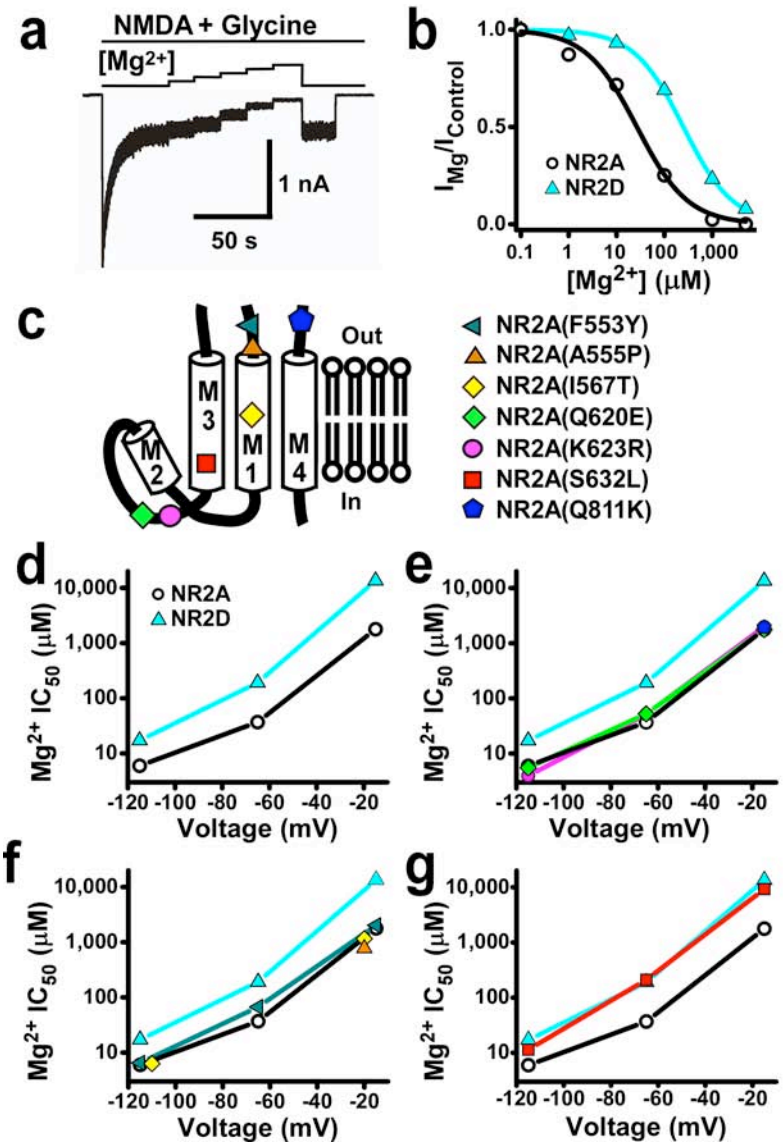

Figure 3 Search for residues that affect the NMDAR subtype specificity of Mg^{2+} block

(**a**) Example trace of NR1/2A receptor-mediated currents at -65 mV and current inhibition by addition of Mg^{2+} at concentrations from 1 μM to 5 mM.
(**b**) [Mg^{2+}]-inhibition curves constructed from the NR1/2A trace in (**a**) (black circles) and similar data from NR1/2D receptors (blue triangles).
(**c**) Transmembrane topology of NR2 subunits and predicted locations of targeted residues.
(**d-g**) Plots of average Mg^{2+} IC_{50}s at -115, -65, and -15 mV in wild-type receptors and receptors containing amino acid residue substitutions (point mutants in which a residue in the NR2A subunit was replaced with the homologous residue in NR2C and NR2D subunits). The mutant subunit represented by each symbol is defined in (**c**) (right).
(**d**) Mg^{2+} IC_{50}s of wild-type NR1/2A and NR1/2D receptors.
(**e**) Mg^{2+} IC_{50}s of NR1/2A(Q620E), NR1/2A(K632R), NR1/2A(Q811K) and wild-type receptors.
(**f**) Mg^{2+} IC_{50}s of NR1/2A(F553Y), NR1/2A(A555P), NR1/2A(I567T) and wild-type receptors.
(**g**) Mg^{2+} IC_{50}s of NR1/2A(S632L) and wild-type receptors. n = 2-24 cells per point. Wild-type NMDAR data presented in (**d**) are replotted in (**e-g**).

Data in this figure were gathered by Dr. Wei Gao.

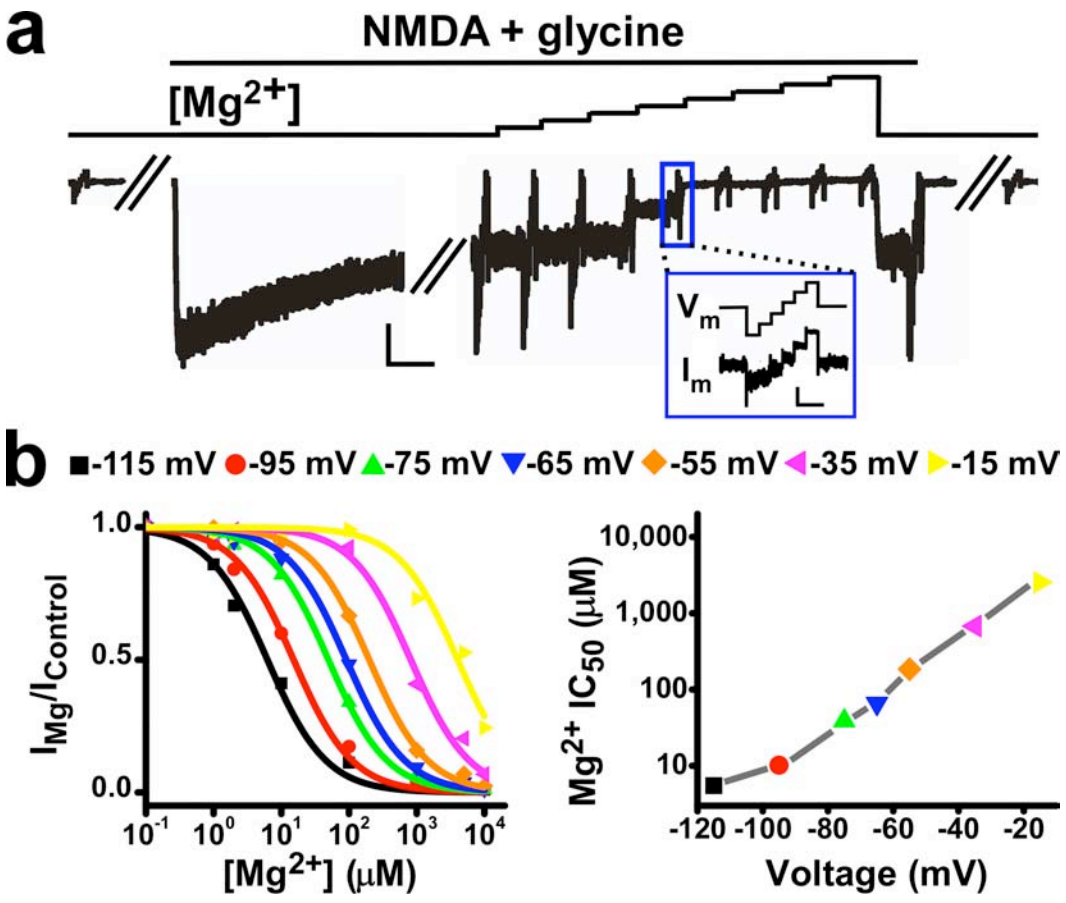

Figure 4 A novel approach for measuring Mg^{2+} IC_{50}s at seven

(**a**) Whole-cell recording current trace of NR1/2A receptor current during rapid measurement of Mg^{2+} IC_{50}s at seven voltages. Large scale bars, 300 pA and 5 s. Inset, I-V curves in each [Mg^{2+}] were measured by quickly stepping the command voltage from -115 to -15 mV in 20 mV increments. Scale bars in inset, 100 pA and 500 ms. See Section 2.2 for a detailed description of the protocol.
(**b**) Left, Mg^{2+} concentration-inhibition curves derived from data in (**a**). NMDAR-mediated current in each [Mg^{2+}] divided by NMDAR-mediated current in 0 Mg^{2+} is plotted against [Mg^{2+}]. Right, plot of the voltage-dependence of Mg^{2+} IC_{50}, based on the single concentration-inhibition curves to the left. At least 3 sets of curves were measured and averaged per cell.

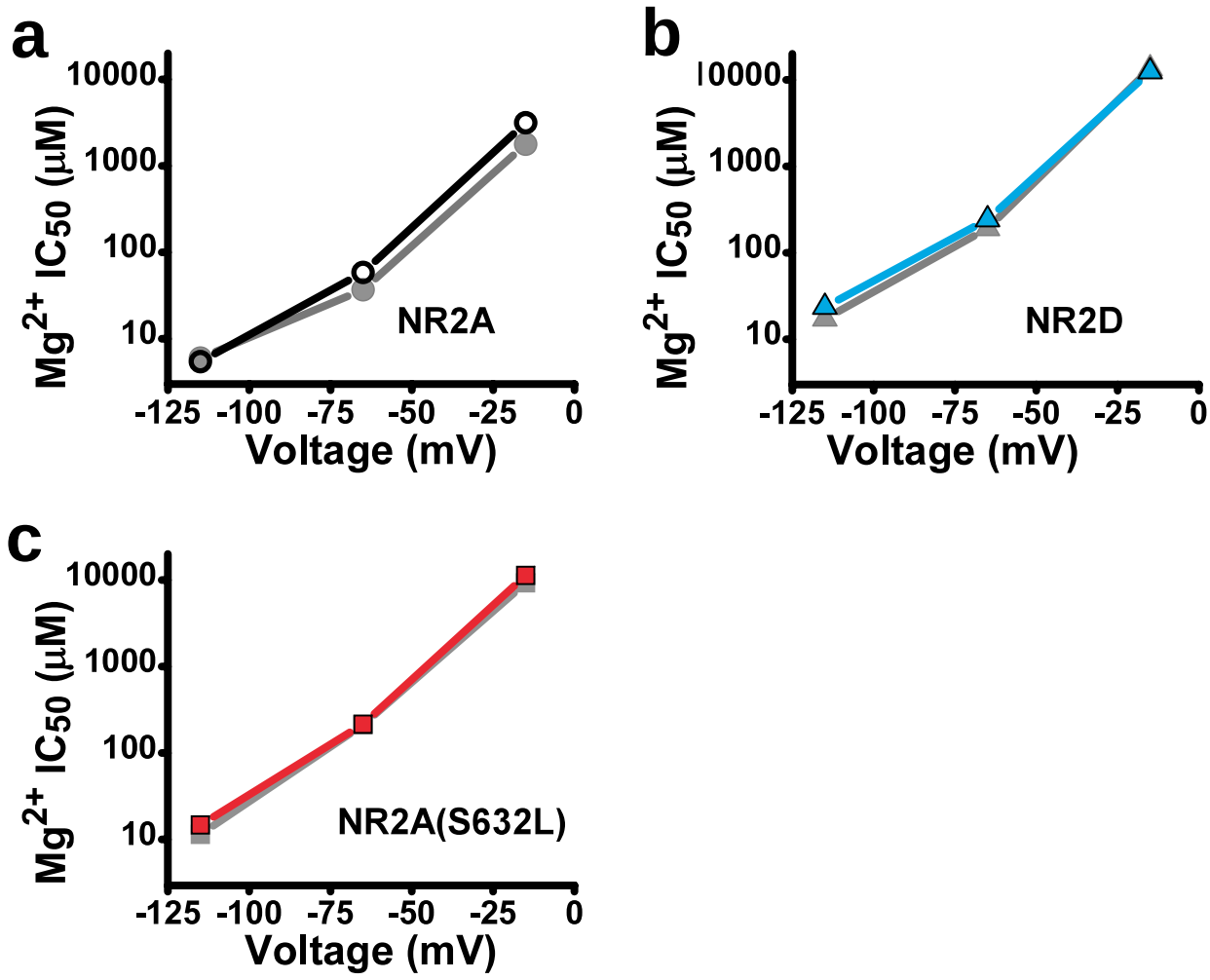

Figure 5 Comparison of Mg^{2+} IC_{50}s determined by two protocols

At -15, -65 and -115 mV, the protocols for gathering Mg^{2+} IC_{50} data yielded similar results for: (**a**) NR1/2A receptors, (**b**) NR1/2D receptors and (**c**) NR1/2A(S632L) receptors. Results from the slower protocol (illustrated in Figure 3a and b) are plotted with grey symbols and lines, and results from the rapid protocol (illustrated in Figure 4) are plotted with black (**a**), blue (**b**), or red (**c**) symbols and lines. See Section 2.2 and Figure 3 for protocol details.

Data in this figure were gathered by Dr. Wei Gao.

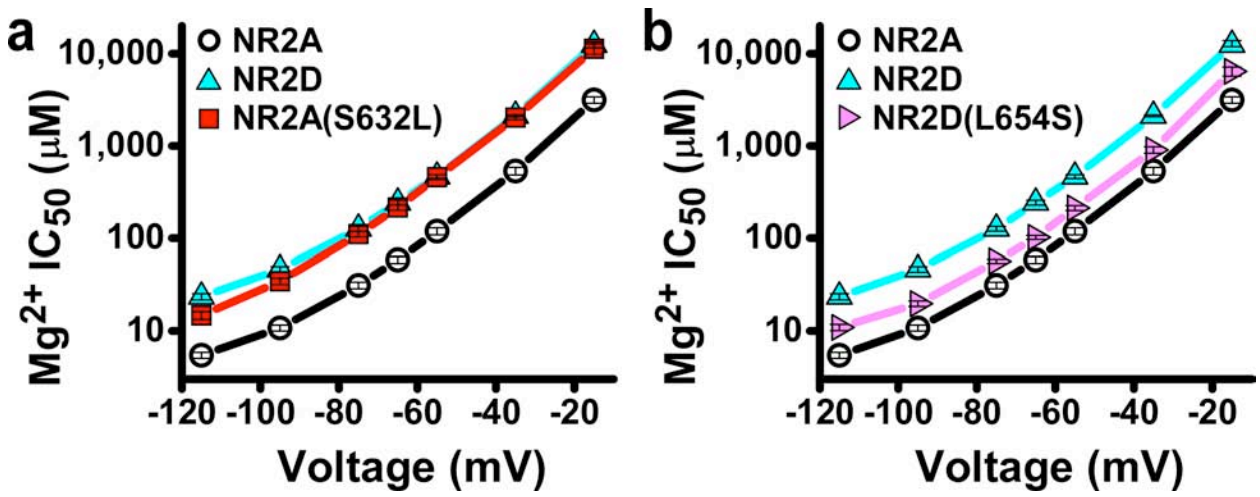

Figure 6 The NR2 S/L site determines the NMDAR subtype specificity of Mg^{2+} IC_{50}

(**a**) NR1/2A(S632L) receptor Mg^{2+} IC_{50}s are similar to NR1/2D receptor IC_{50}s across a wide range of voltages. Plot of the voltage-dependence of Mg^{2+} IC_{50}s of NR1/2A, NR1/2D, and NR1/2A(S632L) receptors. IC_{50}s in this figure and in Figure 19 were determined using a rapid measurement protocol (Figure 4).
(**b**) NR1/2D(L654S) receptor Mg^{2+} IC_{50}s approach those of NR1/2A receptors across a wide range of voltages.

Data in this figure were gathered by Dr. Wei Gao.

2.4 STRUCTURAL DETERMINANTS OF VARIATION IN SINGLE-CHANNEL PROPERTIES

2.4.1 Single-channel conductance

After the surprising discovery that a single residue in NR2 subunits drastically affects the NR2 subtype specificity of Mg^{2+} IC_{50}, I asked whether this residue contributes to another fundamental NR2 subtype-dependent property, single-channel conductance. Single-channel conductance, along with reversal potential, defines the amount of current that passes through an open channel at any voltage. It is a hallmark difference between NMDAR subtypes, and determination of single-channel conductance is an important tool for identifying NMDAR subunit composition of native channels in the central nervous system (Cull-Candy et al., 1998; Farrant et al., 1994).

I recorded single-channel currents in NR1/2A and NR1/2A(S632L) receptors (Figure 7a) to determine single-channel current amplitudes (Figure 7b) and conductance (Figure 7c), and compared them to NR1/2D receptor single-channel data gathered previously in Dr. Johnson's lab (Qian et al., 2005). Across voltages, the single-channel current amplitudes of NR1/2A(S632L) receptors were noticeably smaller than those of NR1/2A receptors (Figure 7a). NR1/2C and NR1/2D receptors display similarly small single-channel amplitudes (Cull-Candy et al., 1998; Qian et al., 2005; Stern et al., 1992). The main state conductance of wild-type NR1/2A receptors was 54.6 ± 2.1 pS, similar to other reported values (Stern et al., 1992; Stern et al., 1994). The main state conductance of NR1/2A(S632L) receptors was 34.8 ± 1.4 pS, significantly different

from the NR1/2A main state conductance (t-test for heterogeneity of slopes, $p < 0.0001$), but indistinguishable from that of NR1/2D receptors (37.4 ± 1.3 pS, measured previously in the Johnson lab (Qian et al., 2005), $p = 0.2522$) and consistent with other reported values (Wyllie et al., 1998; Wyllie et al., 1996).

Another single-channel property that strongly distinguishes NMDAR subtypes is a prominent subconductance state of ~20 pS that is exhibited by NR1/2C and NR1/2D receptors, but not by NR1/2A or NR1/2B receptors. I observed that NR1/2A(S632L) receptors exhibit a remarkably similar subconductance state of 17.0 ± 0.7 pS (Figure 7c). This conductance is not significantly different from the subconductance state of NR1/2D receptors previously measured in our lab under the same conditions (Qian et al., 2005) (20.2 ± 1.3 pS; $p = 0.051$); these data agree with prior reports of the NR1/2D subconductance state (Wyllie et al., 1998; Wyllie et al., 1996).

I could not consistently resolve a subconductance state in NR1/2A receptors, although in some patches I observed infrequent occupancy of a 40 pS subconductance state (Figure 8), as has been previously reported (Stern et al., 1992; Stern et al., 1994). NR1/2A(S632L) receptors evidenced no similar subconductance state.

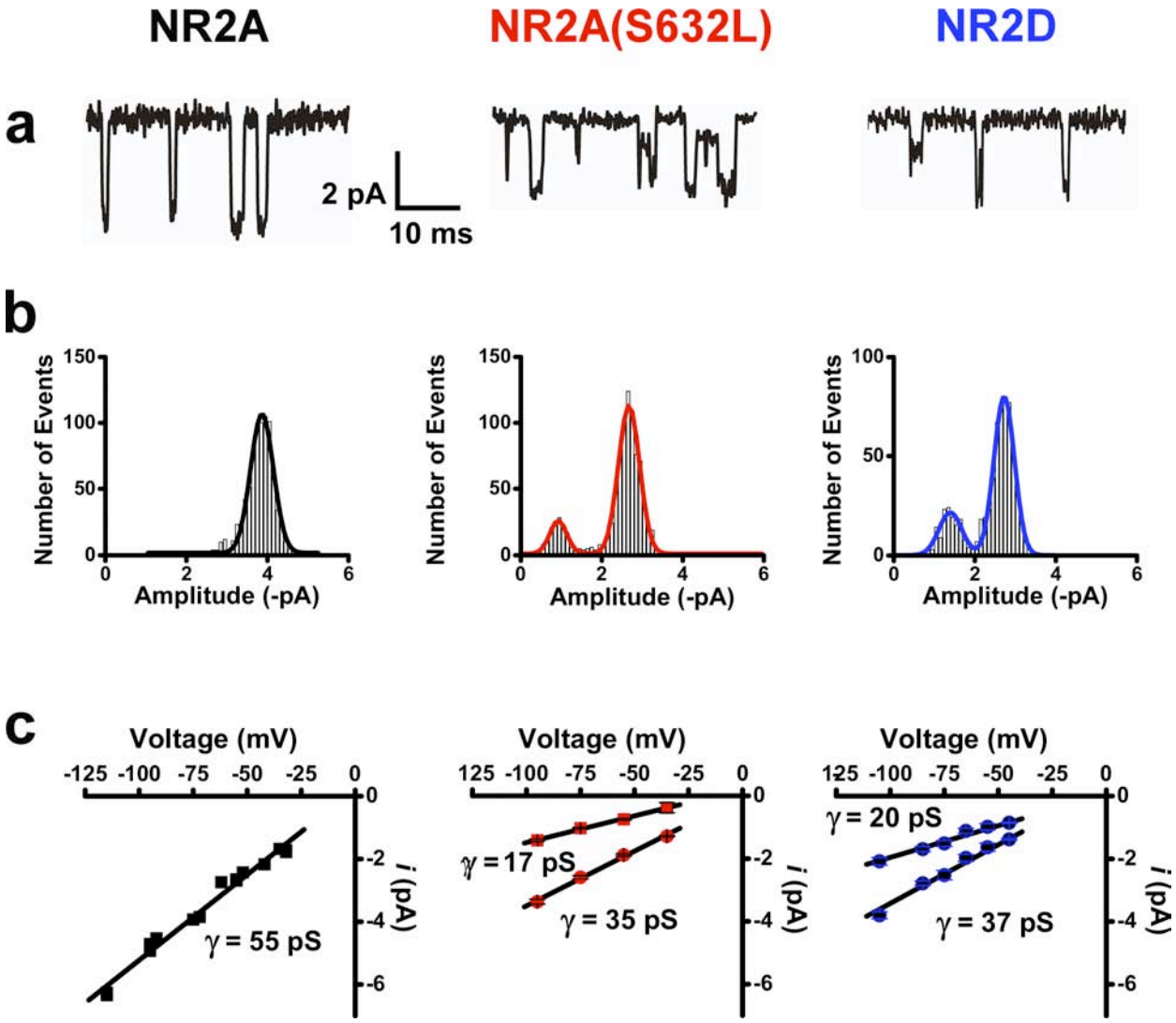

Figure 7 The NR2 S/L site controls the subtype specificity of NMDAR single channel conductance

(**a**) Representative single-channel current traces of NR1/2A (left), NR1/2A(S632L) (center) and NR1/2D (right) receptors recorded in outside-out patch configuration at -75 mV.
(**b**) Representative single-channel current amplitude histograms and fits of NR1/2A receptors (left), NR1/2A(S632L) receptors (center), and NR1/2D receptors (right) at -75 mV.
(**c**) *i*-V plots of single-channel currents and linear regression fits. The slope of the linear fit to each *i*-V plot (single-channel conductance) is shown next to each fit. Left, NR1/2A receptors, (n = 4 patches) center, NR1/2A(S632L) receptors (n = 4 patches), right, NR1/2D receptors. NR1/2D receptor data are from Qian et al. (2005).

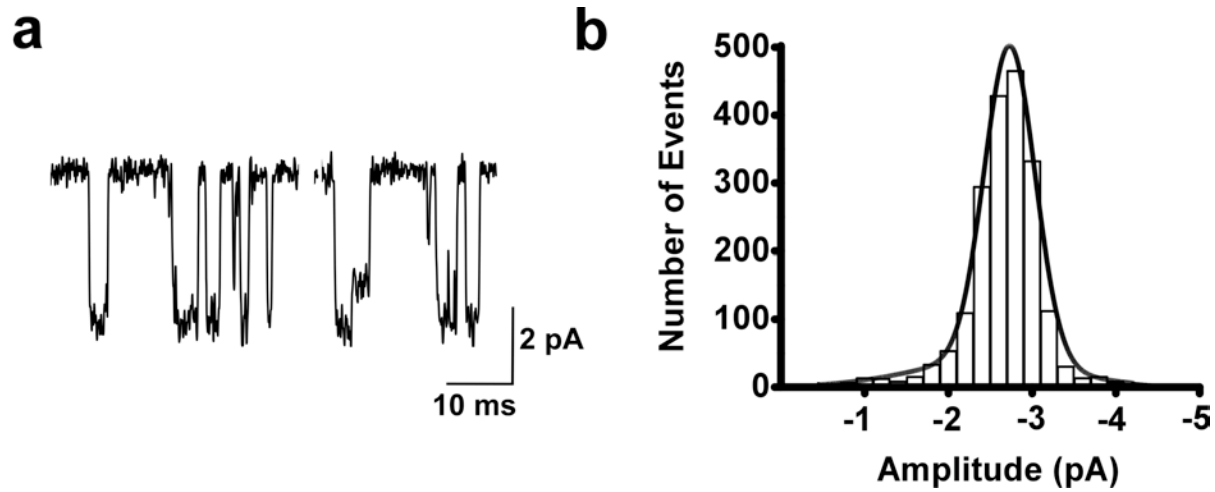

Figure 8 Single-channel conductance of NR1/2A receptors

(**a)** Single-channel current trace demonstrating NR1/2A receptor main- and subconductance states recorded in an outside-out patch recording configuration at -55 mV
(**b**) **S**ingle-channel current amplitude histogram corresponding to the patch from which traces in (**a**) were sampled. The histogram was best fit by two Gaussian distributions, corresponding to mean amplitudes of -2.4 pA and -2.7 pA.

2.4.2 Channel kinetics

As discussed in Section 1.4.2, NMDAR channel kinetics are subtype-specific. NR2 subunit NTDs strongly regulate the variation among NMDAR subtypes of a number of kinetic parameters, including P_{open} and channel open duration (Gielen et al., 2009; Yuan et al., 2009). Although the NTD+L is clearly the primary determinant of subtype-specific variation in these channel properties, other structural influences on NMDAR kinetics must exist. Substitution of the NR2A NTD for the NR2B NTD, for example, does not fully change the open-time phenotype of NR1/2B receptors to that of NR1/2A receptors.

To determine whether the NR2 S/L site affects channel kinetics, I evaluated open periods (the length of time during which the channel is open, regardless of main or sub state occupation) and shut times of NR1/2A and NR1/2A(S632L) receptors, and compared them to those of NR1/2D receptors (Qian et al., 2005). Open period distributions were reliably and adequately fit by two components (τ's) (Figure 9). The mean durations of each NR1/2A receptor open period component were similar to those of NR1/2A(S632L) receptors, but were different from those of NR1/2D receptors (Table 2.1). Moreover, the duration of the largest open period component of NR1/2A(S632L) receptors, 1.72 s, was more similar to the duration of the largest open period component of NR1/2A receptors (2.26 ms) than to that of NR1/2D receptors (0.52 ms).

Examples of shut time distributions are presented in Figure 9. Each shut time distribution was fit with three or four components. As with the open periods, mean NR1/2A(S632L) receptor shut time τ's were more similar to NR1/2A receptors than they were to NR1/2D receptors (Table

2.2) . Thus, the NR2 S/L site appears to affect channel permeation properties more than it affects channel kinetics.

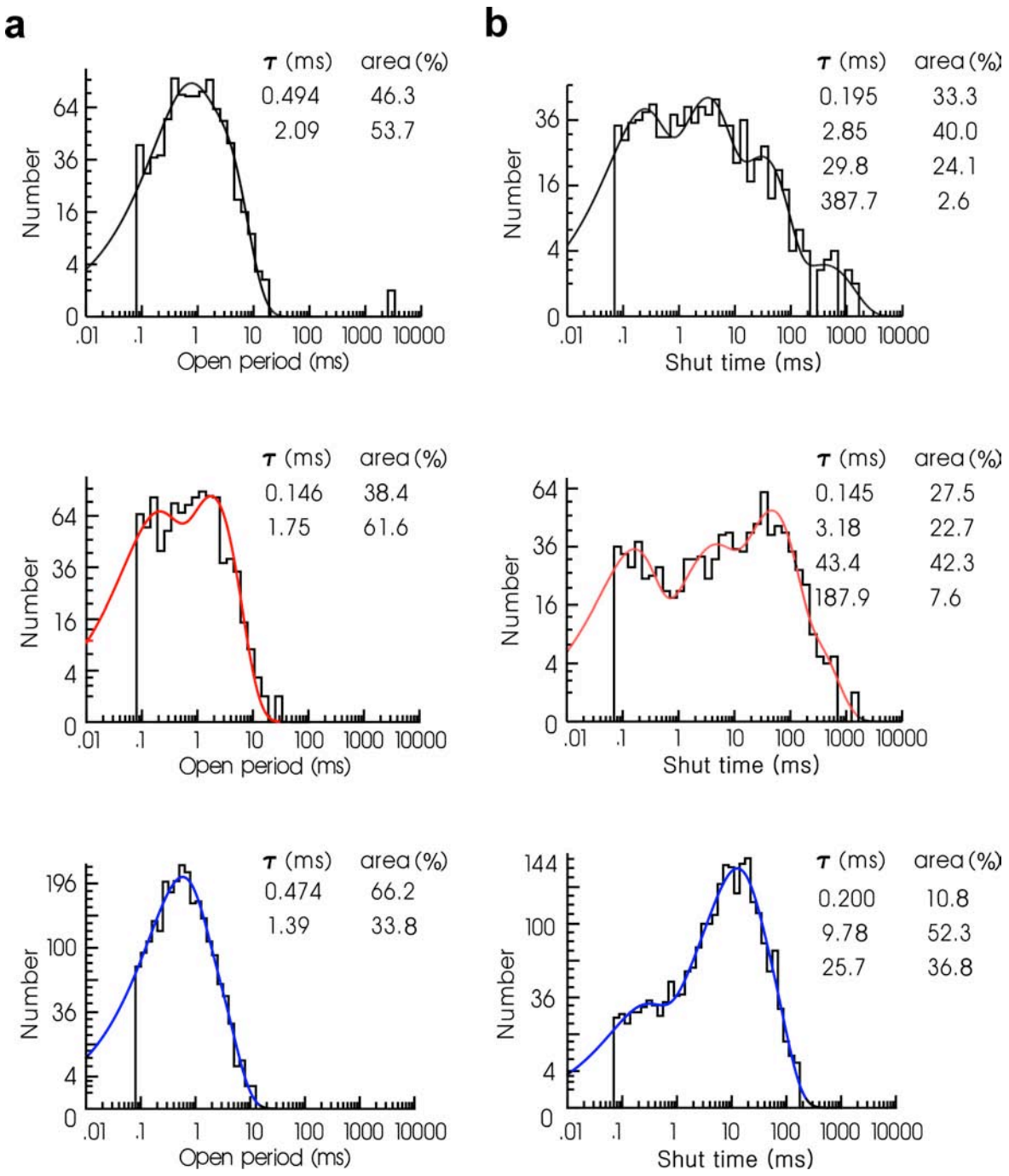

Figure 9 The NR2 S/L site does not strongly affect single-channel kinetics

(**a**) Representative open period distribution histograms derived from outside-out patch recordings of NR1/2A receptors (top, black fits), NR1/2A(S632L) receptors (middle, red fits), and NR2D receptors (bottom, blue fits).
(**b**) Representative shut time distribution histograms derived from the same recordings as in (**a**). NR1/2D receptor data from Qian et al. (2006)

Table 2.1 Effects of the NR2 S/L site on open period distributions

	τ_1, ms (%)	τ_2, ms (%)	Mean of τ's, ms	n
NR1/2A	0.11 (31%)	2.26 (69%)	0.80	3
NR1/2A(S632L)	0.13 (29%)	1.72 (71%)	0.63	3
NR1/2D[2]	0.58 (87%)	1.22 (13%)	0.33	4

Table 2.2 Effects of the NR2 S/L site on shut time distributions

	τ_1, ms (%)	τ_2, ms (%)	τ_3, ms (%)	τ_4, ms (%)	n
NR1/2A	0.21 (23%)	4.9 (33%)	48.1 (39%	537 (4%)	3
NR1/2A(S632L)	0.15 (32%)	2.6 (23%)	36.7 (35%)	233 (10%)	3
NR1/2D[2]	0.14 (18%)	0.85 (5%)	10.1 (37%)	140 (38%)	4

2.5 STRUCTURAL DETERMINANTS OF CALCIUM PERMEABILITY

2.5.1 Variation in Ca^{2+} permeability among NMDAR subtypes

NR1/2A receptors and NR1/2B receptors display similarly high permeabilities to Ca^{2+} (Schneggenburger, 1996), whereas NR1/2C receptors display lower Ca^{2+} permeability than NR1/2A receptors (Burnashev et al., 1992b; Burnashev et al., 1995). There has been no report of NR1/2D receptor Ca^{2+} permeability, and there has been no report of a systematic comparison of Ca^{2+} permeabilities across NMDAR subtypes. Furthermore, the wide variation among studies in the magnitudes of Ca^{2+} permeability of the same NMDAR subtype makes comparison across

[2] NR1/2D receptor data from Qian et al. (2005)

studies challenging. For instance, values of NR1/2A receptor fractional Ca^{2+} current (P_f, the fraction of total current carried by Ca^{2+}) vary from 11% (Burnashev et al., 1995) to 18.5% (Schneggenburger, 1996). Therefore, my goal has been to quantify the relative Ca^{2+} permeabilities of each wild-type diheteromeric NMDAR subtype, as well to test for a role of the NR2 S/L site in determining the subtype specificity of Ca^{2+} permeability.

To assess the relative Ca^{2+} permeabilities of wild-type NMDARs, I measured the V_{rev}s of each NMDAR subtype in biionic conditions, with 152 mM intracellular Cs^+ and either 146 mM extracellular Cs^+, 1.8 mM extracellular Ca^{2+}, or 10 mM extracellular Ca^{2+}. Figure 10a illustrates the voltage-clamp step protocol used to determine V_{rev}s and the resulting current through NR1/2A receptors in 1.8 mM Ca^{2+}. NMDAR-mediated current was quantified by subtracting the averaged baseline current (before and after agonist application) at each voltage from current recorded at each voltage during application of 1 mM glutamate plus 50 μ M glycine. The NMDAR-mediated current was then plotted against voltage (Figure 10b), and V_{rev} was determined to be the point at which the fitted I-V function crossed the x-axis (see Section 2.2).

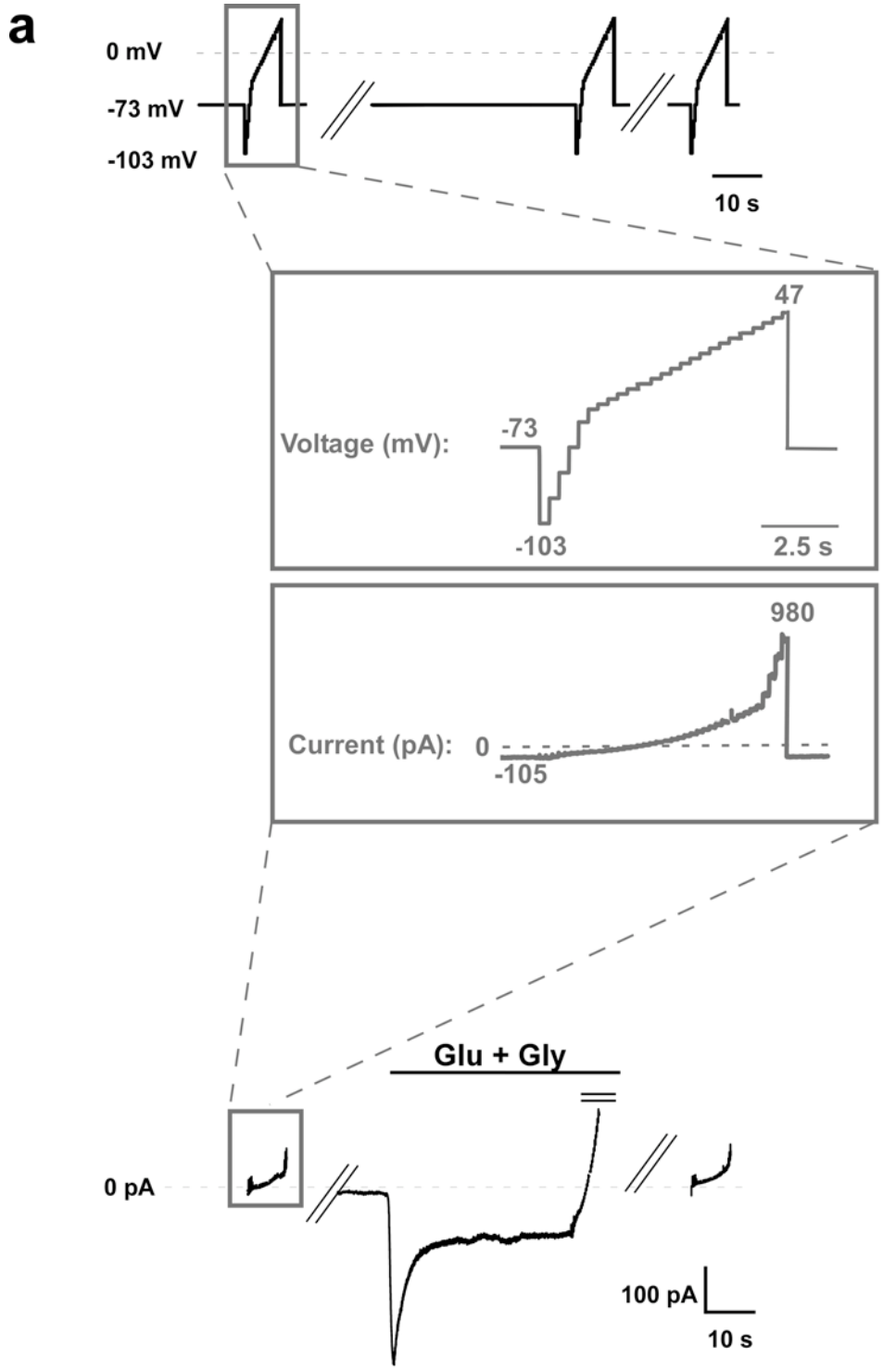

Figure 10 Protocol for V_{rev} determination under biionic conditions

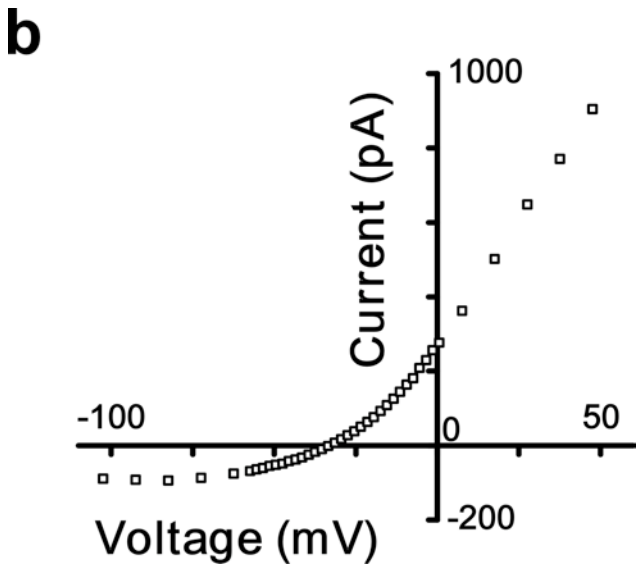

Figure 10 (continued)

(**a**) Voltage command (black trace, top) and resulting current traces (black traces, bottom) from a cell expressing NR1/2A receptors in 1.8 mM extracellular Ca2+. In absence of agonists, the command voltage was held at -73 mV, and then was stepped through a series of voltages from -103 mV to 47 mV). Agonists (glutamate + glycine) were applied for 60 seconds to allow for desensitization, and again the commanded voltage was stepped from -103 mV to 47 mV. The steps were once again commanded after agonist washout. Grey insets, voltage command step protocol (top inset) and currents recorded during this protocol (bottom inset). Outward current larger than 150 pA in the presence of agonists is not shown in the bottom current trace (black), but is depicted in the inset. Note the lack of voltage dependence of current at voltages more negative than -73 mV (plotted in (**b)**).
(**b**) I-V plot of Ca^{2+}-mediated current through NR1/2A receptors, from data presented in (**a**), as well as outward current larger than 150 pA.

Average V_{rev}s in the presence of 146 mM extracellular Cs^+ were similar across NMDAR subtypes (Table 2.3). In both 1.8 mM and 10 mM extracellular Ca^{2+}, however, NR1/2A and NR1/2B receptor V_{rev}s diverged from those of NR1/C and NR1/2D receptors (Table 2.4 and Table 2.5).

NMDAR subtypes displayed a narrow distribution of V_{rev}s derived from individual experiments in 1.8 mM Ca^{2+} (Table 2.4). As expected, the V_{rev}s of NR1/2A and NR1/2B receptors (n = 3 per subtype) were more depolarized than those of NR1/2C receptors (n = 2) and NR1/2D receptors (n = 1). Using averaged V_{rev}s, I determined P_{Ca}/P_{Cs} for each NMDAR subtype in each [Ca^{2+}] with a modified Lewis equation (Equation 3) (Lewis, 1979). P_{Ca}/P_{Cs} values of NR1/2A and NR1/2B receptors in 1.8 mM Ca^{2+} were similar, and each was higher the P_{Ca}/P_{Cs} of NR1/2C receptors (Table 2.6). Based on a sample of one V_{rev} value in 1.8 mM Ca^{2+}, the NR1/2D receptor P_{Ca}/P_{Cs} was also smaller than those of NR1/2A and NR1/2B receptors (Figure 11 and Table 2.1). P_{Ca}/P_{Cs} values were also calculated with ionic activities, rather than concentrations (Table 5.2).

Results in 10 mM extracellular Ca^{2+} revealed a largely similar pattern: NR1/2A receptors and NR1/2B receptors displayed more depolarized V_{rev}s than did NR1/2C receptors (n = 3 per subtype). These results are similar to those of previous reports (Burnashev et al., 1992b; Schneggenburger, 1996; Wollmuth and Sakmann, 1998). Like the distributions of V_{rev}s in 1.8 mM Ca^{2+}, those in 10 mM Ca^{2+} were tightly clustered by NMDAR subtype for NR1/2A, NR1/2B, and NR1/2C receptors. Surprisingly, however, the distribution of V_{rev}s for NR1/2D receptors in 10 mM Ca^{2+} (n = 5) appeared to be bimodal, with two values near the V_{rev}s of

NR1/2C receptors and three values that were even more depolarized than the V_{rev}s of NR1/2A and NR1/2B receptors (Table 2.5).

Table 2.3 NMDA receptor reversal potentials in 146 mM Cs^+

NMDAR Subtype	Mean V_{rev}	Range	n
NR1/2A	-6.0 mV	(-6.4 mV) - (-5.7 mV)	2
NR1/2B	-4.6 mV	(-4.6 mV)	1
NR1/2C	-6.0 mV	(-6.0 mV)	1
NR1/2D	-5.3 mV	(-6.5 mV) - (-4.5 mV)	5
NR1/2A(S632L)	-4.4 mV	(-5.5 mV) - (-3.7 mV)	3

Table 2.4 NMDA receptor reversal potentials in 1.8 mM Ca^{2+}

NMDAR Subtype	Mean V_{rev}	Range	n
NR1/2A	-35.1 mV	(-37.9 mV) - (-32.6 mV)	3
NR1/2B	-35.2 mV	(-35.9 mV) - (-34.0 mV)	3
NR1/2C	-42.0 mV	(-42.4 mV) - (-41.5 mV)	2
NR1/2D	-47.7 mV	(-47.7 mV)	1
NR1/2A(S632L)	-40.4 mV	(-41.5 mV) - (-39.3 mV)	2

Table 2.5 NMDA receptor reversal potentials in 10 mM Ca^{2+}

NMDAR Subtype	Mean V_{rev}	Range	n
NR1/2A	-12.6 mV	(-13.7 mV) - (-11.7 mV)	3
NR1/2B	-9.7 mV	(-12.0 mV) - (-8.5 mV)	3
NR1/2C	-20.0 mV	(-21.7 mV) - (-18.2 mV)	3
NR1/2D (low)	-15.6 mV	(-18.3 mV) - (-12.9 mV)	2
NR1/2D (high)	-2.5 mV	(-3.7 mV) - (-1.5 mV)	3
NR1/2A(S632L)	-15.7 mV	(-16.7 mV) - (-14.5 mV)	3

Table 2.6 NMDAR subtype dependence of P_{Ca}/P_{Cs}

NMDAR Subtype	$[Ca^{2+}]$ (mM)	P_{Ca}/P_{Cs}
NR1/2A	1.8	7.7
NR1/2B	1.8	7.3
NR1/2C	1.8	5.6
NR1/2D	1.8	4.2
NR1/2A(S632L)	1.8	5.9
NR1/2A	10	4.5
NR1/2B	10	5.0
NR1/2C	10	3.1
NR1/2D ("low permeability")	10	3.7
NR1/2D ("high permeability")	10	7.8
NR1/2A(S632L)	10	3.6

P_{Ca}/P_{Cs} values were calculated using ion concentrations, rather than activities (see Appendix C, Table 5.2 for values calculated using ion activities).

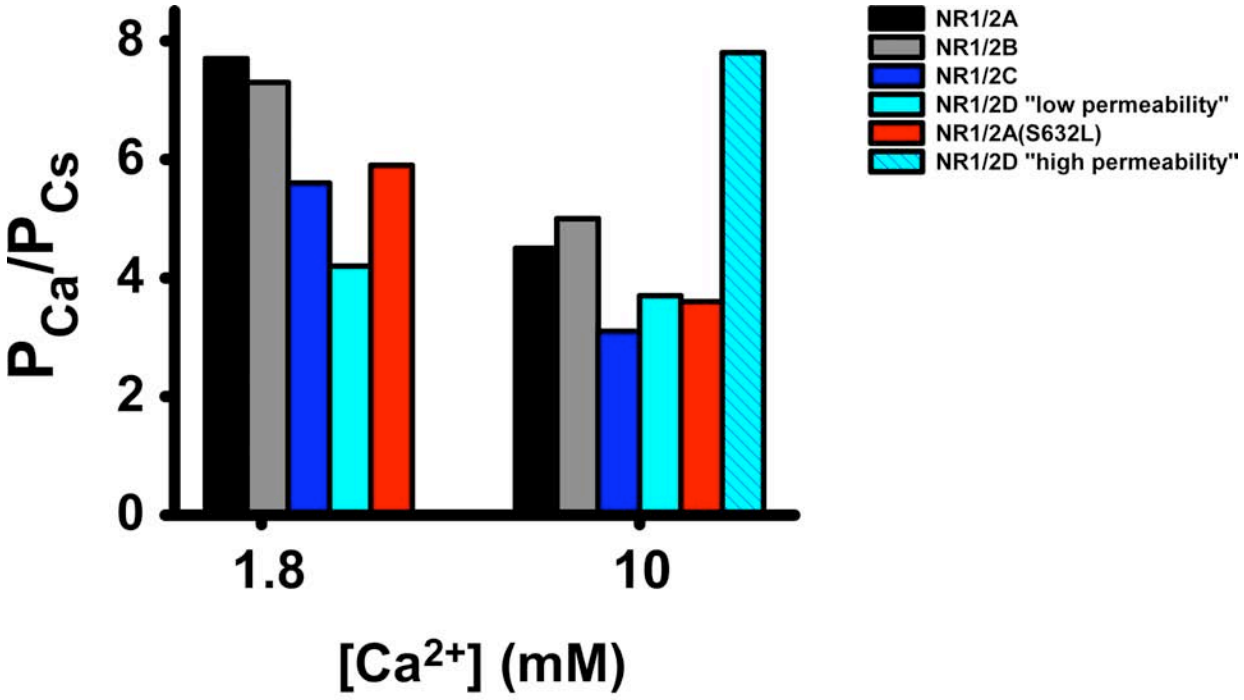

Figure 11 NMDAR subtype-dependence of P_{Ca}/P_{Cs} and influence of the NR2 S/L site on Ca^{2+} permeability

Graph of P_{Ca}/P_{Cs} versus NMDAR subtype in 1.8 mM and 10 mM Ca^{2+}. NR1/2D receptor data are split into two groups: "low-permeability" NR1/2D receptors and "high-permeability" NR1/2D receptors (see text). More data are required to determine whether actual distribution of NR1/2D receptor V_{rev}s is bimodal.

Consistent with a previous study (Wollmuth and Sakmann, 1998), the P_{Ca}/P_{Cs} value of each NMDAR subtype in 10 mM Ca^{2+} was lower than the P_{Ca}/P_{Cs} value in 1.8 mM Ca^{2+}. NR1/2A and NR1/2B receptor P_{Ca}/P_{Cs} values were similar to each other, whereas the NR1/2C receptor P_{Ca}/P_{Cs} was lower (Figure 11 and Table 2.6). I calculated two provisional P_{Ca}/P_{Cs} values for NR1/2D receptors in 10 mM Ca^{2+}, due to the apparent bimodal nature of the NR1/2D receptor V_{rev} distribution (Table 2.5 and Table 2.6). The P_{Ca}/P_{Cs} of "low-permeability" NR1/2D receptors was similar to that of NR1/2C receptors, whereas the P_{Ca}/P_{Cs} of "high-permeability NR1/2D receptors" was higher even than those of NR1/2A or NR1/2B receptors (Figure 11 and Table 2.6). These surprising results indicates that, under certain conditions, NR1/2D receptors might be far more permeable to Ca^{2+} than any other NMDAR subtype. Due to small sample sizes (Table 2.5), however, no firm conclusions regarding the relative permeability to Ca^{2+} of NR1/2D receptors can be drawn.

2.5.2 Influence of the NR2 S/L Site on Ca^{2+} permeability of NMDARs

Because the NR2 S/L site regulates the subtype specificity of other channel permeability properties (see Sections 2.4 and 2.4), I hypothesized that it also influences the subtype specificity of Ca^{2+} permeability. Therefore, I assessed P_{Ca}/P_{Cs} of NR1/2A(S632L) receptors in the same manner as that described for the evaluation of wild-type receptor P_{Ca}/P_{Cs}'s.

As with NR1/2A, NR1/2B, and NR1/2C receptors, measured NR1/2A(S632L) receptor V_{rev}s were tightly distributed. NR1/2A(S632L) receptor V_{rev}s in 1.8 mM Ca^{2+} (n = 2) were strikingly similar to NR1/2C receptor V_{rev}s, but more depolarized than that of NR1/2D receptors (Table 2.4). P_{Ca}/P_{Cs} of NR1/2A(S632L) receptors was 5.9 (Figure 11), decreased 86% from the

P_{Ca}/P_{Cs} of NR1/2A receptors toward that of NR1/2C receptors (Equation 4) and 51% toward that of NR1/2D receptors (Equation 5).

In 10 mM Ca^{2+}, NR1/2A(S632L) receptor V_{rev}s (n = 3) were again tightly clustered, with an average value similar to the "low-permeability" NR1/2D receptor average V_{rev} and roughly halfway between the NR1/2C receptor average V_{rev} and those of NR1/2A and NR1/2B receptors (Table 2.5). Like wild-type NMDARs, NR2(S632L) receptor relative permeability to Ca^{2+} decreased when [Ca^{2+}] increased; P_{Ca}/P_{Cs} of NR1/2A(S632L) receptors in 10 mM Ca^{2+} was 3.6 (Figure 11). This value reflects a 64% decrease, from the NR1/2A receptor P_{Ca}/P_{Cs} toward the NR1/2C receptor P_{Ca}/P_{Cs} (Equation 4) and a 112% decrease from the NR1/2A receptor P_{Ca}/P_{Cs} toward the P_{Ca}/P_{Cs} of the putative "low-permeability" NR1/2D receptors (Equation 5). Based on the these provisional calculations, the NR2 S/L site may therefore account for 88% of the subtype specificity of relative Ca^{2+} permeability among NMDARs (averaged percent decrease of NR1/2A(S632L) receptor P_{Ca}/P_{Cs}, from the N1/2A receptor P_{Ca}/P_{Cs} toward the NR1/2C or the "low-permeability" NR1/2D receptor P_{Ca}/P_{Cs} (see Methods, Section 2.2)).

2.6 DISCUSSION

Based on the results of this study and recent previous work, the spectrum of NMDAR subtype-dependent properties can be divided into two clusters. One cluster of properties is related to channel gating and binding of ligands that control gating, and includes maximal channel open probability, pH sensitivity, Zn^{2+} inhibition, agonist potency, and deactivation kinetics. The NMDAR subtype dependence of this gating property cluster depends principally on a large region distant from the NR2 S/L site: the NTD+L region (Gielen et al., 2009; Yuan et

al., 2009). We demonstrate here that the NMDAR subtype dependence of a second cluster, properties of the open channel, depends, in contrast, on a single amino acid difference in the M3 transmembrane region. Together, differences in and near the NTD and at the NR2 S/L site underlie the great majority of functional variation among NMDAR subtypes.

The NR2 S/L site powerfully regulates ion permeation of the NMDAR channel, as demonstrated by its effects on single-channel conductance states and Ca^{2+} permeability. The influence of the NR2 S/L site on Mg^{2+} block also may be mediated by an effect on ion permeation; the single greatest difference between the kinetics of Mg^{2+} block of NR1/2A and NR1/2D receptors is an enhanced rate of Mg^{2+} permeation through NR1/2D receptors (Qian et al., 2005; Qian and Johnson, 2006). The NR2 S/L site, situated near the intracellular end of the pore (Figure 3), appears to be well-located to affect ion permeation. The extent to which the NR2 S/L site affects Mg^{2+} IC_{50}, however, decreases as voltage becomes more negative, in both NR1/2D(L654S) and NR1/2A(S632L) receptors (Figure 6). Furthermore, the interactions between the NR2 S/L site and NR1(W608) that shape Mg^{2+} IC_{50} appear to become less pronounced as voltage becomes more negative (Figure 19). Because Mg^{2+} permeates the pore more frequently at hyperpolarized voltages, these observations suggest that the NR2 S/L site may affect Mg^{2+} IC_{50} in a manner that does not involve changes in Mg^{2+} permeation. One possibility is that the NR2 S/L site contributes to subtype-specific properties of an internal permeant ion binding site, which is known to affect channel block by Mg^{2+} in a subtype-specific manner (Antonov et al., 1998; Antonov and Johnson, 1999; Qian et al., 2002; Qian and Johnson, 2006; Zhu and Auerbach, 2001a).

The subtype dependence of channel block by Mg^{2+} is not solely determined by the NR2 S/L site. This is clear from Mg^{2+} IC_{50} measurements of NR1/2D(L654S) receptors, in which

mutation of the NR2 S/L site accounted for most, but not all, of the difference in Mg^{2+} IC_{50}s between NR1/2A and NR1/2D receptors (Figure 6**)**. Furthermore, previous studies have implicated both other transmembrane regions and the ABD in regulating the NMDAR subtype dependence of Mg^{2+} block (Kuner and Schoepfer, 1996; Wrighton et al., 2008). In a series of experiments related to those presented here, Kuner and Schoepfer (1996) assayed Mg^{2+} block of NR1/2C receptors in which the NR2C subunit was modified to contain parts of the NR2B subunit. They found that sections of NR2 subunits in or near the transmembrane domain, including M3, strongly influenced the NR2 subtype dependence of Mg^{2+} IC_{50}. The authors noted that receptors containing an NR2C subunit with a leucine-to-serine substitution at the NR2 S/L site exhibited increased voltage dependence of Mg^{2+} block, similar to that of NR1/2B receptors, but no change in Mg^{2+} IC_{50} at -100 mV. In contrast, our experiments showed that the NR1/2D(L654S) receptor Mg^{2+} IC_{50} at a similar voltage (-95 mV) was significantly higher than the wild-type Mg^{2+} IC_{50}. Furthermore, we noted no change in the voltage dependence of channel block by Mg^{2+} between NR1/2D and NR1/2D(L654S) receptors. Indeed, the voltage dependence of Mg^{2+} IC_{50} did not differ among the wild-type receptors we examined. The apparent discord with our findings may stem from the different preparations used: Kuner and Schoepfer (1996) recorded from Xenopus oocytes, which resulted in multiple differences in experimental conditions compared to those of the study presented here, including permeant ion concentrations, which can strongly affect Mg^{2+} block (Antonov and Johnson, 1999; Qian et al., 2002; Schoepfer et al., 1994; Zhu and Auerbach, 2001a, b). Hence, differences between the internal solution of oocytes and the intracellular solutions used for whole-cell recordings in HEK cells may contribute to disparities between results presented here and those in Kuner and Schoepfer (1996).

Variation in Ca^{2+} permeability among NMDAR subtypes has been less well-characterized than variation in channel block by Mg^{2+}. Results presented here represent preliminary results of the first systematic study of Ca^{2+} permeability across all four diheteromeric NMDAR subtypes, as well as the first report of NR1/2D receptor permeability to Ca^{2+}. Although sample sizes must be increased before statistical analyses of P_{Ca}/P_{Cs}'s can be performed, the emerging results suggest both expected and unexpected scenarios. As predicted based on prior studies (Burnashev et al., 1992b; Burnashev et al., 1995; Schneggenburger, 1996, 1998; Wollmuth and Sakmann, 1998), NR1/2A and NR1/2B receptor relative permeabilities of Ca^{2+} were found to be quite similar to each other, and higher than the relative permeability of Ca^{2+} to NR1/2C receptors. Due to the grouping of open-channel properties into similar NR1/2A and NR1/2B receptor properties, versus similar NR1/2C and NR1/2D receptors, I hypothesized that NR1/2D receptors would evidence a Ca^{2+} permeability similar to that of NR1/2C receptors. Results of this study support this hypothesis: in 1.8 mM Ca^{2+}, P_{Ca}/P_{Cs} of NR1/2D receptors is similar to that of NR1/2C receptors, and in 10 mM Ca^{2+}, the "low-permeability" NR1/2D receptor cluster of V_{rev}s yields a P_{Ca}/P_{Cs} value that is very close to that of NR1/2C receptors. Surprisingly, a second apparent cluster of NR1/2D V_{rev}s emerged in 10 mM Ca^{2+}, which led to a P_{Ca}/P_{Cs} value that far exceeded those of NR1/2A and NR1/2B receptors. Because of the low sample size of NR1/2D V_{rev}s in 1.8 mM (n = 1), I was unable to explore the distribution of NR1/2D receptor V_{rev}s in 1.8 mM Ca^{2+}. More data must be gathered before any conclusions are formed about the permeability to Ca^{2+} of NR1/2D receptors.

Neuronal NMDARs display a wide range of Ca^{2+} permeabilities, even within one subtype. The P_fs of NMDARs in individual spines of hippocampal pyramidal neurons were demonstrated to vary by a factor of 10; half of this variation was due to variation in Ca^{2+}

permeation through NR1/2B receptors (Sobczyk et al., 2005). This variation may be due to modifications at a number of phosphorylation and glycosylation sites (Traynelis et al., 2010). For example, phosphorylation of the NMDAR CTD by protein kinase A has been reported to increase the Ca^{2+} permeability of NMDARs (Skeberdis et al., 2006). Variation in the phosphorylation state of NR1/2D receptors may contribute to the variation in NR1/2D V_{rev}s reported here. Alternatively, the apparent bimodal nature of the NR1/2D V_{rev} distribution (Table 2.5) may be artifactual, arising from variation in experimental conditions. I believe that this is unlikely, however, because two of the divergent NR1/2D V_{rev}s in 10 mM Ca^{2+} were derived from experiments conducted less than two hours apart (V_{rev} = -2.5 mV and V_{rev} = -13.2 mV). These cells derived from the same split of cells and were therefore plated at the same time. They had undergone the same transfection and were bathed in the same solutions during whole-cell recording. The sole disparity that I observed was that the coverslips onto which the two cells had been plated rested in different petri dishes during cell growth and transfection.

Research presented in Section 2.5 permit a preliminary comparison of relative Ca^{2+} permeabilities across diheteromeric NMDAR subtypes. The P_{Ca}/P_{Cs} values reported here are higher than have previously been reported. For instance, P_{Ca}/P_{Cs} of NR1/2A receptors has been measured at about 5.7 and 6.4 in similar experiments (under biionic conditions, in 1.8 mM extracellular Ca^{2+}, at 21˚ C - 23˚ C, calculated without activity coefficients) (Jatzke et al., 2002; Watanabe et al., 2002), whereas my preliminary measurement is higher (7.7, Figure 11). My sample sizes are small, however, so more data are needed to make a fair comparison of my results to those of other groups. Furthermore, the variation between the P_{Ca}/P_{Cs} of NR1/2A receptors reported here and values reported elsewhere is well within the variation between studies in NMDAR Ca^{2+} permeability values quantified in another manner (P_f, fractional Ca^{2+}

current; discussed below). The NR1/2A receptor P_{Ca}/P_{Cs} value here, compared to the most different P_{Ca}/P_{Cs} value reported in other studies (Wollmuth and Sakmann, 1998), varies a factor of 1.4, whereas NR1/2A P_f values vary by factors of 1.2 - 1.7 (Jatzke et al., 2002; Schneggenburger, 1996; Wollmuth and Sakmann, 1998).

The calcium permeability of NMDARs has been assessed in several manners, each of which has unique advantages. To determine the percent of NMDAR-mediated current that is carried by Ca^{2+} ions (P_f), some groups have quantified Ca^{2+} influx with an indicator dye while voltage-clamping the cell to measure total current influx (Jatzke et al., 2002; Schneggenburger, 1996). P_f measurements are made in the presence of both mono- and divalent cations, and thus assess Ca^{2+} permeability under more physiological conditions than P_{Ca}/P_{Cs} measurements in biionic conditions. Because interactions of permeant ions with NMDARs at one binding site can modulate the interactions of permeant ions with NMDARs at a different binding site (Antonov and Johnson, 1999; Zhu and Auerbach, 2001a, b), assessing Ca^{2+} permeability in the presence of several ion species provides useful information (Burnashev et al., 1995). Indeed, the relative permeability of Ca^{2+} to NMDARs is strongly affected by the presence or absence of other ion species (Jatzke et al., 2002). P_{Ca}/P_{Cs} measurements performed in biionic conditions convey different information, assessing the relative ease with which ions permeate the pore in absence of NMDAR interactions with other ion species (Schneggenburger, 1996; Wollmuth and Sakmann, 1998). P_{Ca}/P_{Cs} measurements performed in the presence of mono- and divalent cations convey yet another type of information.

Jatzke et al. (2002) argued that P_f measurements provide the most useful information, and that P_{Ca}/P_{Cs} measurements made in the presence of both mono- and divalent cations contain more useful information than measurements made under biionic conditions (Jatzke et al., 2002). The

presence of multiple permeant ion species in the external solution, however, can obscure some channel interactions with ions. For example, the concentration dependence of relative Ca^{2+} permeability, likely due to channel block by Ca^{2+}, was noted in biionic experiments conducted by Jatzke et al. (2003), but this phenomenon was not observed in similar experiments when monovalent ions were included in the extracellular solution. Hence, each method of quantifying Ca^{2+} permeation through NMDARs is likely to yield interesting information.

To my knowledge, this study is the first to identify a structural basis of NMDAR subtype-dependent variation in single-channel conductance, as well as the first study to examine structural determinants of subtype-specific Ca^{2+} permeability. Results presented here demonstrate the critical role of the NR2 S/L site in forming the subtype specificity of these fundamental open-channel properties.

3.0 STRUCTURAL MODELS OF NMDARS

3.1 INTRODUCTION

Although biochemical and electrophysiological experiments provide a wealth of information regarding protein structure, the level of detail that can be discerned from these type of studies is limited. More extensive structural information can be gleaned from examination of the crystal structures of a protein. Furthermore, predictions based on crystallized protein structures, coupled with experimental testing of these predictions, often provide insight into structural mechanisms of protein function (Doyle et al., 1998; Sobolevsky et al., 2009).

Creating iGluR crystals and solving their structures has proven difficult. In the absence of an iGluR crystal structure, previous studies have relied on molecular models to generate hypotheses regarding iGluR structure and function (Tikhonov et al., 1999; Wood et al., 1995). Several lines of evidence suggest that mammalian iGluRs are evolutionarily related to prokaryotic ion channels, on which many iGluR models are based. Like iGluRs, bacterial cyclic nucleotide-gated (CNG) and voltage-gated Na^+, K^+, and Ca^{2+} channels are tetrameric or pseudo-tetrameric and contain a reentrant loop that forms the selectivity filter of channel (Heinemann et al., 1992; MacKinnon, 1995; Rosenmund et al., 1998; Wood et al., 1995).

The structure of the iGluR M2-M3 region is similar to homologous sections of prokaryotic CNG- and voltage--gated channels, while iGluR ABDs and NTDs are structurally

similar to prokaryotic amino acid binding proteins (Jan and Jan, 1992; Mayer et al., 2001; Panchenko et al., 2001; Tikhonov, 2007). Perhaps the strongest evidence for an evolutionary relationship between mammalian iGluRs and K^+ channels stems from studies on GluR0, a bacterial glutamate receptor with a K^+-selective ion channel. The GluR0 ABD shares roughly 20% sequence identity with mammalian iGluRs, and 20% sequence identity with GlnBP, the prokaryotic glutamine binding protein (though sequence identity between all three is merely 4% (Mayer et al., 2001)). Furthermore, the crystal structure of the GluR0 ABD is strikingly similar to the structures of the GluA2 and bacterial periplasmatic amino acid binding proteins (Mayer et al., 2001). The GluR0 pore loop and subsequent transmembrane α-helix share 41% sequence identity with the homologous region of the tetrameric KcsA channel and 44% homology with the homologous region of the *rattus* GluA2 subunit (Chen et al., 1999). The high conservation among these proteins of both sequence and structure provides strong support for the hypothesis that iGluRs are derived from the ancient insertion of DNA encoding a K^+ channel into DNA encoding a periplasmatic amino acid binding protein (Tikhonov and Magazanik, 2009). Thus, a wealth of evidence indicates that mammalian iGluRs are evolutionarily related to bacterial K^+ channels (and, by extension, bacterial CNG channels, which are related to K^+ channels (Jan and Jan, 1990)).

The structural homology of iGluRs and voltage- and CNG-gated ion channels, as well as their evolutionary link, make prokaryotic ion channels good candidates for templates with which structural models of iGluRs can be created. Structural homology modeling has been used successfully by several groups to predict iGluR structure and its functional implications (Panchenko et al., 2001; Tikhonov, 2007; Wood et al., 1995).

I used structural homology modeling to predict ways in which the NR2 S/L site might influence the pore. The NR2 S/L site is unlikely to interact with permeant and blocking ions directly, due to its location at the base of the M3 region (Figure 3c). I therefore hypothesized that the NR2 S/L site exerts its influence over Mg^{2+} block, single-channel conductance, and Ca^{2+} permeability through interactions with amino acid residues that are closer to the pore. Models were created based on the crystal structures of three channels: the prokaryotic KcsA channel, the prokaryotic NaK channel, and the eukaryotic GluA2 AMPAR channel. KcsA and NaK channel-based models yielded similar predictions regarding which residues might interact with the NR2 S/L site, whereas the GluA2 receptor-based model yielded a different prediction.

3.2 METHODS

Structural modeling. Templates on which to base models were selected to represent a variety of tetrameric ion channel structures that NMDARs might resemble. For KcsA channel- and NaK channel-based models, sequence alignments were performed by hand, first by aligning the selectivity filters, and then by placing emphasis on aligning: (a) predicted NMDAR transmembrane domains (Beck et al., 1999; Kuner et al., 1996; Sobolevsky et al., 2002a; Wollmuth and Sobolevsky, 2004) with the transmembrane domains of the templates, and (b) conserved residues (Chiu et al., 1999; Chiu et al., 2002) with each other (Figure 13c and Figure 15c). The sequence alignment for the GluA2 receptor-based model is from Sobolevsky et al. (2009) (Figure 17b).

The structural homology modeling program Modeller (Eswar et al., 2007) (versions 8.2 and 9.7) was used to create 200 energetically-plausible conformations of the M2-M3 region of the NMDA receptor, based on homologous regions of: (a) the crystalized NaK channel bound with K^+ and Ca^{2+} ions (PBD ID 2AHZ), and (b) the crystalized KcsA channel bound with K^+ ions (PDB ID 1BL8). The same method was used to create 50 models of the entire NMDA receptor minus the C-terminal domain, based on the crystalized GluA2 receptor (PDB ID 3KG2). For each template, the five models with the lowest DOPE (discrete optimized protein energy) scores were viewed. Predictions and hypotheses were based on the most commonly-observed configuration among the five lowest-energy models of the interface between the NR2 S/L site and NR1 subunit residues. The molecular visualization programs RasTop (version 2.1) and VMD (version 1.8.7) were used to view wild-type and mutant NMDAR models and to generate Figure 14, Figure 16 and Figure 18.

3.3 NMDAR CHANNEL MODEL BASED ON THE KCSA CHANNEL

Each KcsA channel subunit is composed of 160 residues that form an intracellular carboxy terminal, two transmembrane domains, a re-entrant loop located toward the extracellular aspect, and an intracellular amino terminal (Gulbis and Doyle, 2004) (Figure 13a). As with iGluRs, the reentrant loops of four subunits form the narrow selectivity filter. Each subunit contributes to the filter a five amino-acid motif, with the backbone carbonyl oxygens of each residue facing into the pore (Zhou et al., 2001). These carbonyl oxygens replace the waters of hydration surrounding K^+ ions to coordinate ion movement through the selectivity filter (Doyle et al., 1998). Smaller Na^+ ions do not bind the all of the carbonyl oxygens of the KcsA

selectivity filter; indeed, rather than binding Na^+ in a low [K^+]/high [Na^+] solution, the KcsA channel will instead enter a non-conductive state in which the filter is collapsed (Lockless et al., 2007). K^+ ions pass through the selectivity filter of the KcsA channel in a single-file manner (Doyle et al., 1998), similar to predicted ion movement through NMDAR channels (Jahr and Stevens, 1993; Zarei and Dani, 1994).

The NR1/2A receptor channel model presented here is limited to the M2-M3 region of the protein, as this region displays the highest structural homology to K^+ channels (Panchenko et al., 2001; Tikhonov et al., 2002; Wood et al., 1995) I arranged the NMDAR subunits in an NR1-2A-1-2A assembly around the pore, due to the known propensity of oligomers for structural symmetry and simplicity (Goodsell and Olson, 2000): whereas an NR1-2A-1-2A subunit assembly requires just one type of interface between NR1 and NR2 subunits, an NR1-1-2A-2A subunit assembly would require two different interfaces (Figure 12). Moreover, recent evidence indicates that recombinant NMDARs adopt this arrangement (Sobolevsky et al., 2009).

The KcsA channel-based NMDAR model is presented in Figure 13b and Figure 14. Visualization of space-filling residues near the NR2 S/L site suggests that the NR2 S/L site might interact directly with two NR1 tryptophans in the p-loop helix: NR1(W608) and NR1(W611) (Figure 14c-e). Both of these tryptophans are near the selectivity filter; thus, a putative interaction between the NR2 S/L site and an NR1 residue in the p-loop might affect the pore-lining region in a manner that influences open channel properties.

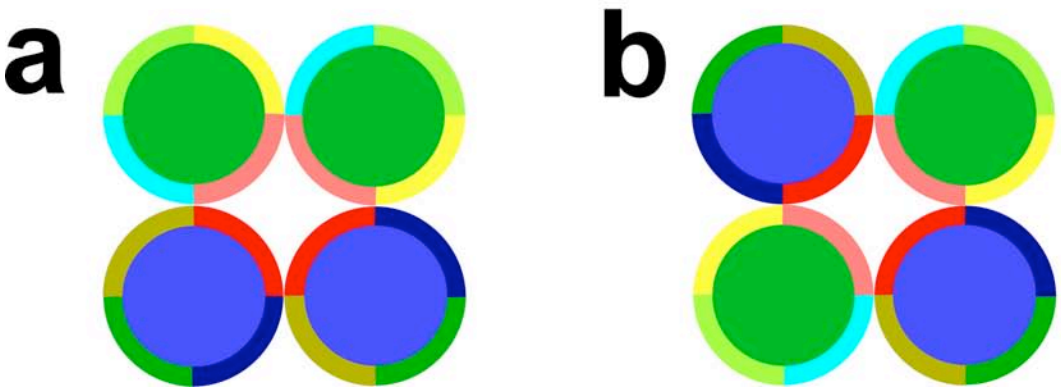

Figure 12 NMDA receptor subunit arrangement around the pore

Green circles, NR1 subunits; blue circles, NR2 subunits. Perimeters of each subunit are colored to aid in orienting each subunit. Red segments, p-loop regions.
(**a**) In an NR1-1-2-2 conformation around the pore, two types of NR1-NR2 subunit interfaces exist: the light blue segment of NR1 interfaces with the dark yellow segment of NR2 (left), and the light yellow segment of NR1 interacts with the dark blue segment of NR2 (right).
(**b**) In an NR1-2A-1-2A arrangement around the pore, the dark blue segment of both NR1 subunits interacts with the light yellow segment of both NR2 subunits.

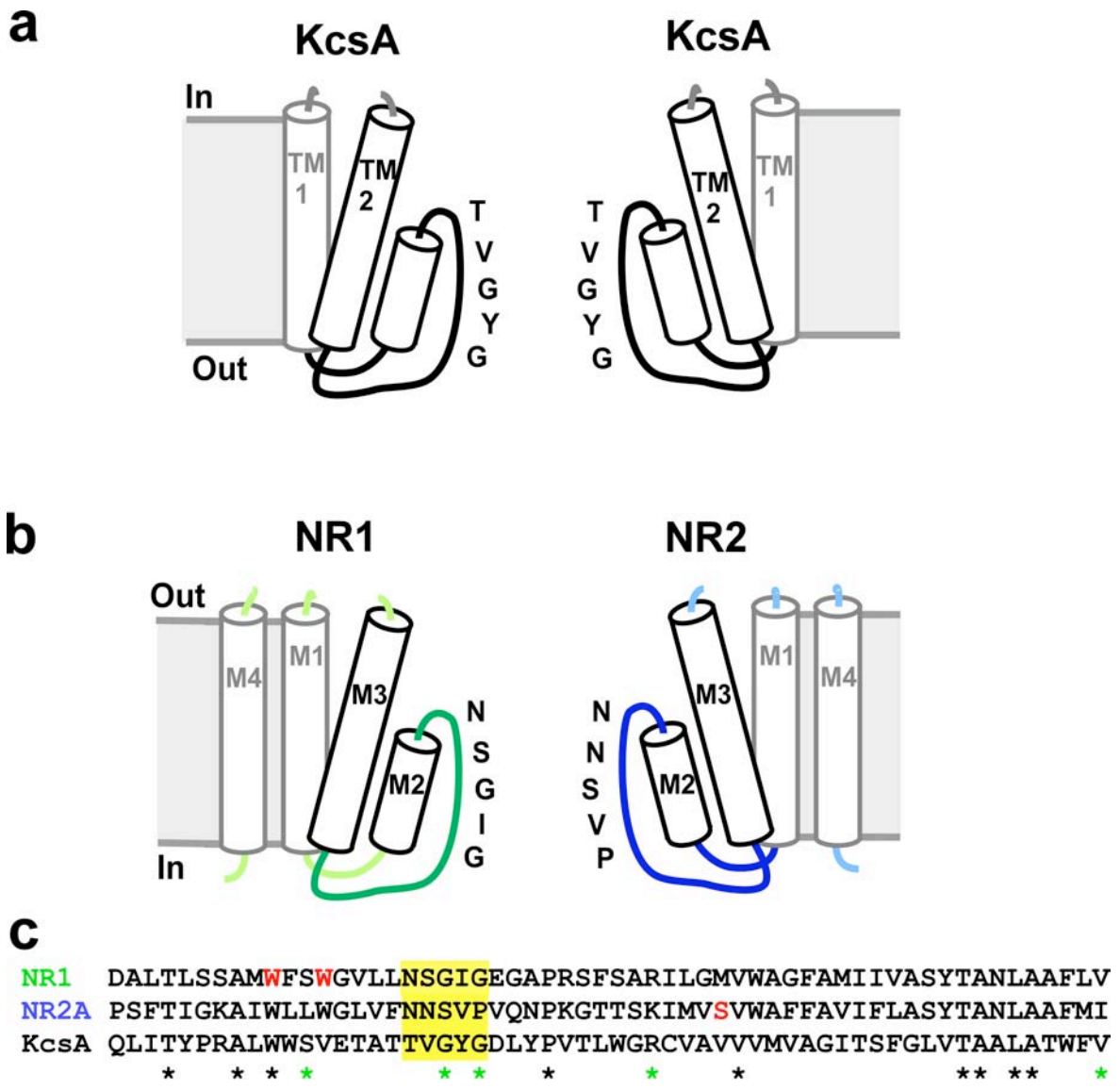

Figure 13 Transmembrane topologies and sequence alignments of KcsA channel and NMDAR subunits

(**a**) Depiction of the transmembrane topology of the crystallized KcsA channel. The structure of the inner helix, TM2, and adjacent p-loop (black lines and outlines) was used as a template on which to base a homology model of the NMDAR channel. The outer helix (TM1, grey outline) was not included in the template. Residues lining the selectivity filter are labeled.

(**a**) Depiction of the transmembrane topology of the NMDAR model based on the KcsA channel. For clarity, only two subunits in the tetramer are depicted; this does not represent subunit arrangement around the pore. The model included the M2-M3 region (black outlines, dark green (NR1) lines and dark blue (NR2A) lines), whereas M1 and M4 regions (grey outlines) were excluded from the model due to lack of homology to the KcsA channel. Residues lining the NR1 and NR2 subunit selectivity filters are labeled.

(**c**) Amino acid sequence alignment of NR1 and NR2A subunit M2-M3 regions, and the homologous region of the KcsA channel subunit. No gaps were inserted into the alignment. Highlighted segments, selectivity filter residues. The NR2 S/L site, NR1(W608), and NR1(W611) are in red font. Asterisks denote residue conservation among all subunits (black) and between NR1 and KcsA subunits (green). None of the residues in this region are unique to KcsA and NR2A subunits.

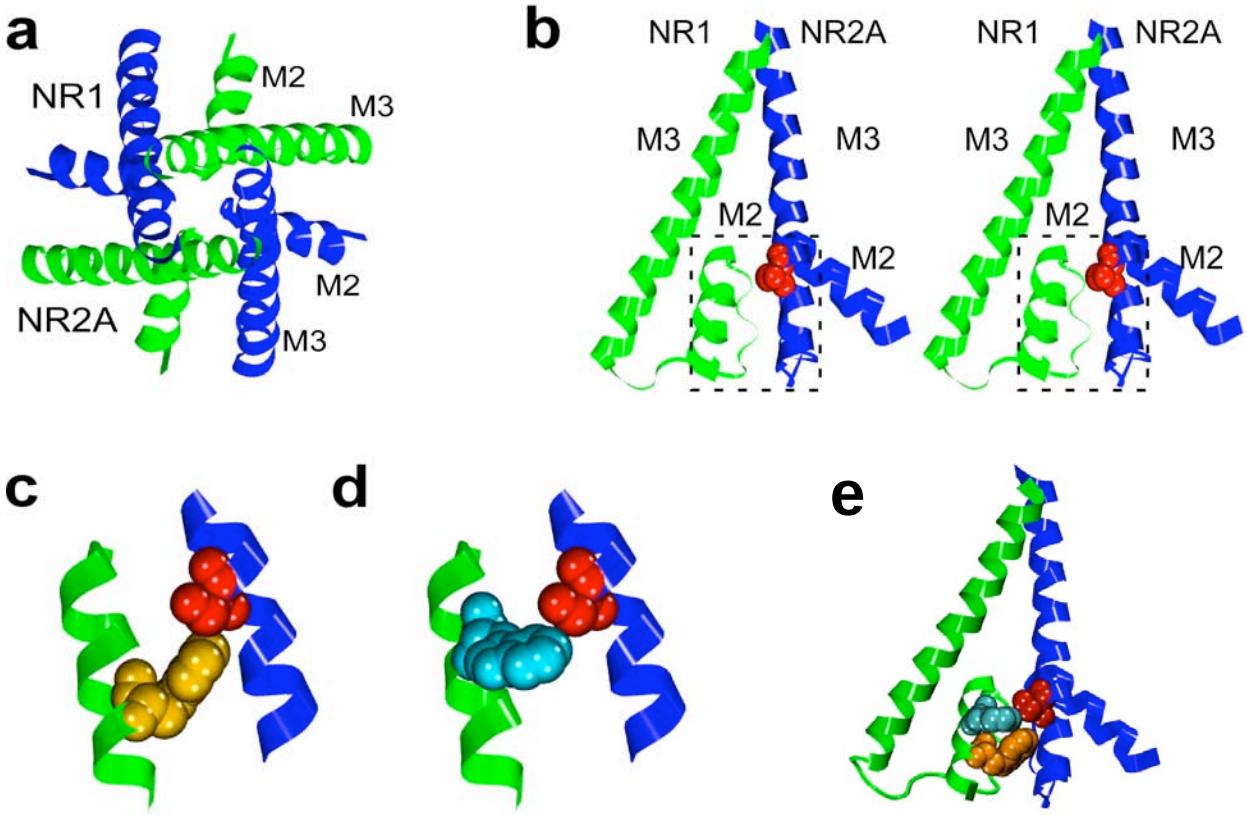

Figure 14 Homology model of the M2-M3 regions of the NR1/2A receptor based on the crystal structure of the KcsA channel

(**a**) Ribbon diagram depiction of the M2-M3 region of the NMDAR homology model, looking from the extracellular surface into the pore. Green ribbons, NR1 subunits; blue ribbons, NR2A subunits.
(**b**) Stereo view ribbon diagram depiction of the M2-M3 regions of the NMDAR model, viewed from outside the channel, looking inward. The NR1 and NR2A subunits on the far side of the channel have been removed for clarity. Green ribbon, NR1 subunit; blue ribbon, NR2A subunit. Red space-filling residue, NR2A(S632). Box, area enlarged and rotated in (**c**) and (**d**).
(**c** and **d**) Depiction of intersubunit residue-residue interactions in the NMDAR model. The M2 α-helix from the NR1 subunit and the adjacent α-helical section of M3 from the NR2A subunit are shown as ribbons. Space-filling residues: red, NR2 S/L site serine; orange, NR1(W608) in (**c**); cyan, NR1(W611) in (**d**).
(**e**) Depiction of intersubunit interactions in the NMDAR model between the NR2 S/L site, NR1(W608) and NR1(W611).

3.4 NMDAR CHANNEL MODEL BASED ON THE NAK CHANNEL

Whereas crystallized K^+ channels have often served as structures on which NMDARs have been modeled, the model presented in this section is based on the crystal structure of the *Bacillus cereus* NaK channel (Shi et al., 2006). The NaK channel is a member of the cyclic nucleotide-gated (CNG) channel family, a group of non-selective tetrameric cation channels. The NaK channel shares high sequence homology with K^+ channels, is probably evolutionarily related to both K^+ channels and NMDARs (Shi et al., 2006; Wood et al., 1995), and, like NMDARs, is permeable to Na^+, K^+, and Ca^{2+} (Alam and Jiang, 2009; Alam et al., 2007; Shi et al., 2006).

The NaK channel consists of an intracellular carboxy terminus, an interfacial helix (M0) running parallel to the membrane, and two transmembrane regions (M1 and M2) separated by a reentrant p-loop (Figure 15a). Like an upside-down NMDAR channel, the NaK channel p-loop extends from near the extracellular surface of the membrane to approximately halfway through the channel. The selectivity filter is composed of three p-loop residues that form two permeant ion binding sites along the narrowest section of the open channel plus two residues that participate in forming an extracellular vestibule. These five residues are homologous to the residues that comprise the KcsA channel selectivity filter (Shi et al., 2006). The external vestibule of the NaK channel selectivity filter is wider than the homologous region of the KcsA channel selectivity filter, and it can accomodate a larger number of water molecules. These water molecules are critical to the coordination of ion movement through the narrowest section of the selectivity filter, allowing Na^+, K^+, and Ca^{2+} ions to remain in contact with a

sufficient number of ligands throughout pore passage (Alam et al., 2007; Noskov and Roux, 2007). The KcsA channel, on the other hand, limits channel permeation to ions that are large enough to interact with the carbonyl oxygens that ring the selectivity filter (namely, K^+ ions) plus one or two water molecules (Noskov and Roux, 2007; Zhou et al., 2001).

Several studies have demonstrated the structural conservation of glutamate receptor M2-M3 regions and the homologous regions of proteins that are related to the NaK channel (Chen et al., 1999; Panchenko et al., 2001); I therefore limited the homology model to these regions. This model has an NR1-2A-1-2A subunit arrangement (Sobolevsky et al., 2009) (Figure 16b) (see Section 3.3.) As in the model that I created based on the KcsA channel, the NR2 S/L site in the NaK channel-based model interfaces with the p-loop helix of the NR1 subunit. When viewed as a space-filling residue, NR2A(S632) appears to be very close to two NR1 tryptophan residues in the p-loop helix which are separated by one α-helical rotation: NR1(W608) and NR1(W611) (Figure 16c-e). Hence, the NaK channel-based NMDAR model yields predictions that are similar to those derived from the KcsA channel-based model.

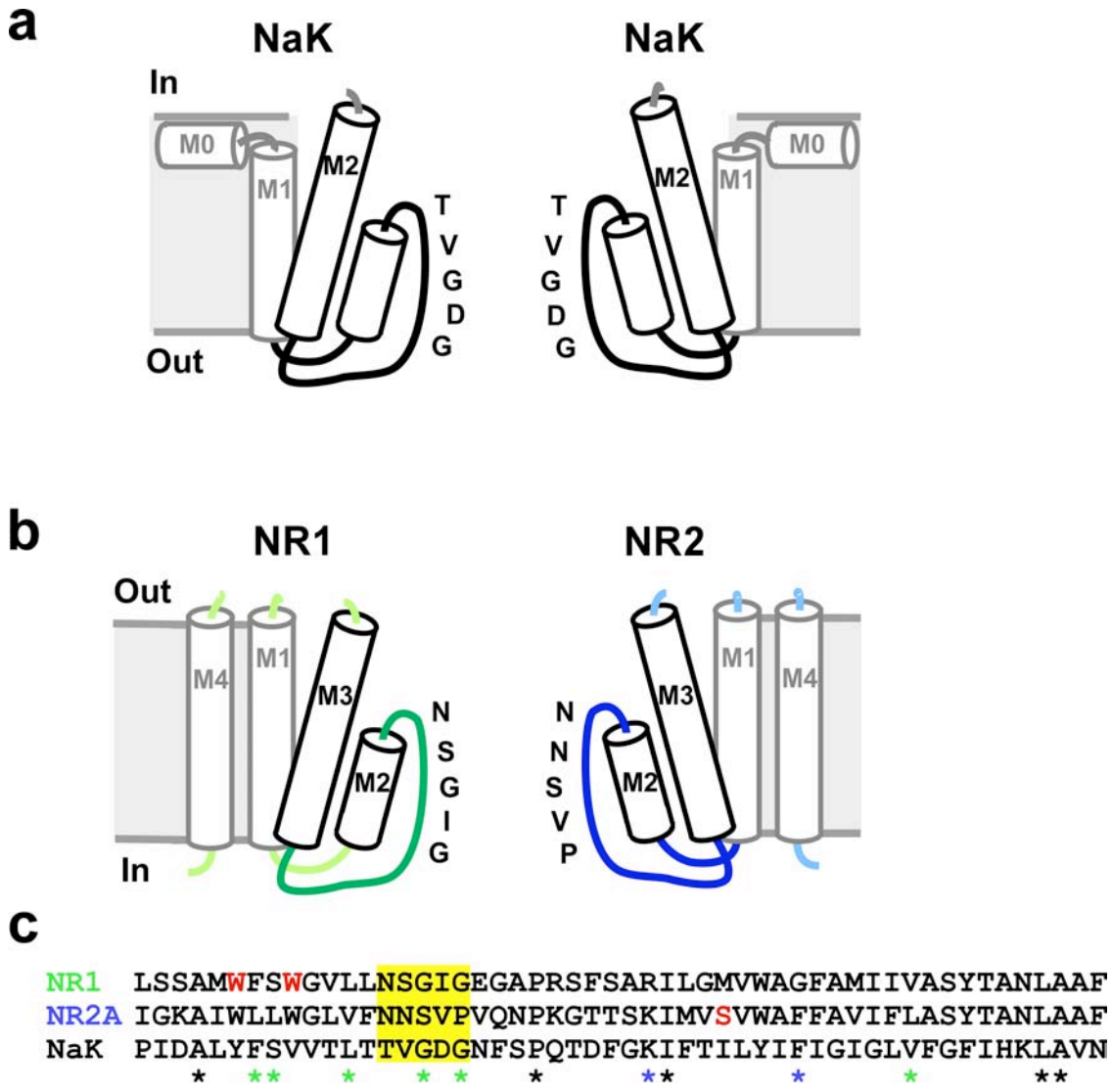

Figure 15 Transmembrane topologies and sequence alignments of NaK channel and NMDAR subunits

(**a**) Depiction of the transmembrane topology of the crystallized NaK channel. The structure of the inner helix, M2, and adjacent p-loop (black lines and outlines) was used as a template on which to base a homology model of the NMDAR channel. M0 and M1 (grey outlines) were not included in the template. Residues lining the selectivity filter are labeled.
(**b**) Depiction of the transmembrane topology of the NMDAR model based on the NaK channel. For clarity, only two subunits in the tetramer are depicted; this does not represent subunit arrangement around the pore. The model included the M2-M3 region (black outlines, dark green (NR1) lines and dark blue (NR2A) lines), whereas M1 and M4 regions (grey outlines) were excluded from the model due to lack of homology to the NaK channel. Residues lining the NR1 and NR2 subunit selectivity filters are labeled.
(**c**) Amino acid sequence alignment used for the NMDAR homology model, showing the M2-M3 region of NR1 and NR2A subunits and homologous region of the NaK channel subunit. No gaps were required in the alignment. Residues along the selectivity filter are highlighted in yellow. The NR2 S/L site, NR1(W608), and NR1(W611) are in red font. Black asterisks mark residues that are the same in NaK channel, NR1 and NR2A subunits. Green asterisks, residues that are the same in NaK channel and NR1 subunits. Blue asterisks, residues that are the same in NaK channel and the NR2A subunit.

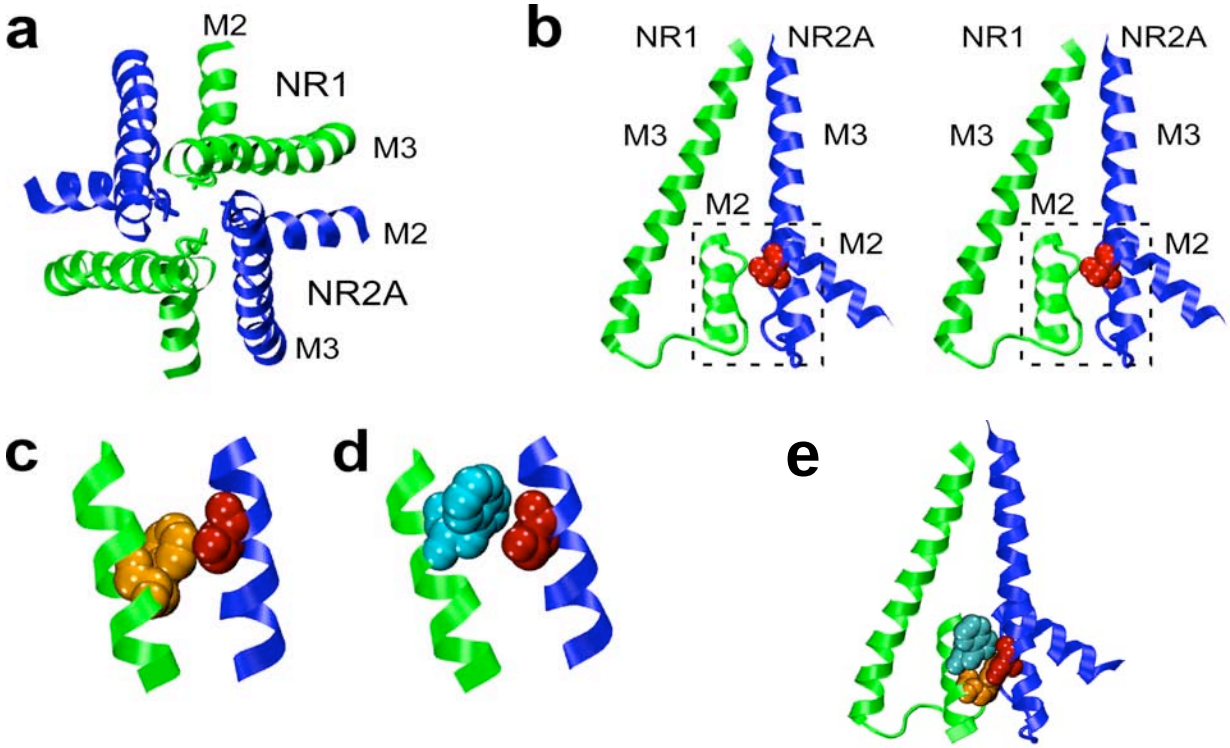

Figure 16 Homology model of the M2-M3 regions of the NMDA receptor based on the crystal structure of the NaK channel

(**a**) Ribbon diagram depiction of the M2-M3 region of the NMDAR homology model, looking from the extracellular surface into the pore. Green ribbons, NR1 subunits; blue ribbons, NR2A subunits.
(**b**) Stereo view ribbon diagram depiction of the M2-M3 regions of the NMDAR model, viewed from outside the channel, looking inward. The NR1 and NR2A subunits on the far side of the channel have been removed for clarity. Green ribbon, NR1 subunit; blue ribbon, NR2A subunit. Red space-filling residue, NR2A(S632). Box, area enlarged and rotated in (**c**) and (**d**).
(**c** and **d**) Depiction of intersubunit residue-residue interactions in the NMDAR model. The M2 α-helix from the NR1 subunit and the adjacent α-helical section of M3 from the NR2A subunit are shown as ribbons. Space-filling residues: red, NR2 S/L site serine; orange, NR1(W608) in (**c**); cyan, NR1(W611) in (**d**).
e) Depiction of intersubunit interactions in the NMDAR model between the NR2 S/L site, NR1(W608) and NR1(W611).

3.5 NMDAR MODEL BASED ON THE GLUA2 AMPA RECEPTOR

The first nearly-complete iGluR crystal structure, that of the homomeric GluA2 AMPA receptor, was published in 2009 (Sobolevsky et al., 2009). Several unexpected structural features of the ion channel were observed. For instance, the GluA2 receptor includes a pre-M1 interfacial helix, similar to the NaK channel interfacial helix and those of inwardly rectifying K^+ channels (Nishida et al., 2007; Shi et al., 2006). The location of the pre-M1 helix, adjacent to M3 and M4 residues near the activation gate, suggests that it may influence GluA2 receptor gating. The position of GluA2 receptor p-loop helices was also unexpected: compared to inverted NaK and K^+ channels, GluA2 receptor p-loop helices are shifted toward the intracellular aspect of the pore, along the axis perpendicular to the membrane (Figure 17a). Disappointingly, the region that connects the p-loop helix to M3, including the selectivity filter, was not resolved. This may be a consequence of inherent instability in a region of the protein that is likely to exist in an extended conformation, or it may be due to crystallization conditions.

AMPARs are closely related to NMDARs (Dingledine et al., 1999), and the GluA2 receptor structure provides valuable insights into NMDARs (Traynelis et al., 2010). I created a model of the NR1/2A receptor based on the GluA2 receptor, again with a subunit assembly of NR1-2A-1-2A around the pore (Figure 18b) (see Section 3.3). The GluA2-based NMDAR model did not suggest a direct interaction between the NR2 S/L site and NR1(W608) or NR1(W611) (Figure 18d). Rather, the NR2 S/L site is closest to the R group of NR1(L614), which is near the N-terminal apex of the p-loop helix (Figure 18e). Interpretation of this

predicted interaction is complicated by the poor resolution of the p-loop helix in the GuA2 receptor crystal structure and the lack of a resolved selectivity filter (Sobolevsky et al., 2009).

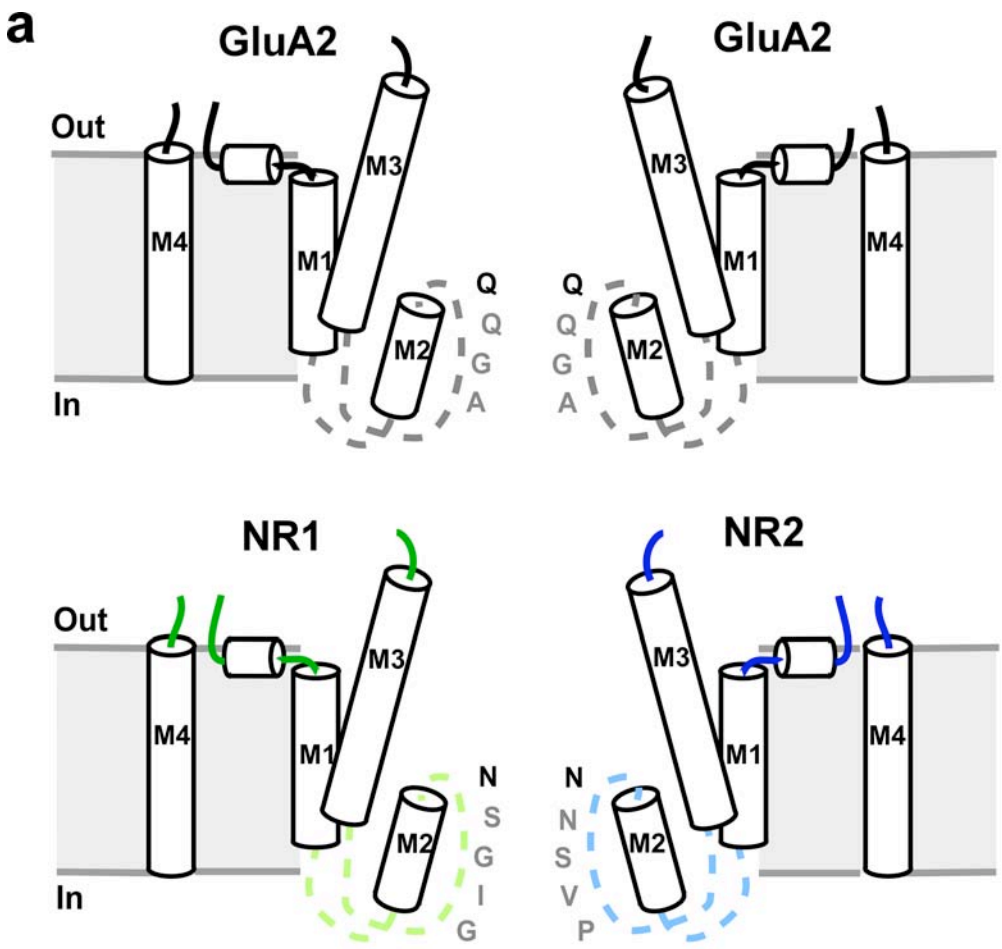

b

```
NR1    DALTLSSAMWFSWGVLLNSGIGEGAPRSFSARILGMVWAGFAMIIVASYTANLAAFLV
NR2A   PSFTIGKAIWLLWGLVFNNSVPVQNPKGTTSKIMVSVWAFFAVIFLASYTANLAAFMI
GluA2  NEFGIFNSLWFSLGAFMQQGA-DISPRSLSGRIVGGVWWFFTLIIISSYTANLAAFLT
         * *     *** *           *** * ** * ** **  **  *********
```

Figure 17 Transmembrane topologies and sequence alignments of GluA2 and NMDAR subunits

(**a**) Depiction of the transmembrane topology of the crystallized GluA2 channel. The structure of the three transmembrane helices plus the helical section of the p-loop (black lines and outlines) was used as a template on which to base a homology model of the NMDAR channel. The residues connecting M1 to M2 and the residues connecting M2 to M3 including the selectivity filter) were not resolved in the crystal structure (grey dashed lines). Residues lining the selectivity filter are labeled in predicted locations.
(**b**) Amino acid sequence alignment used for the NMDAR homology model, showing the M2-M3 region of NR1 and NR2A subunits and homologous region of the GluA2 subunit. Residues in grey font were not resolved in the GluA2 crystal structure. Selectivity filter residues are highlighted in yellow. The NR2 S/L site, NR1(W608), and NR1(W611) are in red font. Black asterisks mark residues that are the same in GluA2, NR1 and NR2A subunits. Black asterisks mark residues that are the same in GluA2, NR1 and NR2A subunits. Green asterisks, residues that are the same in GluA2 and NR1 subunits. Blue asterisks, residues that are the same in GluA2 and NR2A subunits.

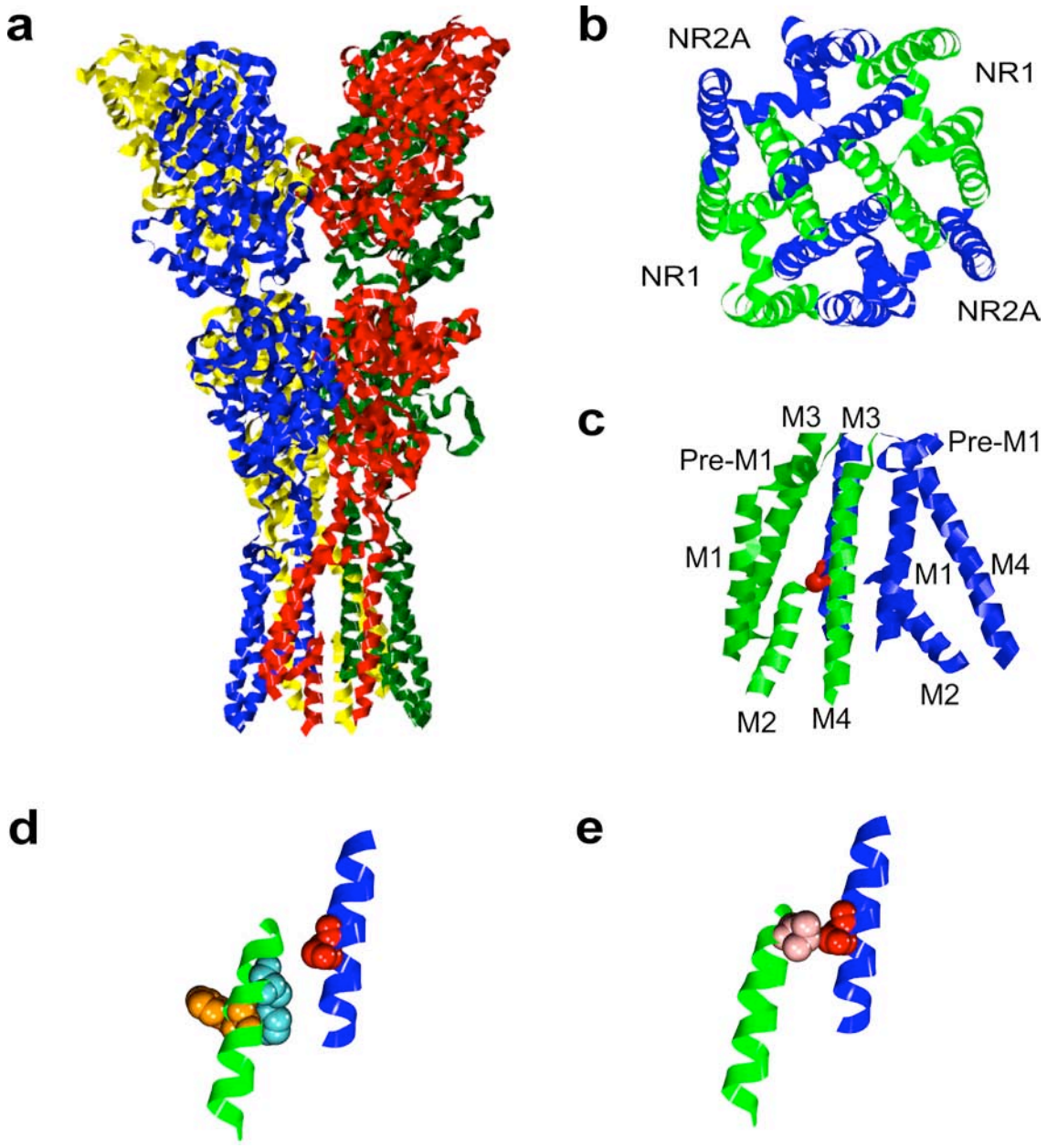

Figure 18 Homology model of the NMDA receptor based on the crystal structure of the GluA2 receptor

(**a**) Ribbon diagram depiction of the NMDAR model based on the structure of the GluA2 receptor, viewed from a perspective orthogonal to the membrane. For clarity, each subunit is portrayed in a different color. Red and yellow ribbons, NR1 subunits; dark green and blue ribbons, NR2A subunits.
(**b**) Ribbon diagram depiction of the transmembrane region plus extended M3 helices of the NMDAR homology model, looking from the extracellular surface into the pore. Green ribbons, NR1 subunits; blue ribbons, NR2A subunits
(**c**) Ribbon diagram depiction of the transmembrane region of the NMDAR model, viewed from outside the channel, looking inward. The NR1 and NR2A subunits on the far side of the channel have been removed for clarity. Green ribbon, NR1 subunit; blue ribbon, NR2A subunit. Red space-filling residue, NR2A(S632). Box, area enlarged and rotated in (**d**) and (**e**).
(**d** and **e**) Depiction of intersubunit residue-residue interactions in the NMDAR model. The M2 α-helix from the NR1 subunit and the adjacent α-helical section of M3 from the NR2A subunit are shown as ribbons. Space-filling residues: red, NR2 S/L site serine; orange, NR1(W608); cyan, NR1(W611) in (**d**); pink, NR1(L614) in (**e**).

3.6 DISCUSSION

Insight into the mechanisms responsible for the relative nonselectivity of NMDAR channels may be gained by examining the selectivity filters of homologous channels with known structures. Previous studies have demonstrated structural similarities between NMDARs and K^+ channels (Jones et al., 2002; Wood et al., 1995). The NaK channel is structurally similar to NMDARs as well, but is cation-nonselective (Alam et al., 2007; Shi et al., 2006). Whereas in K^+ channels, four K^+ binding sites are formed along the selectivity filter by four rings of carbonyl oxygens projecting into the channel (Doyle et al., 1998; Jiang et al., 2002; Long et al., 2005), the NaK channel selectivity filter contains only two rings of carbonyl oxygens (Shi et al., 2006). NaK channel residues along the pore-lining section of the p-loop that do not contribute to these carbonyl oxygen rings form an external vestibule that is wider than the perimeter delineated by the carbonyl oxygen rings; this vestibule appears to contribute to non-specific cation permeability (Alam et al., 2007). NMDAR cation non-specificity may similarly depend on a relatively short selectivity filter and wide vestibule.

It is not surprising to me that the NMDAR homology models presented in this section provide divergent predictions; as templates, each of the known structures on which NMDAR channels have been modeled contain weaknesses . Notably, all the crystal structures on which NMDAR homology models have been based display four-fold symmetry, whereas NMDARs do not, and the asymmetry may be significant in the channel region (Sobolevsky et al., 2002b). The GluA2 receptor has the advantage of sharing many structural similarities and a close

evolutionary relation to NMDARs, but the pore region was not fully resolved in the GluA2 receptor crystal structure, providing weaker constraints on the homology model I created. Furthermore, unlike NMDARs, the GluA2 channel is Ca^{2+}-impermeable (Dingledine et al., 1999). The NaK channel has the advantage of Ca^{2+} permeability and a well-resolved pore, but the disadvantage of a far more distant evolutionary relation to NMDARs. In past studies, K^+ channels have proven useful as iGluR model templates, but these channels are far more selective than iGluRs. Thus, experimental testing of predictions based on any currently available homology model will be important for model validation.

4.0 MECHANISTIC BASIS OF NR2 S/L SITE EFFECTS

4.1 INTRODUCTION

As discussed in Section 2.6, the NR2 S/L site is unlikely to interact directly with ions in the solvent. Both the KcsA-based and the NaK-based models presented in Sections 3.3 and 3.4 suggest possible interactions between the NR2 S/L site and two NR1 subunit residues: W611 and W608. To determine whether either of these NR1 residues couples with the NR2 S/L site to influence NR2 subunit-dependent channel properties, I performed mutant cycle analyses (Corradi et al., 2007; Hidalgo and MacKinnon, 1995). In a mutant cycle analysis, the effects of two or more point mutations are evaluated to probe for functional evidence of an interaction between residues at these sites. Chang and Kuo (2008) performed mutant cycle analyses to show that the NR1 and NR2B subunit alanine residues at position A7 in the SYTANLAAF motif of M3 interact at the activation gate, and that the small sidechains of these residues are necessary for gate closure. Thus, mutant cycles have provided insight into NMDAR structure and function. Although mutant cycle analyses are traditionally performed with free energy measurements, I performed these analyses with Mg^{2+} IC_{50} measurements.

4.2 METHODS

Electrophysiology. Mg^{2+} IC_{50} data at seven voltages were gathered in the whole-cell recording configuration, using the rapid measurement protocol described in Section 2.2 (Figure 4) Solutions, recording instruments, and IC_{50} calculations are also described in Section 2.2.

Mutant cycle analyses. For each mutant cycle, we measured the Mg^{2+} IC_{50}s of four NMDAR subunit combinations: wild-type (wt) NR1 and wt NR2A subunits (wt/wt receptors); wt NR1 and mutant NR2A subunits (wt/mut receptors); mut NR1 and wt NR2A subunits (mut/wt receptors); and mut NR1 and mut NR2A subunits (mut/mut receptors). If there is no interaction between the NR1 and NR2 subunit residues, then inclusion of a mutant NR1 subunit in an NMDAR should result in the same degree of functional change, regardless of whether that mutant NR1 subunit is expressed with a wild-type or mutant NR2A subunit. That is, if the mutated residues do not interact, then the magnitude of change in Mg^{2+} IC_{50} from wt/wt to mut/wt should be equal to the magnitude of change from wt/mut to mut/mut. Likewise, the magnitude of change in Mg^{2+} IC_{50} from wt/wt to wt/mut should be the same as that from mut/wt to mut/mut. Mutant cycle analyses are commonly quantified by calculation of a coupling coefficient Ω (Corradi et al., 2007; Hidalgo and MacKinnon, 1995; Ranganathan et al., 1996). In my experiments, an interaction between residues was assessed indirectly by measuring the Mg^{2+} IC_{50}s of each subunit combination, resulting in the following equation for Ω:

$$\Omega = \frac{\left(Mg^{2+}\ IC_{50}, wt/mut\right) \times \left(Mg^{2+}\ IC_{50}, mut/wt\right)}{\left(Mg^{2+}\ IC_{50}, wt/wt\right) \times \left(Mg^{2+}\ IC_{50}, mut/mut\right)} \qquad \textbf{Equation 6}$$

When $\Omega = 1$, there is no evidence for interaction between two residues; $\Omega > 1$ or $\Omega < 1$ argues for an interaction between the residues of interest (Hidalgo and MacKinnon, 1995; Kizelsztein et al., 2000; Ranganathan et al., 1996).

Several point mutants at each NR1 and NR2 subunit site of interest were created. Mutant cycle measurements were performed if whole-cell recordings from HEK293T cells expressing each mutant receptor necessary for the cycle typically yielded NMDAR current amplitudes more negative than -100 pA at -65 mV in 0 Mg^{2+}. Cells with smaller current amplitudes could not be used to reliably measure [Mg^{2+}]-inhibition curves, especially at less negative voltages. Thus, we performed a mutant cycle using NR1(W611A) and NR2A(S632L) subunits (Figure 19a), rather than using the mutant subunits that we initially created, NR1(W611S) and NR2A(S632W); NR1(W611S)/2A(S632W) receptors did not pass sufficiently large currents. Furthermore, I attempted to supplement the mutant cycle experiment that used the mutant subunits NR1(W608S) and NR2A(S632W) (Figure 19b) with a mutant cycle experiment that paralleled the NR1(W611A)-NR2A(S632L) experiments. I observed no NMDAR-mediated current, however, in NR1(W608A)/2A(S632L) receptors. In each mutant cycle presented here, data at -15 mV were excluded because some mutants did not pass enough current to accurately estimate Mg^{2+} IC_{50}s at that voltage.

Statistical analysis. Mg^{2+} IC_{50} data are presented as mean Mg^{2+} IC_{50} value (averaged across cells) ± s.e.m. Two-way ANOVA interaction tests of log-transformed Mg^{2+} IC_{50} data were performed on mutant cycle data (Figure 19). These tests assess the independence of two factors (in this case, Factor 1 is the effect of the mutation at the NR2 S/L site and Factor 2 is the effect of the mutation at a site in the NR1 subunit). Whereas untransformed IC_{50} measurement data do not follow a normal distribution, log-transformed IC_{50} data are normally distributed (Fleming et

al., 1972). Because ANOVA tests assume normal distributions of data, the log transformation was used. Interactions were considered significant at $P < 0.05$.

4.3 NR1(W611) - NR2A(S632) MUTANT CYCLE

I first probed for an interaction between NR1(W611) and NR2A(S632). Initially, I attempted to perform experiments with the mutant subunits NR1(W611S) and NR2A(S632W). I predicted that mutating the NR1 tryptophan to serine might partially compensate for the effects of mutating the NR2A serine to tryptophan. Currents through NR1(W611S)/2A(S632W) receptors, however, were too small to measure Mg^{2+} IC_{50}s accurately. I constructed several more NR1(W611) point mutants, but observed that a number of the mutant subunits did not appear to form functional channels when co-expressed with wild-type or mutant NR2A subunits. NR1(W611A), however, produced currents large enough to permit Mg^{2+} IC_{50} measurements when coexpressed with NR2A and when coexpressed with NR2A(S632L). Mutating NR1(W611) to A had little effect on Mg^{2+} IC_{50}s when coexpressed with NR2A, and little effect on Mg^{2+} IC_{50}s when coexpressed with NR2A(S632L) (Figure 19a). I tested for statistical evidence of an interaction between NR1(W611) and the NR2 S/L site at each voltage; at no voltage was there evidence for an interaction between NR1(W611) and NR2A(S632) (at -115 mV, $p = 0.51$; -95 mV, $p = 0.38$; -75 mV, $p = 0.53$; -65 mV, $p = 0.09$; -55 mV, $p = 0.26$; -35 mV, $p = 0.06$). Thus, my data do not provide evidence for an interaction between NR1(W611) and NR2A(S632).

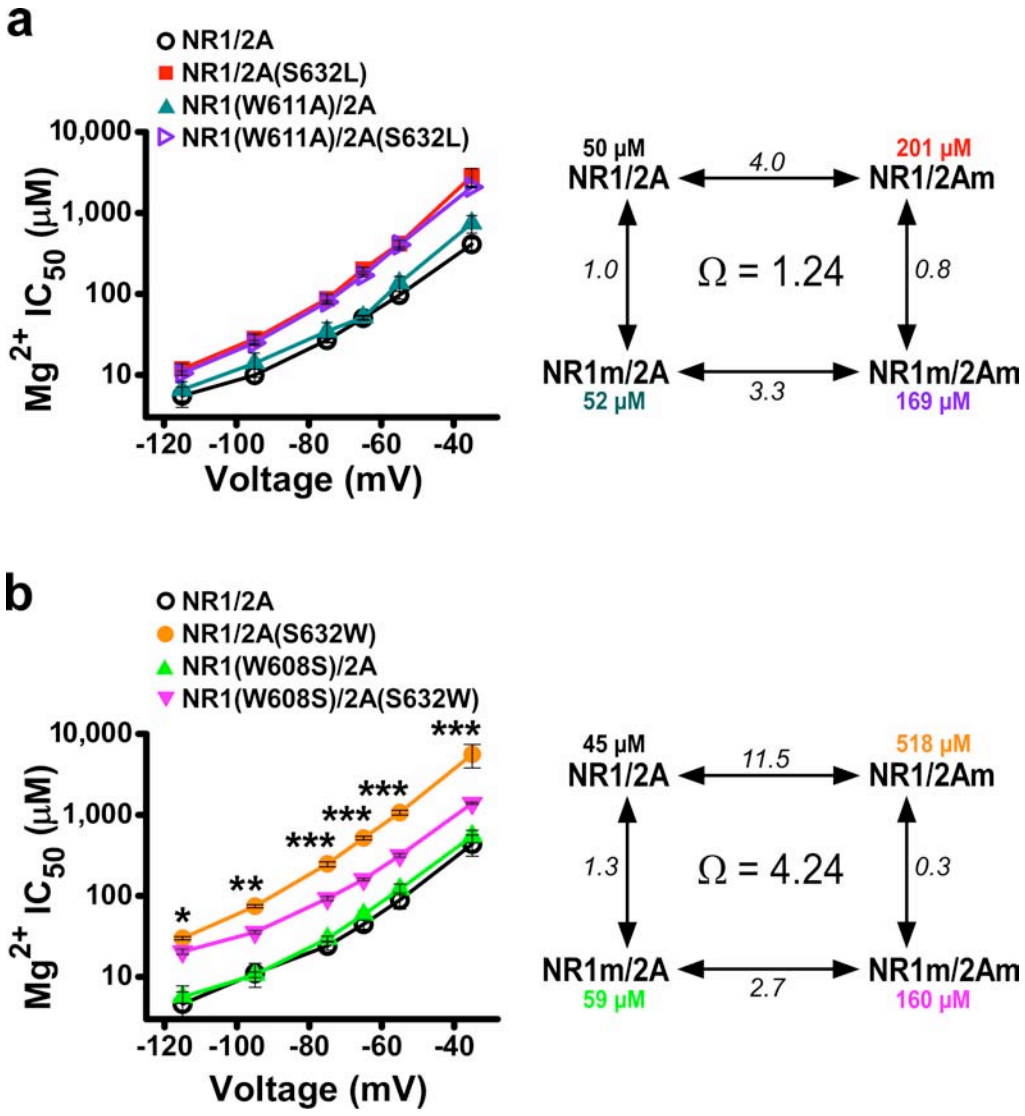

Figure 19 Mutant cycle determination of intersubunit interactions that control the NMDAR subtype specificity of Mg^{2+} block

(**a** and **b**) Mutant cycle results and schematics. Left, plot of the voltage-dependence of wild-type and mutant NMDAR Mg^{2+} IC_{50}s (n = 4 for each NMDAR subunit combination). Data at -15 mV were excluded because some mutants did not pass enough current to accurately estimate Mg^{2+} IC_{50}s at that voltage. Statistical significance of the mutant cycle was tested with a two-way ANOVA interaction test at each voltage (see Section 4.2). *p < 0.05; ** p < 0.01; ***p < 0.001.

Right, mutant cycle schematic and representative mutant cycle results at a single voltage (-65 mV). Above each NMDAR subunit combination label is the Mg^{2+} IC_{50}. Adjacent to each arrow is the fold-change of Mg^{2+} IC_{50}s, comparing the mean Mg^{2+} IC_{50} of NMDARs containing a wild-type subunit to the mean Mg^{2+} IC_{50} of NMDARs containing a mutant subunit. NR1m and 2Am represent mutant subunits. If an NR1 residue does not interact with the NR2 S/L site, the identity of the NR2 subunit (wild-type or mutant) in an NMDAR should not impact the magnitude of difference (fold-change) in Mg^{2+} IC_{50} between NMDARs with a wild-type NR1 subunit and NMDARs with a mutant NR1 subunit. The coupling coefficient Ω (Equation 6) at -65 mV is in the center of the schematic.

(**a**) NR1(W611)-NR2A(S632) mutant cycle. Ω = 1.6, averaged across voltages.

(**b**) NR1(W608)-NR2A(S632) mutant cycle. Ω = 3.5, averaged across voltages.

4.4 NR1(W608) - NR2A(S632W) MUTANT CYCLE

To determine whether NR1(W608) interacts with the NR2 S/L site, I attempted to perform mutant cycle experiments that paralleled the NR1(W611A)-NR2A(S632L) experiments, using NR1(W608A) and NR2A(S632L). I observed no NMDAR-mediated current, however, in NR1(W608A)/2A(S632L) receptors (for functional outcomes of other mutant NMDAR transfections, see Appendix B). Next, I replaced NR1(W608) with a serine, creating NR1(W608S), and replaced the NR2A serine with a tryptophan, creating NR2A(S632W). NR1(W608S) formed functional channels with NR2A, as well as with NR2A(S632W). Expression of NR1(W608S) with wild-type NR2A slightly increased the Mg^{2+} IC_{50} values from those of NR1/2A receptors (Figure 19b). If there is no interaction between NR1(W608) and NR2A(S632), I would expect that coexpressing the NR1(W608S) and NR2A(S632W) would yield a similar small increase in Mg^{2+} IC_{50}s, compared to those of NR1/2A(S632W) receptors. Mutating NR2A(S632) to W, however, markedly *decreased* Mg^{2+} IC_{50}s of NMDARs when coexpressed with NR1(W608S) subunits. Statistically significant interactions were found at every voltage (at -115 mV, $p = 0.03$; -95 mV, $p = 0.01$; -75 mV, $p = 0.00001$; -65 mV, $p < 0.00001$; -55 mV, $p = 0.00004$; -35 mV, $p = 0.001$). Thus, mutating NR1(W608) to serine partially compensates for the effects of mutating NR2A(S632) to tryptophan. These data unveil a critical intersubunit interaction that regulates the subtype specificity of NMDAR channel block by Mg^{2+}.

4.5 DISCUSSION

The NMDAR homology models in Section 3.0 and the results presented in this section suggest that the NR2 S/L site regulates NR2 subtype specificity of Mg^{2+} block through interactions with NR1(W608). The mechanism by which NR1(W608) affects the pore, however, is unknown. A cysteine accessibility study showed that NR1(W608) is solvent-accessible from the intracellular aspect of the membrane (Kuner et al., 1996), suggesting that the residue is situated close to the pore. Jin et al. (2007) showed that mutation of NR1(W608) to leucine does not affect channel block by Mg^{2+}, though NR1(W608L)/2B receptors exhibit weaker channel block by some permeant polyamine derivatives. Modification of the homologous residue in NR2B subunits, also a tryptophan, strongly affects Mg^{2+} block and permeation (Williams et al., 1998).

Mutant cycles test for functional, but not structural, interactions between residues. Hence, it is possible that the NR2 S/L site and NR1(W608) interact in an allosteric manner. Though theories abound, little is known about the structure of the NMDAR selectivity filter. Electrophysiological studies indicate that the narrowest part of the open NR1/2A receptor pore has a mean diameter of 5.5 Å (Villarroel et al., 1995), and suggest that the NR1 N-site and NR2A N+1 site are near or included in this narrowest section (Wollmuth et al., 1996). Further elucidation of the effects of interactions between the NR2 /L site and NR1(W608) may provide insight into the structure of NMDAR selectivity filters.

Two of the three NMDAR models I created argue for a direct interaction between the NR2 S/L site and NR1(W608) (the models based on the KcsA and NaK channels). The GluA2 receptor-based NMDAR model, however, argues against a direct interaction. The argument against a direct interaction is strengthened by the close evolutionary relationship between NMDARs and AMPARs. A mutant cycle analysis testing the predictions of the GluA2-based

model would provide useful information not only on the relationship between the NR2 S/L site and NR1(L614), but also on the utility of NMDAR channel models based on AMPAR structures. I did not perform this experiment, however, because the structure of the GluA2 receptor was not available when I performed mutant cycle experiments. At that time, I had created only the KcsA channel- and NaK channel-based models, and therefore based my mutant cycle experiments on the predictions that these models generated. Results presented in this chapter demonstrate both the usefulness of homology models and the importance of testing predictions based on homology models.

Intriguingly, the p-loop tryptophan at NR1(W608) is highly conserved. All known mammalian iGluR subunits contain a tryptophan at the position homologous to NR1(W608), with the exception of the NR3A and NR3B subunits. In fact, this tryptophan is present at the homologous sites of nematode (*Caenorhabditis elegans*) and insect (*Drosophila melanogaster*) iGluRs, as well as in predicted iGluR subunits and glutamate binding proteins of the plant *Arabidopsis* (Chiu et al., 2002; Sprengel et al., 2001). Furthermore, the tryptophan at this site is conserved in the prokaryotic GluR0 channel and in some prokaryotic and eukaryotic potassium channels (Sprengel et al., 2001). Thus, NR1(W608) and the tryptophans at equivalent sites in NMDAR subunit homologs are likely to play a critical role in the function of these proteins.

It is possible that the high conservation of this residue has been driven by a functional role beyond its effects on channel properties. For instance, the p-loop tryptophan may serve a critical role in protein folding, translocation, or membrane insertion. If so, then the effects of NR1(W608) on NMDAR pore properties may have diverged from the effects of tryptophans at homologous sites in other ion channels. Just as the highly-conserved asparagine in the SYTANLAAF motif has developed to contribute to Ca^{2+} permeability in NMDARs (Jatzke et al.,

2003; Watanabe et al., 2002), but not in Ca^{2+}-permeable AMPARs, the tryptophans at NR1(W608) and in related channels may have developed to differentially contribute to pore properties.

Alternatively, conservation of the p-loop tryptophan may be driven by a fundamental role in pore function. In this case, studies on the role of this conserved tryptophan in the KcsA channel, KcsA(W67), may provide insight into the role of NR1(W608). KcsA(W67) participates in a hydrogen bond network that strongly influences the KcsA channel selectivity filter (Cordero-Morales et al., 2006; Cuello et al., 2010a; Cuello et al., 2010b). In wild-type receptors, KcsA(W67) appears to bond with nearby residues in a way that promotes selectivity filter instability. This instability is proposed to cause frequent channel inactivation, in which the selectivity filter collapses.

Two KcsA channel p-loop helix residues, KcsA(W67) and KcsA(E71), and three selectivity filter region residues, KcsA(Y78), KcsA(G79), and KcsA(D80), participate in the hydrogen bond network. In wild-type channels, KcsA(W67) faces the selectivity filter and forms bonds with both KcsA(E71) and KcsA(D80) to promote selectivity filter destabilization and inactivation. When KcsA(E71) is mutated to an alanine, however, creating KcsA(E71A), the hydrogen bond network is disrupted and inactivation becomes far less frequent. KcsA(W67) sidechain position is more variable in crystallized channels containing KcsA(E71A): KcsA(W67) can either face the selectivity filter, or it can face the transmembrane domain homologous to M3 in NMDAR subunits (Cordero-Morales et al., 2006; Cuello et al., 2010a). The two p-loop conformations created by two KcsA(W67) sidechain locations have been proposed to underlie different conductance states (Cordero-Morales et al., 2006).

The residues involved in the KcsA channel hydrogen bond network have similar counterparts at homologous sites in the NR1 subunit. For example, the residue properties of NR1(E621), the NR1 subunit residue homologous to KcsA(D80), are similar to the residue properties of aspartate. Furthermore, the glycine at KcsA(G79) in the KcsA channel is conserved in NR1 subunits. Finally, NR1(G612), the NR1 subunit residue homologous to the residue mutated to alanine in the KcsA(E71A) channel, is similar in size and polarity to alanine. Given the importance of these KcsA channel residues in creating variation in KcsA(W67) sidechain position, the homologous residues of NR1 subunits may contribute to a similar variable positioning of the NR1(W608) sidechain. If so, the NR2 S/L site (which is likely to be adjacent to NR1(W608)) might exert its effects on the pore by influencing NR1(W608) sidechain position, which may influence selectivity filter stability. It would be interesting to compare models of NR1/2A and NR1/2D receptor channels based on the structure of the crystallized KcsA(E71A) channel; this modeling must wait, however, until the structure is published later this year.

5.0 GENERAL DISCUSSION

5.1 RELATIONSHIPS BETWEEN NMDAR OPEN CHANNEL PROPERTIES

The open-channel NMDAR properties that are regulated by the NR2 S/L site are intricately linked. For instance, both Ca^{2+} permeability and channel block by Mg^{2+} primarily depend on asparagine residues in the selectivity filter (Burnashev et al., 1992b; Sharma and Stevens, 1996a; Wollmuth et al., 1998a; Wollmuth et al., 1996) (see Sections 1.3.4 and 1.3.5). Furthermore, the dissimilarity between NR1/2A receptor and NR1/2D receptor Mg^{2+} IC_{50}s likely stems in part from different Mg^{2+} permeation rates, which are proposed to arise from variations in the energy barrier to permeation at or near the selectivity filter (Qian and Johnson, 2006). The interaction between the NR2 S/L site and the p-loop residue NR1(W608) (Section 4.4) provides further evidence that Mg^{2+} block variation among NMDAR subtypes arises from dissimilarities at the level of the selectivity filter. Hence, the NR2 S/L site may influence both Mg^{2+} IC_{50} and relative Ca^{2+} permeability by affecting the selectivity filter.

The mechanism by which the NR2 S/L site regulates single-channel conductance may similarly overlap with mechanism by which this site regulates relative Ca^{2+} permeability. Like Ca^{2+} permeability, single-channel conductance of NMDARs is highly dependent on internal and external permeant ion concentrations (Ascher and Nowak, 1988; Premkumar and Auerbach, 1996). Both main- and subconductance states are strongly regulated by the concentration of

external Ca^{2+} ($[Ca^{2+}]$): as $[Ca^{2+}]$ decreases, single-channel conductance increases (Ascher and Nowak, 1988; Gibb and Colquhoun, 1992; Jahr and Stevens, 1993; Wyllie et al., 1996). It is possible, therefore, that the effects of the NR2 S/L site on single-channel conductance reflect an effect of the NR2 S/L site on channel block by Ca^{2+}. One way to separate the influence of the NR2 S/L site on single-channel conductance from the influence of this site on relative Ca^{2+} permeability would be to assess the single-channel conductances of wild-type and NR1/2A(S632L) receptors in a Ca^{2+}-free external solution. If, in absence of external Ca^{2+}, NR1/2A(S632L) receptor single-channel conductance is shifted from that of NR1/2A receptors toward that of NR1/2D receptors, then the effects of the NR2 S/L site on single-channel conductance could not be due to an effect on Ca^{2+} block.

The structural origins of main- and subconductance states in NMDARs are unclear. One hypothesis is that the two states reflect structural differences in or near the external vestibule, which may affect Ca^{2+} binding in or near this location. Observations of weakly voltage-dependent NMDAR channel block by Ca^{2+} led to the proposal that Ca^{2+} binding in or near the external vestibule slows monovalent cation permeation (Premkumar and Auerbach, 1996; Wollmuth and Sakmann, 1998) (Jahr and Stevens, 1993; Premkumar et al., 1997); NMDARs in subconductance state conformations may have a higher affinity for Ca^{2+} at this external site (Premkumar and Auerbach, 1996). Thus, the increased Ca^{2+} affinity of the external Ca^{2+} binding site in a subconductance state conformation (compared to Ca^{2+} affinity of the site in a main state conformation) may create the subconductance state by reducing both divalent and monovalent cation permeation when Ca^{2+} is bound. Varying external $[Ca^{2+}]$s, however, does not alter NR1/2D receptor transition rates between main- and subconductance states (Wyllie et al., 1996). Furthermore, NMDARs adopt subconductance state conformations in the absence of divalent

cations (Gibb and Colquhoun, 1992; Wyllie et al., 1996). Thus, it is likely that other structural difference between main- and subconductance states exist, in addition to potential structural differences in the external vestibule.

Another hypothesis regarding the structural origin of main- and subconductance states is that the permeation barrier formed by the selectivity filter can adopt two configurations with different ion permeation energetics, each representing a conductance state (Premkumar et al., 1997). Indeed, an NR2A subunit point mutation at the N+1 site in the selectivity filter appears to eliminate the subconductance state (Wollmuth et al., 1998b). Further supporting the hypothesis that main- and subconductance states involve different energy barriers at the selectivity filter, mutations at the apex of the selectivity filter (the Q/R/N site) dramatically alter both main- and subconductance states (Premkumar and Auerbach, 1996), as well as sub state occupancy (Premkumar et al., 1997; Schneggenburger and Ascher, 1997). Finally, additional support that the selectivity filter permeation barrier differs between main- and subconductance states is provided by the NR2 S/L site research presented in this document. The NR2 S/L site, which strongly regulates both main- and sub conductance states, is adjacent to the selectivity filter-forming p-loop; hence, it is well-located to affect the permeation barrier formed by the selectivity filter.

5.2 COMPARISONS WITH PREVIOUS STUDIES

The subtype dependence of many NMDAR channel properties has been extensively studied (Traynelis et al., 2010). Comparison across studies of some properties, however, is complicated by large variations in experimental conditions between studies. Variation in

permeant ion concentrations of intracellular and extracellular solutions, for instance, affects all of the open channel NMDAR properties characterized in this document (Section 2.0). The single-channel conductances and kinetics of wild-type NMDARs that are reported in this document are consistent with values from several other studies, in part because the solutions in which these measurements are made are similar (Cull-Candy et al., 1998; Stern et al., 1992; Wyllie et al., 1996).

In contrast, measures of Mg^{2+} IC_{50} and P_{Ca}/P_{Cs} are more variable (Antonov and Johnson, 1999; Ascher and Nowak, 1988; Jatzke et al., 2002; Kuner and Schoepfer, 1996; Mayer and Westbrook, 1987; Schneggenburger, 1996; Zarei and Dani, 1994). For instance, Kuner and Schoepfer (1996) noted less voltage dependence of NR1/2C and NR1/2D receptor Mg^{2+} IC_{50}s, compared to those of NR1/2A and NR1/2B receptors, at voltages between -80 and -30 mV; this phenomenon that was not observed in the study presented here (we observed, on average, an e-fold change in Mg^{2+} IC_{50} per 14 mV for both NR1/2A and NR1/2D receptors between -75 and -35 mV, similar to previously published values for NMDARs of indeterminate subunit composition (Ascher and Nowak, 1988; Jahr and Stevens, 1990; Kleckner and Dingledine, 1991)) (Table 5.2). It is possible that disparities between results presented in this document and those presented by Kuner and Schoepfer (1996) stem from different recording conditions: whereas we performed experiments in HEK cells, Kuner and Schoepfer (1996) used oocytes, which have a different intracellular solution than our CsCl intracellular solution. Like Kuner and Schoepfer (1996), however, Kleckner and Dingledine (1991) expressed NMDARs in oocytes - but noted no variation in the voltage dependence of Mg^{2+} IC_{50}s in NMDARs derived from hippocampal mRNA gathered at several developmental stages. Indeed, I could find no other study that noted NMDAR subtype-specific voltage dependence of Mg^{2+} IC_{50}s. Several groups

have measured the voltage dependence of Mg^{2+} IC_{50}s in spinal neurons (likely containing NR2C subunits, but possibly also containing NR2A subunits) or hippocampal neurons (likely containing NR2A and/or NR2B subunits), but I could find no single study that compared these measures in two populations of neurons. Nevertheless, it is noteworthy that the voltage dependence of Mg^{2+} block of NMDARs in spinal neurons is lower than that of hippocampal neurons, when comparing across studies (Ascher and Nowak, 1988; Jahr and Stevens, 1990; Mayer and Westbrook, 1985).

For similar reasons, comparison of the relative Ca^{2+} permeabilities presented in this document with previously published relative Ca^{2+} permeabilities is challenging. As discussed in Section 2.6, several measures of Ca^{2+} permeability have been used. Even among studies that performed relative Ca^{2+} permeability measurements under biionic conditions, comparisons are complicated by the use of different monovalent cation species (Burnashev et al., 1995; Jatzke et al., 2002), different means of determining relative permeability (Iino et al., 1990; Tsuzuki et al., 1994; Wollmuth and Sakmann, 1998), and different concentrations of Ca^{2+} (Burnashev et al., 1995; Watanabe et al., 2002). For instance, Iino et al. (1990) calculated the P_{Ca}/P_{Cs} of NMDARs in cultured hippocampal neurons based on whole-cell recording determination of the reversal potential in a single biionic solution containing internal Cs^+ and external Ca^{2+}, whereas Tsuzuki et al. (1994) calculated the P_{Ca}/P_{Na} of NR1/2B receptors in oocytes based on single-channel recording determination of the reversal potential in multiple biionic solutions, containing internal K^+ and external Ca^{2+}, Na^+, or K^+. Previously published NMDAR relative Ca^{2+} permeabilities are enumerated in Table 5.2. When possible, data that I gathered are compared to data from previously published studies. For instance, using the equation presented in Iino et al. (1990) and inserting ion concentrations, rather than activities, I find a P_{Ca}/P_{Cs} of 3.7 for NR1/2A receptors

and 4.4 for NR1/2B receptors in 10 mM Ca^{2+}; in contrast, Iino et al. (1990) found a P_{Ca}/P_{Cs} of 6.2 in 10 mM Ca^{2+} for hippocampal neurons (likely containing NR2A and/or NR2B subunits). Iino et al. (1990) also calculated P_{Ca}/P_{Cs} using ion activities, yielding a value of 14.3 (Table 5.2); I performed similar calculations, which yielded lower values compared to Iino et al. (1990) (Table 5.2).

For comparison to the P_{Ca}/P_{Cs} data presented in this document, three studies are most relevant (in that each assessed NR1/2A receptor P_{Ca}/P_{Cs} in HEK cells, under conditions similar to those presented here and using similar calculations). In these studies, P_{Ca}/P_{Cs} in 1.8 mM Ca^{2+} was 5.7 (Jatzke et al., 2002), 6.1 (Wollmuth and Sakmann, 1998), and 6.4 (Watanabe et al., 2002). The NR1/2A receptor P_{Ca}/P_{Cs} value in 1.8 mM Ca^{2+} that I report, 7.7, is higher than previously published values (Table 5.2). In contrast, my measurement of the NR1/2A receptor P_{Ca}/P_{Cs} in 10 mM Ca^{2+} (4.5) is similar to previously reported values under similar conditions (4.2, Wollmuth and Sakmann (1998); 4.0[3], Jatzke et al. (2002)) (Table 5.2). I could find no reports of NR1/2B, NR1/2C, or NR1/2D receptor P_{Ca}/P_{Cs} measured under comparable conditions. Across methodologically-different studies, however, the consistent trend was NR1/2A and NR1/2B receptor Ca^{2+} permeabilities are higher than those of NR1/2C and NR1/2D receptors (Burnashev et al., 1995; Monyer et al., 1994; Monyer et al., 1992; Schneggenburger, 1996). In this aspect, my research is consistent with previously published research.

[3] Estimate based on a graph of P_{Ca}/P_{Cs} values in 1.8 mM, 10 mM and 110 mM Ca^{2+}

5.3 PHYSIOLOGICAL IMPLICATIONS OF THE NR2 S/L SITE

In physiological concentrations of divalent cations (1 mM Mg^{2+} and 1.8 mM Ca^{2+}), NR1/2A receptor P_fs peak at -20 mV, whereas NR1/2C receptor P_fs peak at -40 mV (Burnashev et al., 1995). Thus, the range of voltages at which NMDARs effectively conduct Ca^{2+} is subtype-specific, and therefore the range of voltages at which NMDARs can act as coincidence detectors is subtype-specific. The NR2 S/L site, which strongly regulates the subtype specificity of Mg^{2+} block and probably regulates the subtype specificity of relative Ca^{2+} permeability, is likely be an important determinant of the conditions under which each NMDAR subtype detects coincident activity.

The NR2 S/L site may also indirectly regulate subtype-specific NMDAR interactions with the clinically beneficial channel blocker memantine, which slows the cognitive decline associated with Alzheimer's disease (Muir, 2006). Memantine binds near the apex of the selectivity filter, at a site that overlaps with the Mg^{2+} binding site (Chen and Lipton, 2005; Kashiwagi et al., 2002); the two channel blockers exhibit competitive binding (Kotermanski and Johnson, 2009). Most of the research on memantine block of NMDARs has demonstrated little subtype selectivity (Dravid et al., 2007; Parsons et al., 2007). Recently, however, memantine was shown to be selective for NR1/2C and NR1/2D receptors in the presence of a physiological concentration of Mg^{2+} (Kotermanski and Johnson, 2009). The weaker channel block by Mg^{2+} of NR1/2C and NR1/2D receptors allows lower concentrations of memantine to inhibit these receptors, compared to the concentrations of memantine necessary to exert similar effects on NR1/2A and NR1/2B receptors, in the presence of Mg^{2+}. Because memantine does not permeate the NMDAR channel, I would predict that the NR2 S/L site does not directly influence memantine block. In the presence of Mg^{2+}, however, the NR2 S/L site may affect memantine

inhibition of NMDARs by regulating the extent to which Mg^{2+} competes with memantine for binding in the pore. To test this, memantine IC_{50}s of wild-type NMDARs and NR1/2A(S632L) receptors at several voltages would be determined in the presence and absence of 1 mM Mg^{2+}. If the ratio of NMDAR memantine IC_{50} in absence of Mg^{2+} to memantine IC_{50} in 1 mM Mg^{2+} is lower in NR1/2A(S632L) receptors than in NR1/2A receptors, there would be evidence to support the hypothesis that the NR2 S/L site indirectly influences subtype-specific NMDAR channel block by memantine.

5.4 FUTURE DIRECTIONS

Many NMDAR properties are now known to be strongly regulated by the NR2 NTD+L region or the NR2 S/L site. The modular control of NMDAR properties by these two regions of the NMDAR protein might be exploited to tease apart the roles of different subtype-specific channel properties in physiological processes. For instance, NMDARs containing NR2D subunits are likely primarily expressed at extrasynaptic locations in some cerebellar neurons (Misra et al., 2000; Momiyama et al., 1996; Vicini and Rumbaugh, 2000); the high affinity for glutamate of NR1/2D receptors may create a unique opportunity for activation by synaptic glutamate spillover. One way of assessing the role of extrasynaptic NR1/2D receptors in sensing glutamate spillover would be to examine neurons that express extrasynaptic NR1/2D receptors with lower sensitivity to glutamate. To examine such neurons, a mouse could be created that conditionally expresses NR2D subunits with a substituted NR2A NTD+L region. Alternatively, cultured neurons from wild-type or NR2D knockout mice could be transfected with NR2D subunits containing the substituted NR2A NTD+L region.

Hypotheses regarding the roles of NMDARs in pathological processes might be tested in a similar manner. For instance, if the NR2 S/L site impacts the subtype-selectivity of memantine in the presence of Mg^{2+}, the hypothesis that the neuroprotective effects of memantine are mediated by interactions with NR1/2C or NR1/2D receptors (Kotermanski and Johnson, 2009) could be addressed. If the clinical utility of memantine relies on subtype-specificity, then memantine might be less neuroprotective in neurons with serine substitutions at the NR2 S/L sites of NR1/2C or NR1/2D receptors. In experiments designed to address this hypothesis, cultured neurons could be transfected with NR2C or NR2D subunits containing a serine at the NR2 S/L site. Assays of NMDA-induced excitotoxicity in the presence and absence of memantine, and in the presence and absence of Mg^{2+}, could be performed in these cultures, as well as in cultures transfected with wild-type NR2C or NR2D receptors. Alternatively, transgenic mice could be created that conditionally express the mutant NR2C or NR2D subunits, and *in vivo* experiments could be performed on the effects of the NR2 S/L site on neuroprotection by memantine. Hence, investigations into structural bases of NMDAR channel properties may yield powerful tools for evaluating hypotheses regarding the roles of NMDARs in both normal and pathological physiology.

APPENDIX A

Mechanism of differential control of NMDA receptor activity by NR2 subunits

Published in final edited form as:
Nature. 2009 June 4; 459(7247): 703–707. doi:10.1038/nature07993.

Mechanism of differential control of NMDA receptor activity by NR2 subunits

Marc Gielen[1], **Beth Siegler Retchless**[2], **Laetitia Mony**[1], **Jon W. Johnson**[2], and **Pierre Paoletti**[1]

[1]Laboratoire de Neurobiologie, Ecole Normale Supérieure, CNRS 46 rue d'Ulm, 75005 Paris, France

[2]Department of Neuroscience, University of Pittsburgh, A210 Langely Hall, Pittsburgh, PA 15260, USA

Abstract

NMDA receptors (NMDARs) are a major class of excitatory neurotransmitter receptors in the central nervous system. They form glutamate-gated ion channels highly permeable to calcium that mediate activity-dependent synaptic plasticity[1]. NMDAR dysfunction is implicated in multiple brain disorders, including stroke, chronic pain and schizophrenia[2]. NMDARs exist as multiple subtypes with distinct pharmacological and biophysical properties largely determined by the type of NR2 subunit (NR2A-NR2D) incorporated in the heteromeric NR1/NR2 complex[1,3,4]. A fundamental difference between NMDAR subtypes is their channel maximal open probability (Po), which spans a 50-fold range from ~0.5 for NR2A-containing receptors to ~0.01 for NR2C- and NR2D-containing receptors; NR2B-containing receptors having an intermediate value (~0.1)[5–9]. These differences in Po confer unique charge transfer capacities and signaling properties on each receptor subtype[4,6,10,11]. The molecular basis for this profound difference in activity between NMDAR subtypes is unknown. Here we demonstrate that the subunit-specific gating of NMDARs is controlled by the region formed by the NR2 N-terminal domain (NTD), an extracellular clamshell-like domain previously shown to bind allosteric inhibitors[12–15], and the short linker connecting the NTD to the agonist-binding domain (ABD). Subtype specificity of NMDAR Po largely reflects differences in the spontaneous (ligand-independent) equilibrium between open-cleft and closed-cleft conformations of the NR2-NTD. This NTD-driven gating control also impacts pharmacological properties, by setting the sensitivity to the endogenous inhibitors zinc and protons. Our results provide a proof-of-concept for a drug-based bidirectional control of NMDAR activity using molecules acting either as NR2-NTD "closers" or "openers" promoting receptor inhibition or potentiation, respectively.

Keywords

glutamate receptors; NMDA; gating; channel; synapse; allosteric modulation

We first explored the role of the NR2-NTD in the difference of Po between NR1/NR2A and NR1/NR2B receptors by evaluating the effect of deleting the entire NR2-NTD on receptor activity. We estimated Po using a method based on the covalent modification of a cysteine introduced in the NR1 subunit (NR1-A652C), which locks open the NMDAR channel[16]. Although this method does not give access to the absolute Po of receptors containing the wild-type (wt) NR1 subunit, it can report relative differences in channel activity[17]. Indeed, the extent

Correspondence and requests for materials should be addressed to P.P. (E-mail: paoletti@biologie.ens.fr).

to which the sulfhydryl-modifying reagent MTSEA potentiates NMDAR currents is inversely related to the channel Po[17]. MTSEA potentiated currents carried by NR1-A652C/NR2B receptors to a much greater extent than currents of NR1-A652C/NR2A receptors (Fig. 1a&d), consistent with the much lower Po of NR2B-containing receptors compared to NR2A-containing receptors[5,6,17]. In contrast, MTSEA-induced potentiations of NR1-A652C/NR2A-ΔNTD and NR1-A652C/NR2B-ΔNTD receptors were indistinguishable (Fig. 1b&d) indicating equal receptor activities. However, receptors incorporating chimeric NR2A-(2B NTD) or NR2B-(2A NTD) subunits displayed MTSEA-induced potentiations similar to those of the parental NR2 subunits, indicating that swapping the NTDs alone did not exchange the Po (Fig. 1d). We therefore swapped both the NTD and the highly divergent short (14 residues) linker segment that connects the NTD to the ABD (Fig. S1). Remarkably, NR1-A652C/NR2A-(2B NTD+L) and NR1-A652C/NR2B-(2A NTD+L) responses supported levels of MTSEA potentiation closer to those of NR2Bwt-containing and NR2Awt-containing receptors, respectively (Fig. 1c&d). Direct measurement of channel activity using single-channel recordings confirmed this exchange of Po (Fig. 1e and Fig S2).

We next extended the analysis to the NR2D subunit. MTSEA-induced potentiations of NR2D-containing receptors were considerable (~300-fold), reflecting the very low Po of NR1/NR2D receptors (Fig. 1d). Deleting the NR2D-NTD resulted in a 4-fold decrease in MTSEA potentiation, indicative of a markedly increased Po (Fig. 1d). This gain-of-function phenotype could be reinforced by grafting on NR2D-ΔNTD the NTD+linker region of the high-Po subunit NR2A. Reversibly, receptors containing the chimeric NR2A-(2D NTD+L) subunit displayed 17-fold higher MTSEA-potentiation than NR2Awt-containing receptors, suggestive of a much lower Po (Fig. 1d). Thus, the low Po of the NR2D-containing receptors is also set by the NR2-NTD.

Since Po estimation using MTSEA relies on a mutated NR1 subunit (NR1-A652C), we checked that the effects observed did not depend on this mutation. We used the time constant of inhibition by MK-801, an NMDAR open-channel blocker, as an alternative method to assess Po[5,18]. Consistent with the higher Po of NR2A- vs NR2B-containing receptors, MK-801 inhibited wt NR1/NR2A receptors significantly faster than wt NR1/NR2B receptors (Fig. S3a&b). Deleting the NR2-NTDs abolished this difference (Fig. S3b). While swapping the NR2-NTD alone did not exchange MK-801 time constants, incorporating the NTD-ABD linker achieved almost complete transfer (Fig. S3a&b). As expected, the onset of MK-801 inhibition at wt NR1/NR2D receptors was much slower than at NR2A- or NR2B-containing receptors. Deleting the NR2D-NTD or replacing the NTD+linker region of NR2D by that of NR2A strongly accelerated MK-801 inhibition, indicative of a much increased Po (Fig. 1f and Fig S3c). Conversely, MK-801 inhibition of receptors incorporating NR2A-(2D NTD+L) was 15-fold slower than at NR2Awt-containing receptors (Fig. S3b). Together with the MTSEA experiments, these results demonstrate that the NR2-NTD+linker region is a major determinant of the NR2 subunit-specific activity of NMDARs.

We next investigated the mechanism by which a distal domain, the NR2-NTD, influences channel activity. Previous studies on allosteric inhibition of NMDARs by NR2-NTD ligands, such as zinc and ifenprodil, suggested that these ligands bind the NTD cleft and promote its closure[12,15,19]. This in turn leads to receptor inhibition through disruption of the NR1/NR2 ABD dimer interface, resembling the mechanism underlying AMPAR desensitization[20–22]. Since the NTD can adopt at least two conformations, a ligand-free open state and a ligand-bound closed state, we hypothesized that the NTD-driven control of Po might result from spontaneous oscillations of the NR2-NTD between an open-cleft conformation, favoring channel opening, and a closed-cleft conformation, favoring pore closure. Such ligand-independent oscillations have been observed in several clamshell-like proteins, including the bacterial maltose-binding-protein[23] (MBP) and the GABA-B receptor[24]. To test this

hypothesis, we introduced cysteines in the NR2-NTD cleft to lock open the NR2-NTDs using thiol-reactive MTS reagents. Based on 3D models, we first introduced a cysteine deep in the cleft of the NR2B-NTD by mutating the hinge residue NR2B-Y282, whose side chain points toward the cleft entrance (Fig. 2a and ref[25]). Application of the positively charged MTSEA potentiated NR1wt/NR2B-Y282C receptors but not control NR1wt/NR2B-Y282S receptors (Fig. 2b). Strikingly, using MTS compounds of same valence but different sizes, we observed that the larger the MTS, the greater the potentiation (Fig. 2b&c). Comparison of the rates of MK-801 inhibition before and after MTS treatment together with direct measurement of single-channel activity revealed that current potentiations reflected an increase in Po (Fig. S4 and S5). Sensitivity to glycine (binding the NR1-ABD) was unaltered by MTS treatment, while sensitivity to glutamate (binding the NR2-ABD) was slightly decreased (Fig. S6), as expected from the known allosteric interaction between the NR2 NTD and ABD[26]. Interestingly, MTS action was significantly faster on resting than activated receptors (Fig. S7), further arguing for a facilitated opening of the NR2-NTD when the ABD is open. Altogether, these results show that trapping open the NR2-NTD enhances receptor activity. They also indicate that the NTD of NR2B-Y282C is not permanently open (since there was a potentiating effect of the MTS compounds) nor closed (since the introduced cysteine was accessible to MTS), but rather alternates between open and closed conformations, the latter favoring pore closure.

Because NR2B-Y282 is a large residue, we considered the possibility that its mutation into a small residue (cysteine or serine) may have artificially increased the flexibility of the NTD hinge, favoring NTD closure. Indeed, such mutations strongly reduced receptor activity (Fig. S8). This effect highlights the unsuspected role of the NR2-NTD hinge in shaping NMDAR Po, reminiscent of the critical role of the MBP hinge in controlling the apparent maltose affinity[27]. To extend our conclusion of spontaneous NR2-NTD oscillations to receptors with unaltered gating properties, we targeted NR2B-NTD H127, since its mutation into cysteine minimally affects receptor activity (Fig. S8). MTS compounds still potentiated NR1wt/NR2B-H127C receptors (but not control NR1wt/NR2B-H127A receptors) in a size-dependent manner. However, potentiations were considerably smaller than with NR1wt/NR2B-Y282C receptors (Fig. 2c and Fig S9a). Two reasons may explain this difference: higher basal Po of NR1wt/NR2B-H127C receptors, and wider opening of the NTD at MTS-modified NR2B-Y282C subunits because of the deeper location in the cleft of Y282. Overall, these results provide the important new information that spontaneous oscillations of the NR2B-NTD contribute to the low Po of wt NR1/NR2B receptors.

We then tested the prediction that the high Po of NR2A-containing receptors results from the NR2A-NTD preferring the open conformation. As for NR2B, we found the Po of NR2A-containing receptors to be significantly reduced by the mutation of NR2A-Y281 into small residues (Fig. S8). A potentiating component was also observed at receptors containing NR2A-Y281C during treatment by MTS compounds, but not at control NR2A-Y281A receptors. However, MTS-induced potentiations were much smaller than at NR2B-Y282C receptors and were independent of MTS size (Fig. 2c and Fig S9b), suggesting that the NR2A-NTD is much less sensitive to steric hindrance than the NR2B-NTD. In addition, no potentiation was observed at NR2A-H128C receptors even with the large MTS-PtrEA (Fig. 2c and Fig S9b). This is consistent with the NR2A-NTD spending most of its time in an open-cleft conformation, thus contributing to the relatively high Po of NR2A-containing receptors.

Our results on chimeric NR2 subunits, showing that the NTD-ABD linker is required for the differential influence of the NR2-NTD on receptor Po, raised the possibility that this element is also crucial during allosteric modulation of NMDARs by NTD-ligands. NR2A-NTD forms a high affinity zinc inhibitory site[12–14]; accordingly, NR1wt/NR2D-(2A NTD+L) receptors were highly sensitive to zinc (Fig. 3a). NR1wt/NR2B-(2A NTD) receptors are also highly sensitive to zinc. Surprisingly, zinc appears much more potent at these receptors than at wt

NR1/NR2A receptors (Fig. 3a), suggesting that the NR2B NTD-ABD linker facilitates NTD-cleft closure. Increasing the chimera length to incorporate the NR2A NTD-ABD linker almost completely restored NR2Awt-like zinc sensitivity (Fig. 3a). This highlights again the importance of the NTD-ABD linker for the communication between the NTD and the gating machinery.

Proton is another allosteric modulator that differentially inhibits NMDAR subtypes[1]. In contrast with the zinc sensor, the proton sensor is thought to be closely associated with the channel gate[28]. Unexpectedly, deleting the NR2-NTDs fully abolished the difference in pH sensitivity between wt NR1/NR2A and NR1/NR2B receptors (Fig. 3b). Moreover, swapping the NTD+linker region between NR2A and NR2B reversed their pH sensitivities, while grafting the NR2A NTD+linker region onto NR2D decreased its proton sensitivity close to that of NR2Awt-containing receptors (Fig. 3b). Proton sensitivity was also decreased when locking open the NR2B-Y282C NTD with MTS-PtrEA (Fig. 3c). Hence, the NR2 dependence of pH sensitivity is unlikely to result from an intrinsic difference in the proton sensor between NR1/NR2 receptor subtypes, but rather from differential access to the proton binding-site owing to the NR2-NTD influence on channel activity.

Our study reveals that the large differences in channel activity conferred by the various NR2 NMDAR subunits originate from a region remote from the agonist-binding/channel gating core. This region comprises the large NR2-NTD and the short linker connecting the NR2-NTD to the ABD. The bilobate NR2-NTD oscillates spontaneously between open-cleft and closed-cleft conformations (Fig. 4), the latter triggering disruption of the ABD dimer interface and subsequent channel closure[20]. The NTD-ABD linker could exert its key influence by tuning the equilibrium between the different conformations of the NR2-NTD. The identity of the NR2-NTD+linker region also determines the sensitivity to zinc and protons, two endogenous allosteric inhibitors of NMDARs that are likely to be critical in the regulation of NMDAR activity under physiological and pathological conditions[1,3]. Through its dynamic conformational equilibrium, the NR2-NTD could serve as a target for either negative or positive subunit-specific allosteric modulators (Fig. 4). Compounds like ifenprodil, which bind the NTD cleft and promote its closure (NTD “closers”), behave as subunit-specific NMDAR inhibitors and show good efficacy as neuroprotectants[2]. We propose that molecules that bind the same cleft but impede its closure (NTD “openers”) would behave as NMDAR potentiators (Fig. 4). Such molecules may prove of significant therapeutic benefit, given the accumulating evidence that major human psychoses, including schizophrenia, are associated with a deficit of NMDAR activity[2,29].

METHODS SUMMARY

cDNA constructs and site-directed mutagenesis

The pcDNA3-based expression plasmids, mutagenesis and sequencing procedure have been described previously[19]. Chimeras were obtained by classical PCR amplification and subsequent subcloning into the parental clone.

Electrophysiology

Recombinant NMDARs were expressed in *Xenopus laevi* oocytes after co-injection of cDNAs (at 10 ng/μl; nuclear injection) coding for the various NR1 and NR2 subunits (ratio 1:1). Oocytes were prepared, injected, voltage-clamped and superfused as described previously[12]. Single-channels were recorded from HEK cell outside-out patches.

Methods

Two electrode voltage-clamp recordings and analysis

For all experiments, except for those aimed at measuring pH sensitivity, the standard external solution contained (in mM): 100 NaCl, 2.5 KCl, 0.3 $BaCl_2$, 5 HEPES (pH 7.3). To chelate trace amounts of contaminant zinc, DTPA (10 μM) was added in all the "0" zinc solutions[31]. For free zinc concentrations in the 1 nM-1 μM range, tricine (10 mM) was used to buffer zinc, while ADA (1 mM) was used to buffer zinc in the 0.1–100 nM range[20]. For the pH sensitivity experiments, an enriched HEPES external solution was used to insure proper pH buffering[20]. Currents were elicited by co-application of saturating concentrations of glutamate and glycine (100 μM each), and measured at a holding potential of −60 mV. MTS compounds were used at 0.2 mM (except for Fig. S7). Experiments were done at room temperature. Data collection and analysis of pH and zinc dose-response curves were performed according to ref[20]. MK-801 time constants of inhibition were obtained by fitting currents with a monoexponential component within a window corresponding to 10%–90% of the maximal inhibition. Data points used for statistical tests were supposed log-normally distributed prior to a Student's t-test (unless otherwise indicated).

Single-channel recordings and analysis

HEK cells were transfected with 2 μg of cDNAs mixed at a ratio of 1 NR1:3 NR2:3 GFP using calcium phosphate precipitation or FuGENE Transfection Reagent (Roche). Positive cells were visualized by GFP epi-fluorescence. Patch pipettes of 5–10 MΩ were filled with a solution containing (in mM): 115 CsF, 10 CsCl, 10 HEPES, 10 EGTA (pH 7.15 with CsOH). Osmolality was 270 mosm/kg. The standard external solution contained (in mM): 140 NaCl, 2.8 KCl, 0.5 $CaCl_2$, 10 HEPES, 0.01 EDTA (pH 7.3 with NaOH). Osmolality was adjusted to 290 mosm/kg with sucrose. EDTA was added to chelate trace amounts of contaminant zinc[31]. Channel openings were activated by 100 μM glycine, with 0.05 or 0.01 μM glutamate in most experiments, or with 100 μM glutamate in some patches (included only if no double openings were observed). The holding potential (after correction for junction potential) was −80 to −90 mV. Experiments were performed at room temperature. Currents were recorded with an Axopatch 200B amplifier (Molecular Devices), sampled at 20 to 50 kHz, low-pass filtered (8-pole Bessel) at 5 to 10 kHz. Prior to analysis of Po within a burst, data were digitally refiltered to give a cascaded low-pass filter cutoff frequency of 2 kHz. pClamp 9 or 10 (Molecular Devices) was used to acquire and analyze the data.

The principal goal of single-channel analysis was to measure the open probability (P_{open}) within bursts of channel openings, which provides a good estimate of the P_{open} within an NMDAR activation[6,32,33]. To idealize single-channel data, transitions were detected using a 50% threshold criterion[34]. Events of ≤200 μs duration were excluded from analysis. Missing and ignoring brief events can significantly influence dwell-time histograms. However, such brief events contribute only a tiny fraction of the total time that a channel spends open or closed. Thus, missed events should not have significantly affected measurements of P_{open}. Histograms are presented as square root vs. log time plots[35]. Shut-time histograms were fitted with 3 or 4 exponential components. A burst was defined as a series of openings separated by closures of duration less than a critical duration, Tcrit. Bursts with two levels of openings were discarded. We calculated Tcrit between the two longest components of the shut-time histograms so that total number of event misclassifications is minimized[34,36]. For NR1wt/NR2Awt and NR1wt/NR2B-(2A NTD+L) receptors, the two longest components of the shut-time distribution differed by a mean factor > 390, while these components were less separated for NR1wt/NR2Bwt and NR1wt/NR2A-(2B NTD+L) (23-fold and 54-fold separation, respectively). For the latter two constructs, the separation between shut-time components results in a greater than desired number of misclassification of shut times[34]. This may have lead to an overestimation

of the P_{open} within a burst. However, for wild-type receptors, our data are overall consistent with previous results[6,33], suggesting that our P_{open} estimates are reliable.

Chemicals

HEPES, L-glutamate, glycine, DTPA, EDTA, tricine and ADA were obtained from Sigma, D-APV from Ascent Scientific, 2-aminoethylmethanethiosulfonatehydrobromide (MTSEA), [2-(trimethylammonium)ethyl]methanethiosulfonatebromide (MTSET) and 3-(triethylammonium)propylmethanethiosulfonatebromide (MTS-PtrEA) from Toronto Research Chemicals, (+)MK-801 from Tocris. MTS compounds were prepared as 40 mM stock solutions in bi-distilled water, aliquoted in small volumes (50 μL) and stored at −20°C; aliquots were thawed just before use.

Construction of Figure 4

The molecular architecture shown in figure 4a was illustrated by the crystal structure of the mGluR1 ligand-binding domain dimer (pdb 1ewv, ref[37]) at the level of the NTD, the NMDAR NR1/NR2A agonist-binding domain dimer (pdb 2a5T, ref[30]) and two subunits of the KcsA tetramer (pdb 1bl8, ref[38]) as the transmembrane region of the receptor. The fourth transmembrane segment and the C-terminal cytoplasmic region are lacking in this structural depiction.

Supplementary Material

Refer to Web version on PubMed Central for supplementary material.

References

1. Dingledine R, Borges K, Bowie D, Traynelis SF. The glutamate receptor ion channels. Pharmacol Rev 1999;51:7–61. [PubMed: 10049997]
2. Kemp JA, McKernan RM. NMDA receptor pathways as drug targets. Nat Neurosci 2002;5:1039–1042. [PubMed: 12403981]
3. Paoletti P, Neyton J. NMDA receptor subunits: function and pharmacology. Curr Opin Pharmacol 2007;7:39–47. [PubMed: 17088105]
4. Cull-Candy SG, Leszkiewicz DN. Role of distinct NMDA receptor subtypes at central synapses. Sci STKE 2004;2004:re16. [PubMed: 15494561]
5. Chen N, Luo T, Raymond LA. Subtype-dependence of NMDA receptor channel open probability. J Neurosci 1999;19:6844–6854. [PubMed: 10436042]
6. Erreger K, Dravid SM, Banke TG, Wyllie DJ, Traynelis SF. Subunit-specific gating controls rat NR1/NR2A and NR1/NR2B NMDA channel kinetics and synaptic signalling profiles. J Physiol 2005;563:345–358. [PubMed: 15649985]
7. Wyllie DJ, Behe P, Colquhoun D. Single-channel activations and concentration jumps: comparison of recombinant NR1a/NR2A and NR1a/NR2D NMDA receptors. J Physiol 1998;510(Pt 1):1–18. [PubMed: 9625862]
8. Dravid SM, Prakash A, Traynelis SF. Activation of recombinant NR1/NR2C NMDA receptors. J Physiol 2008;586:4425–4439. [PubMed: 18635641]
9. Popescu G, Robert A, Howe JR, Auerbach A. Reaction mechanism determines NMDA receptor response to repetitive stimulation. Nature 2004;430:790–793. [PubMed: 15306812]
10. Liu Y, et al. NMDA receptor subunits have differential roles in mediating excitotoxic neuronal death both in vitro and in vivo. J Neurosci 2007;27:2846–2857. [PubMed: 17360906]
11. Liu L, et al. Role of NMDA receptor subtypes in governing the direction of hippocampal synaptic plasticity. Science 2004;304:1021–1024. [PubMed: 15143284]
12. Paoletti P, et al. Molecular organization of a zinc binding N-terminal modulatory domain in a NMDA receptor subunit. Neuron 2000;28:911–925. [PubMed: 11163276]

13. Low CM, Zheng F, Lyuboslavsky P, Traynelis SF. Molecular determinants of coordinated proton and zinc inhibition of N-methyl-D-aspartate NR1/NR2A receptors. Proc Natl Acad Sci U S A 2000;97:11062–11067. [PubMed: 10984504]
14. Choi YB, Lipton SA. Identification and mechanism of action of two histidine residues underlying high-affinity Zn^{2+} inhibition of the NMDA receptor. Neuron 1999;23:171–180. [PubMed: 10402203]
15. Perin-Dureau F, Rachline J, Neyton J, Paoletti P. Mapping the binding site of the neuroprotectant ifenprodil on NMDA receptors. J Neurosci 2002;22:5955–5965. [PubMed: 12122058]
16. Jones KS, VanDongen HM, VanDongen AM. The NMDA receptor M3 segment is a conserved transduction element coupling ligand binding to channel opening. J Neurosci 2002;22:2044–2053. [PubMed: 11896144]
17. Yuan H, Erreger K, Dravid SM, Traynelis SF. Conserved structural and functional control of N-methyl-D-aspartate receptor gating by transmembrane domain M3. J Biol Chem 2005;280:29708–29716. [PubMed: 15970596]
18. Blanke ML, VanDongen AM. Constitutive activation of the N-methyl-D-aspartate receptor via cleft-spanning disulfide bonds. J Biol Chem 2008;283:21519–21529. [PubMed: 18450751]
19. Rachline J, Perin-Dureau F, Le Goff A, Neyton J, Paoletti P. The micromolar zinc-binding domain on the NMDA receptor subunit NR2B. J Neurosci 2005;25:308–317. [PubMed: 15647474]
20. Gielen M, et al. Structural rearrangements of NR1/NR2A NMDA receptors during allosteric inhibition. Neuron 2008;57:80–93. [PubMed: 18184566]
21. Sun Y, et al. Mechanism of glutamate receptor desensitization. Nature 2002;417:245–253. [PubMed: 12015593]
22. Mayer ML. Glutamate receptors at atomic resolution. Nature 2006;440:456–462. [PubMed: 16554805]
23. Tang C, Schwieters CD, Clore GM. Open-to-closed transition in apo maltose-binding protein observed by paramagnetic NMR. Nature 2007;449:1078–1082. [PubMed: 17960247]
24. Kniazeff J, et al. Locking the dimeric GABA(B) G-protein-coupled receptor in its active state. J Neurosci 2004;24:370–377. [PubMed: 14724235]
25. Mony L, et al. Structural basis of NR2B-selective antagonist recognition by N-methyl-D-aspartate receptors. Mol Pharmacol 2009;75:60–74. [PubMed: 18923063]
26. Zheng F, et al. Allosteric interaction between the amino terminal domain and the ligand binding domain of NR2A. Nat Neurosci 2001;4:894–901. [PubMed: 11528420]
27. Marvin JS, Hellinga HW. Manipulation of ligand binding affinity by exploitation of conformational coupling. Nat Struct Biol 2001;8:795–798. [PubMed: 11524684]
28. Low CM, et al. Molecular determinants of proton-sensitive N-methyl-D-aspartate receptor gating. Mol Pharmacol 2003;63:1212–1222. [PubMed: 12761330]
29. Lisman JE, et al. Circuit-based framework for understanding neurotransmitter and risk gene interactions in schizophrenia. Trends Neurosci 2008;31:234–242. [PubMed: 18395805]
30. Furukawa H, Singh SK, Mancusso R, Gouaux E. Subunit arrangement and function in NMDA receptors. Nature 2005;438:185–192. [PubMed: 16281028]
31. Paoletti P, Ascher P, Neyton J. High-affinity zinc inhibition of NMDA NR1-NR2A receptors. J Neurosci 1997;17:5711–5725. [PubMed: 9221770]
32. Erreger K, Traynelis SF. Zinc inhibition of rat NR1/NR2A N-methyl-D-aspartate receptors. J Physiol 2008;586:763–778. [PubMed: 18048453]
33. Schorge S, Elenes S, Colquhoun D. Maximum likelihood fitting of single channel NMDA activity with a mechanism composed of independent dimers of subunits. J Physiol 2005;569:395–418. [PubMed: 16223763]
34. Colquhoun, D.; Sigworth, FJ. Single-Channel Recording. Sakmann, B.; Neher, E., editors. New York: Plenum Press; 1995. p. 483-587.
35. Sigworth FJ, Sine SM. Data transformations for improved display and fitting of single-channel dwell time histograms. Biophys J 1987;52:1047–1054. [PubMed: 2447968]

36. Jackson MB, Wong BS, Morris CE, Lecar H, Christian CN. Successive openings of the same acetylcholine receptor channel are correlated in open time. Biophys J 1983;42:109–114. [PubMed: 6301575]

37. Kunishima N, et al. Structural basis of glutamate recognition by a dimeric metabotropic glutamate receptor. Nature 2000;407:971–977. [PubMed: 11069170]

38. Doyle DA, et al. The structure of the potassium channel: molecular basis of K^+ conduction and selectivity. Science 1998;280:69–77. [PubMed: 9525859]

Acknowledgements

This work was supported by Ministère de la Recherche (MG, LM), UPMC and FRM (MG), NIH grant R01 MH045817 (JWJ), INSERM, ANR, GlaxoSmithKline and Equipe FRM grant (PP). We thank Boris Barbour, Pierre-Jean Corringer, Jacques Neyton and David Stroebel for comments on the manuscript; Stéphanie Carvalho, Mariano Casado and Marie Gendrel for experimental help.

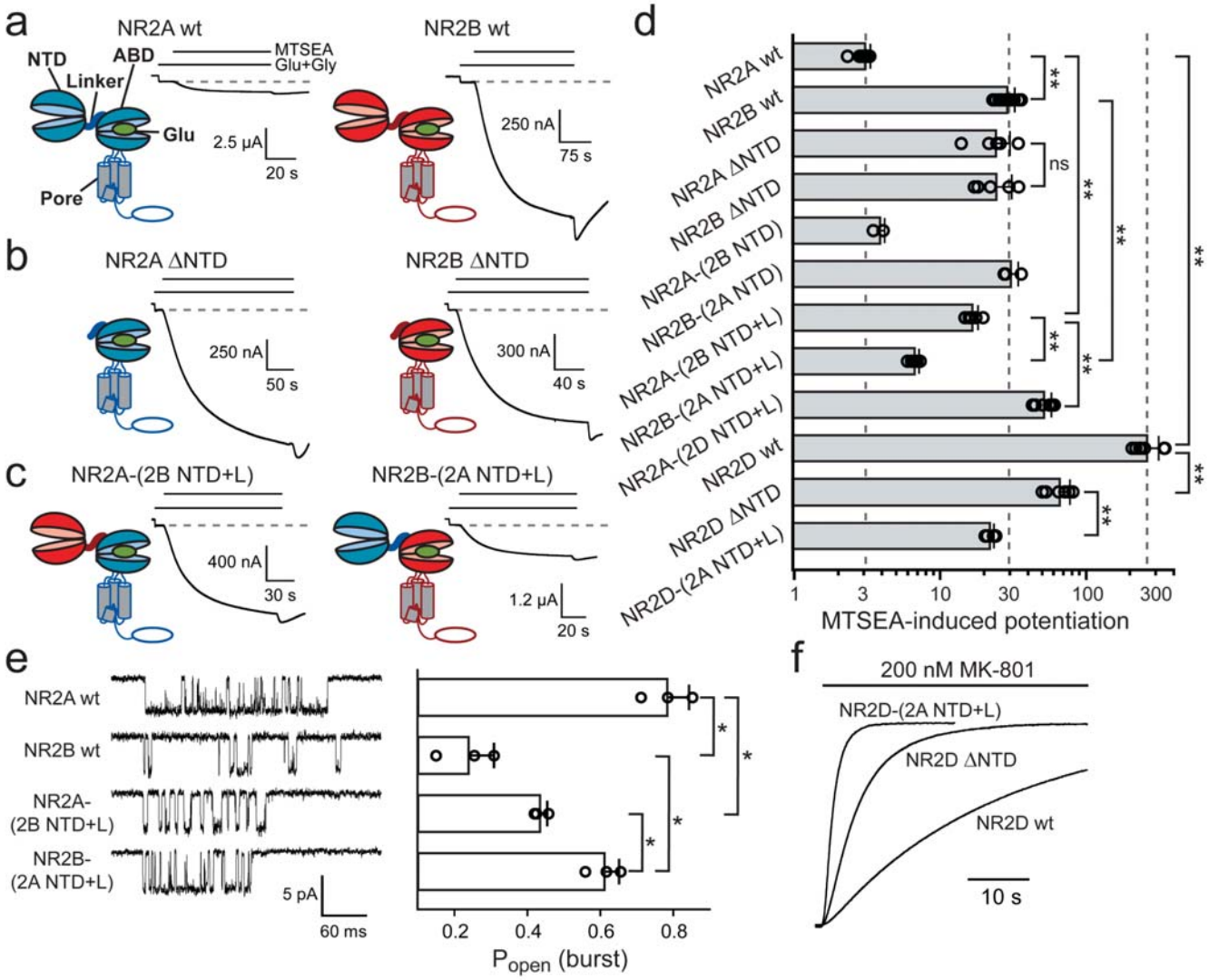

Figure 1. The NR2 NTD+linker region controls NMDAR Po

a–c Potentiation by MTSEA of receptors incorporating NR1-A652C and the indicated NR2 subunits. NTD, N-terminal domain; ABD, agonist-binding domain. **d** Pooled data (mean +/− s.d.), from top to bottom: 3.2 +/− 0.3 (n=12), 30 +/− 4 (n=14), 25 +/− 6 (n=6), 25 +/− 7 (n=5), 4.0 +/− 0.3 (n=3), 32 +/− 4 (n=3), 17 +/− 2 (n=6), 6.9 +/− 0.5 (n=5), 53 +/− 7 (n=9), 270 +/− 60 (n=7), 68 +/− 12 (n=6) and 23 +/− 2 (n=5) (**p<0.001). **e** Po within bursts of openings for receptors incorporating NR1wt and the indicated NR2 subunit. Left: representative traces of bursts. Right (from top to bottom): 0.78 +/− 0.06 (n=3), 0.24 +/− 0.07 (n=3), 0.43 +/− 0.02 (n=3) and 0.61 +/− 0.04 (n=3) (*p<0.05, Student's t-test). **f** Kinetics of inhibition by MK-801 at receptors incorporating NR1wt and NR2Dwt (τ_{on} = 32 s), NR2D-ΔNTD (5.7 s) or NR2D-(2A NTD+L) (1.6 s). Error bars represent s.d.

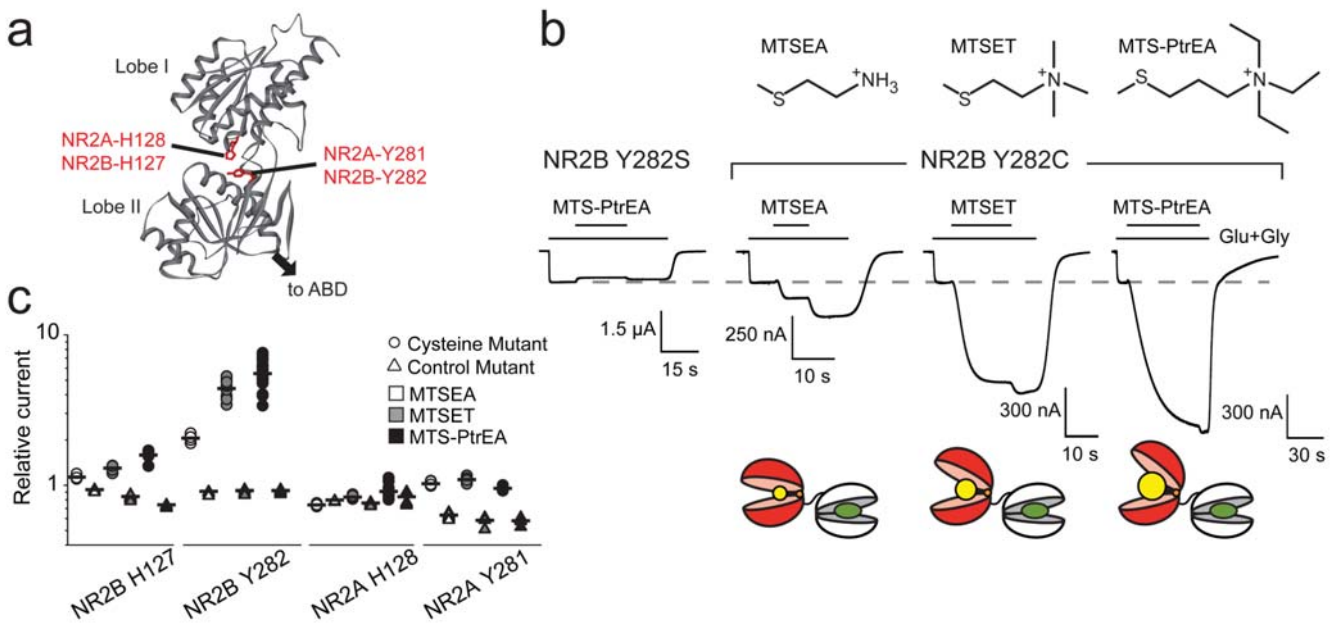

Figure 2. Locking open the NR2-NTD increases NMDAR activity

a 3D model of NR2B-NTD. **b** Top: chemical formula of the transferable moiety of MTSEA, MTSET and MTS-PtrEA. Middle: Recordings from NR1wt/NR2B-Y282C and control NR1wt/NR2B-Y282S receptors during MTS treatment. The potentiation upon MTS wash likely reflects the washout of a reversible pore-blocking effect of the positively charged MTS. Bottom: Schematic representations of the NTD-ABD tandem of NR2B-Y282C after MTS-modification (MTS head group in yellow). **c** Relative currents after application of MTSEA, MTSET and MTS-PtrEA to receptors incorporating NR1wt and the indicated NR2 subunit. See Table S1 for values.

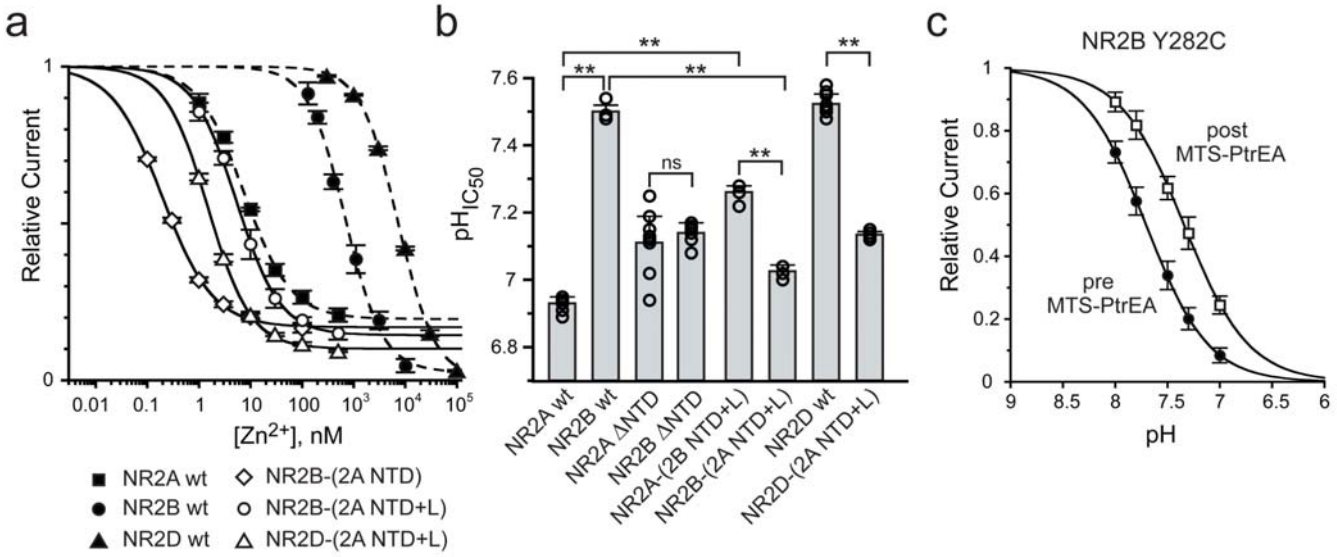

Figure 3. The NR2 NTD+linker region controls zinc and proton sensitivities of NMDARs

a Zinc sensitivity of receptors incorporating NR1wt and ($Inhib_{max}$, IC_{50}): NR2Awt (81%, 7.5 nM [n=6]), NR2Bwt (98%, 720 nM [n = 13]), NR2Dwt (100%, 7.8 μM [n=3]), NR2B-(2A NTD) (83%, 0.20 nM [n=4]), NR2B-(2A NTD+L) (86%, 5.4 nM [n=4]) or NR2D-(2A NTD +L) (90%, 1.5 nM [n=5]). n_H in the 0.9–1.2 range. **b** pH_{IC50} of receptors incorporating NR1wt and the indicated NR2 subunit. See Table S2 for values. (**p<0.001). **c** Proton sensitivity of NR1wt/NR2B-Y282C receptors before (pH_{IC50} = 7.70, n_H = 1.5 [n=3]) and after (pH_{IC50} = 7.34, n_H = 1.4 [n=3]) MTS-PtrEA modification. Error bars represent s.d.

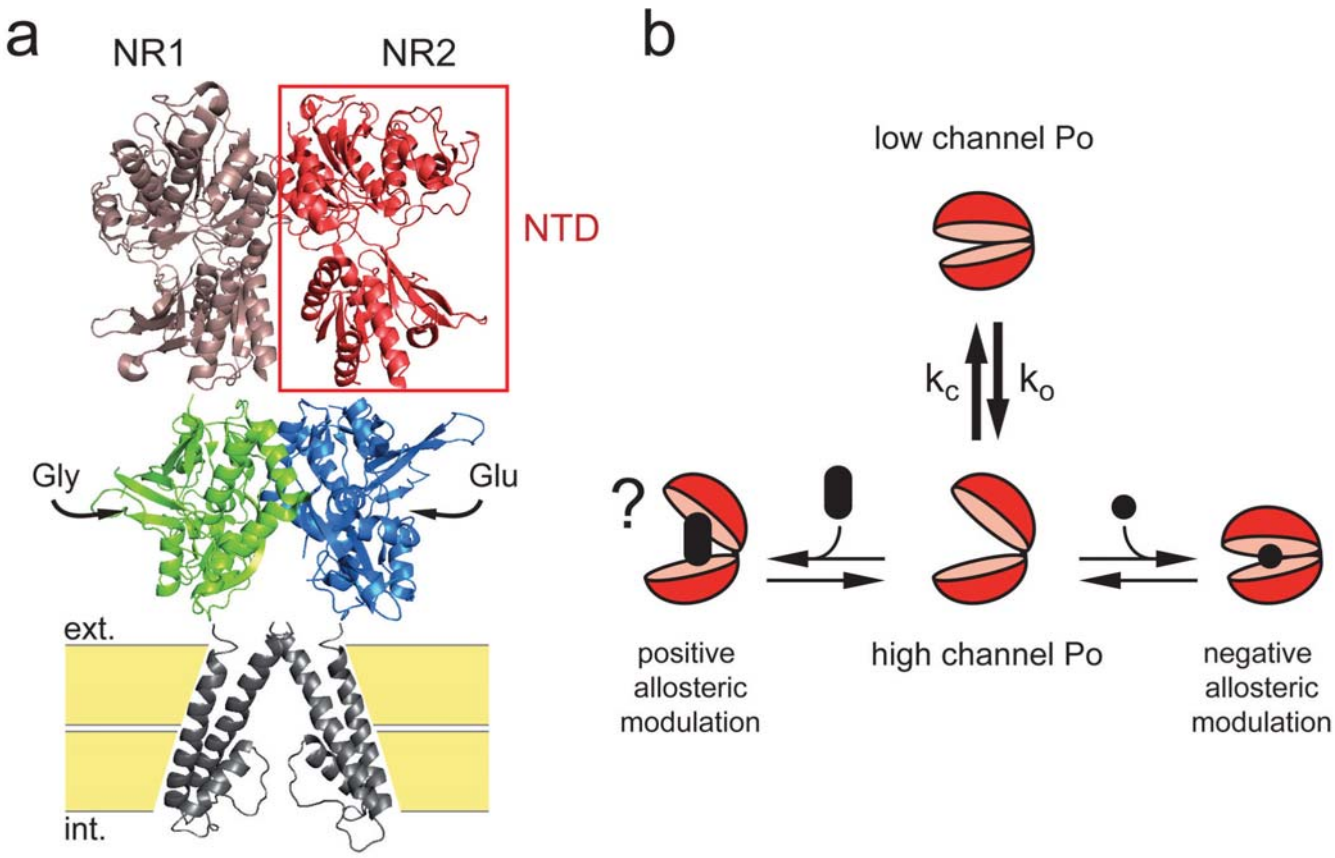

Figure 4. Model for the control of NMDAR activity by the NR2 N-terminal domain

a Structural depiction of an NMDAR. The full receptor is a tetramer but only a NR1/NR2 dimer is shown[30]. **b** In its ligand-free state, the NR2-NTD alternates between open- and closed-cleft conformations, the latter favoring pore closure. In the model, this equilibrium determines the subtype-specificity of NMDAR Po (ko/kc[NR2B] < ko/kc[NR2A]). The NTD is also the target of subunit-specific allosteric inhibitors such as zinc[12–14,19] or ifenprodil[15,25], which bind the NTD central cleft and promote domain closure. We hypothesize that a molecule binding in the same cleft, but preventing its closure, behaves as a positive allosteric modulator, enhancing receptor activity.

APPENDIX B

FUNCTIONAL OUTCOMES OF MUTANT NMDAR EXPRESSION

Table 5.1 Functional outcomes of mutant NMDAR expression

NMDAR Subunit Composition	Outcome
NR1(L614A)/2A	-
NR1(W611K)/2A	-
NR1(W611F)/2A	+
NR1(L614S)/2A	-
NR1(W611F)/2A(S632F)	+
NR1(W611F)/2A(S632L)	+
NR1(W611K)/2A(S632K)	-
NR1(W611K)/2A(S632L)	-
NR1(W611A)/2A(S632L)	+
NR1(W611K)/2A(S632D)	-
NR1(W608A)/2A(S632L)	-
NR1(W608A)/2A(S632W)	-
NR1(W611A)/2A(S632W)	#
NR1(L615A)/2A(S632L)	+
NR1(W611S)/2A(S632W)	#
NR1(W611K)/2A(S632D)	-

\+ Sufficient NMDAR-mediated current to yield consistent Mg^{2+} IC_{50} measurements
\- No detectable NMDAR-mediated current at -65 mV
\# NMDAR-mediated currents too small to yield consistent Mg^{2+} IC_{50} measurements

APPENDIX C

COMPARISON OF NMDAR RELATIVE PERMEABILITIES FROM PREVIOUS STUDIES

Table 5.2 Comparison to previously published relative Ca^{2+} permeability values

Study	Conditions	Measure, $[Ca^{2+}]$	NMDAR Subtype	Calculation basis	Value
Siegler Retchless	Biionic, HEK	$P_{Ca}/P_{Cs,}$ 1.8 mM	NR1/2A	ΔE_{rev} / ΔE_{rev}*	7.7 / 18.5
	Biionic, HEK	$P_{Ca}/P_{Cs,}$ 1.8 mM	NR1/2B	ΔE_{rev} / ΔE_{rev}*	7.3 / 17.5
	Biionic, HEK	$P_{Ca}/P_{Cs,}$ 1.8 mM	NR1/2C	ΔE_{rev} / ΔE_{rev}*	5.6 / 13.4
	Biionic, HEK	$P_{Ca}/P_{Cs,}$ 1.8 mM	NR1/2D	ΔE_{rev} / ΔE_{rev}*	4.2 / 10.1
	Biionic, HEK	$P_{Ca}/P_{Cs,}$ 10 mM	NR1/2A	ΔE_{rev} / ΔE_{rev}*	4.5 / 10.4
	Biionic, HEK	$P_{Ca}/P_{Cs,}$ 10 mM	NR1/2B	ΔE_{rev} / ΔE_{rev}*	5.0 / 11.6
	Biionic, HEK	$P_{Ca}/P_{Cs,}$ 10 mM	NR1/2C	ΔE_{rev} / ΔE_{rev}*	3.1 / 7.2
	Biionic, HEK	$P_{Ca}/P_{Cs,}$ 10 mM	NR1/2D (low permeability)	ΔE_{rev} / ΔE_{rev}*	3.7 / 8.6
	Biionic, HEK	$P_{Ca}/P_{Cs,}$ 10 mM	NR1/2D (high permeability)	ΔE_{rev} / ΔE_{rev}*	7.8 / 18.1
	Biionic, HEK	$P_{Ca}/P_{Cs,}$ 1.8 mM	NR1/2A	E_{rev} / E_{rev} *	6.6 / 15.4
	Biionic, HEK	$P_{Ca}/P_{Cs,}$ 1.8 mM	NR1/2B	E_{rev} / E_{rev} *	6.6 / 15.3
	Biionic, HEK	$P_{Ca}/P_{Cs,}$ 1.8 mM	NR1/2C	E_{rev} / E_{rev} *	4.8 / 11.1
	Biionic, HEK	$P_{Ca}/P_{Cs,}$ 10 mM	NR1/2A	E_{rev} / E_{rev} *	3.7 / 8.6
	Biionic, HEK	$P_{Ca}/P_{Cs,}$ 10 mM	NR1/2B	E_{rev} / E_{rev} *	4.4 / 10.2
	Biionic, HEK	$P_{Ca}/P_{Cs,}$ 10 mM	NR1/2C	E_{rev} / E_{rev} *	2.5 / 5.8

Study	Conditions	Measure, $[Ca^{2+}]$	NMDAR Subtype	Calculation basis	Value
Mayer & Westbrook (1987)	Multiple ions, hippocampal & spinal neurons	$P_{Ca}/P_{Na,}$ 0.3 - 50 mM		ΔE_{rev}* fit	10.6
	Multiple ions, hippocampal & spinal neurons	$P_{Ca}/P_{Na,}$ 0.3 - 50 mM		ΔE_{rev} fit	4.03
Iino et al. (1990)	Biionic, hippocampal neurons	$P_{Ca}/P_{Cs,}$ 10 mM		E_{rev} / E_{rev}*	6.2 / 14.3
Zarei & Dani (1994)	Multiple ions, hippocampal neurons	$P_{Ca}/P_{Cs,}$ 1.5 - 30 mM		ΔE_{rev}*	12
Tsuzuki et al. (1994)	Biionic, oocytes, single-channel	$P_{Ca}/P_{Na,}$ 83 mM	NR1/2B	ΔE_{rev}	3.6
Burnashev et al. (1995)	Biionic, HEK	$P_{Ca}/P_{Cs,}$ 102 mM	NR1/2A	E_{rev}*	4.12
	Biionic, HEK	$P_{Ca}/P_{Cs,}$ 102 mM	NR1/2C	E_{rev}*	2.72
	Multiple ions, HEK	$P_{Ca}/P_{Cs,}$ 102 mM	NR1/2A	P_f*	3.1
	Multiple ions, HEK	$P_{Ca}/P_{Cs,}$ 102 mM	NR1/2C	P_f*	2.23
Schneggenberger (1996)	Multiple ions, HEK	$P_{Ca}/P_{Na,}$ 0.1 - 10 mM	NR1/2A	ΔE_{rev} fit	3.6

Study	Conditions	Measure, $[Ca^{2+}]$	NMDAR Subtype	Calculation basis	Value
Schneggenberger (1996)	Multiple ions, HEK	$P_{Ca}/P_{Na,}$ 0.1 - 10 mM	NR1/2A	ΔE_{rev}* fit	5.1
Wollmuth et al. (1996)	Biionic, oocytes, macropatches	$P_{Ca}/P_{K,}$ 1 mM	NR1/2A	ΔE_{rev}	7.1
Iino et al (1997)	Multiple ions, oocytes, single-channel	$P_{Ca}/P_{Na,}$ 0.1 - 30 mM	NR1/2B	ΔE_{rev}* fit	17
Wollmuth & Sakmann (1998)	Biionic, HEK	$P_{Ca}/P_{Cs,}$ 1.8 mM	NR1/2A	ΔE_{rev}	6.1
	Biionic, HEK	$P_{Ca}/P_{Cs,}$ 10 mM	NR1/2A	ΔE_{rev}	4.2
	Biionic, HEK	$P_{Ca}/P_{Cs,}$ 100 mM	NR1/2A	ΔE_{rev}	2.6
	Biionic, HEK	$P_{Ca}/P_{Cs,}$ 0.18 - 100	NR1/2A	ΔE_{rev} fit	4.8
Watanabe et al. (2002)	Biionic, HEK	$P_{Ca}/P_{Cs,}$ 1.8 mM	NR1/2A	ΔE_{rev}	6.4
Jatzke et al. (2002)	Biionic, HEK	$P_{Ca}/P_{Cs,}$ 1.8 mM	NR1/2A	ΔE_{rev}	5.7◆
	Biionic, HEK	$P_{Ca}/P_{Na,}$1.8	NR1/2A	ΔE_{rev}	7.2
	Multiple ions, HEK	$P_{Ca}/P_{Na,}$ 1.8 mM	NR1/2A	P_f / P_f *	3 / 3.8
	Biionic, HEK	$P_{Ca}/P_{Cs,}$ 10 mM	NR1/2A	ΔE_{rev}	4.0◆
	Biionic, HEK	$P_{Ca}/P_{Na,}$ 10 mM	NR1/2A	ΔE_{rev}	5.1◆
	Biionic, HEK	$P_{Ca}/P_{Cs,}$ 110 mM	NR1/2A	ΔE_{rev}	2.5◆
	Biionic, HEK	$P_{Ca}/P_{Na,}$ 110 mM	NR1/2A	ΔE_{rev}	3.6◆

Unless otherwise noted, data were gathered in the whole-cell recording configuration.

* Calculations based on ionic activities (*a)*, rather than concentrations, where:

$$a_{ion} = \gamma\ [\text{ion}]$$

Activity coefficients (γ) values varied among studies. Wollmuth and Sakmann (1998), for instance, used γ = 0.31, 0.30, 0.26 and 0.72 for 1.8 mM Ca^{2+}, 10 mM Ca^{2+}, 110 mM Ca^{2+} and 143.5 mM Cs^{+}, respectively (I used these values for my calculations, as well). In contrast, Jatzke et al. (2002) and Burnashev et al. (1995) used γ = 0.57 for 1.8 mM Ca^{2+}, γ = 0.52 for 102 mM Ca^{2+}, and γ = 0.72 for 143.5 mM Cs^{+}.

- Values estimated from graphs and comments in text

ΔE_{rev} calculations were performed by comparinng the reversal potentials (V_{rev}, or E) of two solutions, as in Wollmuth & Sakmann (1998):

$$\Delta E_{rev} = V_{rev(Ca)} - V_{rev(Cs)} = \frac{RT}{F} \ln \frac{4\frac{P_{Ca}}{P_{Cs}} \times [Ca^{2+}]_o}{[Cs]_o \times (1 + e^{\frac{V_{rev(Ca)}}{(RT)/F}})}$$

E_{rev} calculations were performed using one reversal potential, as in Iino et al. (1990):

$$\frac{P_{Ca}}{P_{Cs}} = \frac{[Cs]_i}{4[Ca]_o} \times e^{\frac{EF}{RT}} \times (e^{\frac{EF}{RT}} + 1)$$

P_f* calculations were performed as in Burnashev et al. (1995) or Jatzke et al. (2002).

ΔE_{rev} fit and **E_{rev} fit** calculations were performed by fitting a function defined by the Goldman-Hodgkin-Katz current equation using E_{rev} or ΔE_{rev} data gathered in several concentrations of external Ca^{2+}, as in Iino et al. (1990).

BIBLIOGRAPHY

Alam, A., and Jiang, Y. (2009). Structural analysis of ion selectivity in the NaK channel. Nat Struct Mol Biol *16*, 35-41.

Alam, A., Shi, N., and Jiang, Y. (2007). Structural insight into Ca2+ specificity in tetrameric cation channels. Proc Natl Acad Sci U S A *104*, 15334-15339.

Antonov, S.M., Gmiro, V.E., and Johnson, J.W. (1998). Binding sites for permeant ions in the channel of NMDA receptors and their effects on channel block. Nat Neurosci *1*, 451-461.

Antonov, S.M., and Johnson, J.W. (1999). Permeant ion regulation of N-methyl-D-aspartate receptor channel block by Mg(2+). Proc Natl Acad Sci U S A *96*, 14571-14576.

Armstrong, N., and Gouaux, E. (2000). Mechanisms for activation and antagonism of an AMPA-sensitive glutamate receptor: crystal structures of the GluR2 ligand binding core. Neuron *28*, 165-181.

Armstrong, N., Jasti, J., Beich-Frandsen, M., and Gouaux, E. (2006). Measurement of conformational changes accompanying desensitization in an ionotropic glutamate receptor. Cell *127*, 85-97.

Armstrong, N., Mayer, M., and Gouaux, E. (2003). Tuning activation of the AMPA-sensitive GluR2 ion channel by genetic adjustment of agonist-induced conformational changes. Proc Natl Acad Sci U S A *100*, 5736-5741.

Armstrong, N., Sun, Y., Chen, G.Q., and Gouaux, E. (1998). Structure of a glutamate-receptor ligand-binding core in complex with kainate. Nature *395*, 913-917.

Ascher, P., and Nowak, L. (1988). The role of divalent cations in the N-methyl-D-aspartate responses of mouse central neurones in culture. J Physiol *399*, 247-266.

Bahring, R., Bowie, D., Benveniste, M., and Mayer, M.L. (1997). Permeation and block of rat GluR6 glutamate receptor channels by internal and external polyamines. J Physiol *502 (Pt 3)*, 575-589.

Bailey, A., Kelland, E.E., Thomas, A., Biggs, J., Crawford, D., Kitchen, I., and Toms, N.J. (2001). Regional mapping of low-affinity kainate receptors in mouse brain using [(3)H](2S,4R)-4-methylglutamate autoradiography. Eur J Pharmacol *431*, 305-310.

Banke, T.G., Dravid, S.M., and Traynelis, S.F. (2005). Protons trap NR1/NR2B NMDA receptors in a nonconducting state. J Neurosci *25*, 42-51.

Beck, C., Wollmuth, L.P., Seeburg, P.H., Sakmann, B., and Kuner, T. (1999). NMDAR channel segments forming the extracellular vestibule inferred from the accessibility of substituted cysteines. Neuron *22*, 559-570.

Benveniste, M., and Mayer, M.L. (1993). Multiple effects of spermine on N-methyl-D-aspartic acid receptor responses of rat cultured hippocampal neurones. J Physiol *464*, 131-163.

Bernard, A., and Khrestchatisky, M. (1994). Assessing the extent of RNA editing in the TMII regions of GluR5 and GluR6 kainate receptors during rat brain development. J Neurochem *62*, 2057-2060.

Bortolotto, Z.A., Lauri, S., Isaac, J.T., and Collingridge, G.L. (2003). Kainate receptors and the induction of mossy fibre long-term potentiation. Philos Trans R Soc Lond B Biol Sci *358*, 657-666.

Bowie, D. (2008). Ionotropic glutamate receptors & CNS disorders. CNS Neurol Disord Drug Targets *7*, 129-143.

Bowie, D., and Mayer, M.L. (1995). Inward rectification of both AMPA and kainate subtype glutamate receptors generated by polyamine-mediated ion channel block. Neuron *15*, 453-462.

Burnashev, N. (1996). Calcium permeability of glutamate-gated channels in the central nervous system. Curr Opin Neurobiol *6*, 311-317.

Burnashev, N., Monyer, H., Seeburg, P.H., and Sakmann, B. (1992a). Divalent ion permeability of AMPA receptor channels is dominated by the edited form of a single subunit. Neuron *8*, 189-198.

Burnashev, N., Schoepfer, R., Monyer, H., Ruppersberg, J.P., Gunther, W., Seeburg, P.H., and Sakmann, B. (1992b). Control by asparagine residues of calcium permeability and magnesium blockade in the NMDA receptor. Science *257*, 1415-1419.

Burnashev, N., Zhou, Z., Neher, E., and Sakmann, B. (1995). Fractional calcium currents through recombinant GluR channels of the NMDA, AMPA and kainate receptor subtypes. J Physiol *485 (Pt 2)*, 403-418.

Chang, H.R., and Kuo, C.C. (2008). The activation gate and gating mechanism of the NMDA receptor. J Neurosci *28*, 1546-1556.

Chaudhry, C., Plested, A.J., Schuck, P., and Mayer, M.L. (2009). Energetics of glutamate receptor ligand binding domain dimer assembly are modulated by allosteric ions. Proc Natl Acad Sci U S A *106*, 12329-12334.

Chen, G.Q., Cui, C., Mayer, M.L., and Gouaux, E. (1999). Functional characterization of a potassium-selective prokaryotic glutamate receptor. Nature *402*, 817-821.

Chen, H.S., and Lipton, S.A. (2005). Pharmacological implications of two distinct mechanisms of interaction of memantine with N-methyl-D-aspartate-gated channels. J Pharmacol Exp Ther *314*, 961-971.

Chen, L., Cooper, N.G., and Mower, G.D. (2000). Developmental changes in the expression of NMDA receptor subunits (NR1, NR2A, NR2B) in the cat visual cortex and the effects of dark rearing. Brain Res Mol Brain Res *78*, 196-200.

Chen, P.E., and Wyllie, D.J. (2006). Pharmacological insights obtained from structure-function studies of ionotropic glutamate receptors. Br J Pharmacol *147*, 839-853.

Chiu, J., DeSalle, R., Lam, H.M., Meisel, L., and Coruzzi, G. (1999). Molecular evolution of glutamate receptors: a primitive signaling mechanism that existed before plants and animals diverged. Mol Biol Evol *16*, 826-838.

Chiu, J.C., Brenner, E.D., DeSalle, R., Nitabach, M.N., Holmes, T.C., and Coruzzi, G.M. (2002). Phylogenetic and expression analysis of the glutamate-receptor-like gene family in Arabidopsis thaliana. Mol Biol Evol *19*, 1066-1082.

Choi, Y.B., and Lipton, S.A. (1999). Identification and mechanism of action of two histidine residues underlying high-affinity Zn2+ inhibition of the NMDA receptor. Neuron *23*, 171-180.

Ciabarra, A.M., Sullivan, J.M., Gahn, L.G., Pecht, G., Heinemann, S., and Sevarino, K.A. (1995). Cloning and characterization of chi-1: a developmentally regulated member of a novel class of the ionotropic glutamate receptor family. J Neurosci *15*, 6498-6508.

Clarke, R., and Johnson, J. (2006). NMDA receptor NR2 subunit dependence of the slow component of magnesium unblock. Journal of Neuroscience *26*, 5825-5834.

Clements, J.D., and Westbrook, G.L. (1991). Activation kinetics reveal the number of glutamate and glycine binding sites on the N-methyl-D-aspartate receptor. Neuron *7*, 605-613.

Clinton, S.M., and Meador-Woodruff, J.H. (2004). Abnormalities of the NMDA Receptor and Associated Intracellular Molecules in the Thalamus in Schizophrenia and Bipolar Disorder. Neuropsychopharmacology *29*, 1353-1362.

Colquhoun, D. (1998). Binding, gating, affinity and efficacy: the interpretation of structure-activity relationships for agonists and of the effects of mutating receptors. British Journal of Pharmacology *125*, 924-947.

Colquhoun, D., and Sigworth, F.J., eds. (1995). Analysis of single ion channel data, 2 edn (New York: Plenum Press).

Conti, F., Minelli, A., and Brecha, N.C. (1994). Cellular localization and laminar distribution of AMPA glutamate receptor subunits mRNAs and proteins in the rat cerebral cortex. J Comp Neurol *350*, 241-259.

Cordero-Morales, J.F., Cuello, L.G., Zhao, Y., Jogini, V., Cortes, D.M., Roux, B., and Perozo, E. (2006). Molecular determinants of gating at the potassium-channel selectivity filter. Nat Struct Mol Biol *13*, 311-318.

Corradi, J., Spitzmaul, G., De Rosa, M.J., Costabel, M., and Bouzat, C. (2007). Role of pairwise interactions between M1 and M2 domains of the nicotinic receptor in channel gating. Biophys J *92*, 76-86.

Cuello, L.G., Jogini, V., Cortes, D.M., Pan, A.C., Gagnon, D.G., Dalmas, O., Cordero-Morales, J.F., Chakrapani, S., Roux, B., and Perozo, E. (2010a). Structural basis for the coupling between activation and inactivation gates in K(+) channels. Nature *466*, 272-275.

Cuello, L.G., Jogini, V., Cortes, D.M., and Perozo, E. (2010b). Structural mechanism of C-type inactivation in K(+) channels. Nature *466*, 203-208.

Cull-Candy, S.G., Brickley, S.G., Misra, C., Feldmeyer, D., Momiyama, A., and Farrant, M. (1998). NMDA receptor diversity in the cerebellum: identification of subunits contributing to functional receptors. Neuropharmacology *37*, 1369-1380.

Das, U., Kumar, J., Mayer, M.L., and Plested, A.J. (2010). Domain organization and function in GluK2 subtype kainate receptors. Proc Natl Acad Sci U S A *107*, 8463-8468.

Dingledine, R., Borges, K., Bowie, D., and Traynelis, S.F. (1999). The glutamate receptor ion channels. Pharmacol Rev *51*, 7-61.

Donevan, S.D., and Rogawski, M.A. (1995). Intracellular polyamines mediate inward rectification of Ca(2+)-permeable alpha-amino-3-hydroxy-5-methyl-4-isoxazolepropionic acid receptors. Proc Natl Acad Sci U S A *92*, 9298-9302.

Doyle, D.A., Morais Cabral, J., Pfuetzner, R.A., Kuo, A., Gulbis, J.M., Cohen, S.L., Chait, B.T., and MacKinnon, R. (1998). The structure of the potassium channel: molecular basis of K+ conduction and selectivity. Science *280*, 69-77.

Dravid, S.M., Erreger, K., Yuan, H., Nicholson, K., Le, P., Lyuboslavsky, P., Almonte, A., Murray, E., Mosely, C., Barber, J.*, et al.* (2007). Subunit-specific mechanisms and proton sensitivity of NMDA receptor channel block. J Physiol *581*, 107-128.

Enkvetchakul, D., Jeliazkova, I., Bhattacharyya, J., and Nichols, C.G. (2007). Control of inward rectifier K channel activity by lipid tethering of cytoplasmic domains. J Gen Physiol *130*, 329-334.

Erreger, K., Chen, P.E., Wyllie, D.J., and Traynelis, S.F. (2004). Glutamate receptor gating. Crit Rev Neurobiol *16*, 187-224.

Erreger, K., Dravid, S.M., Banke, T.G., Wyllie, D.J., and Traynelis, S.F. (2005). Subunit-specific gating controls rat NR1/NR2A and NR1/NR2B NMDA channel kinetics and synaptic signalling profiles. J Physiol *563*, 345-358.

Erreger, K., Geballe, M.T., Kristensen, A., Chen, P.E., Hansen, K.B., Lee, C.J., Yuan, H., Le, P., Lyuboslavsky, P.N., Micale, N., *et al.* (2007). Subunit-specific agonist activity at NR2A-, NR2B-, NR2C-, and NR2D-containing N-methyl-D-aspartate glutamate receptors. Mol Pharmacol *72*, 907-920.

Erreger, K., and Traynelis, S.F. (2008). Zinc inhibition of rat NR1/NR2A N-methyl-D-aspartate receptors. J Physiol *586*, 763-778.

Eswar, N., Webb, B., Marti-Renom, M.A., Madhusudhan, M.S., Eramian, D., Shen, M.Y., Pieper, U., and Sali, A. (2007). Comparative protein structure modeling using MODELLER. Curr Protoc Protein Sci *Chapter 2*, Unit 2 9.

Farrant, M., Feldmeyer, D., Takahashi, T., and Cull-Candy, S.G. (1994). NMDA-receptor channel diversity in the developing cerebellum. Nature *368*, 335-339.

Fayyazuddin, A., Villarroel, A., Le Goff, A., Lerma, J., and Neyton, J. (2000). Four residues of the extracellular N-terminal domain of the NR2A subunit control high-affinity Zn2+ binding to NMDA receptors. Neuron *25*, 683-694.

Fleming, W.W., Westfall, D.P., De la Lande, I.S., and Jellett, L.B. (1972). Log-normal distribution of equieffective doses of norepinephrine and acetylcholine in several tissues. J Pharmacol Exp Ther *181*, 339-345.

Fukaya, M., Kato, A., Lovett, C., Tonegawa, S., and Watanabe, M. (2003). Retention of NMDA receptor NR2 subunits in the lumen of endoplasmic reticulum in targeted NR1 knockout mice. Proc Natl Acad Sci U S A *100*, 4855-4860.

Furukawa, H., and Gouaux, E. (2003). Mechanisms of activation, inhibition and specificity: crystal structures of the NMDA receptor NR1 ligand-binding core. Embo J *22*, 2873-2885.

Furukawa, H., Singh, S.K., Mancusso, R., and Gouaux, E. (2005). Subunit arrangement and function in NMDA receptors. Nature *438*, 185-192.

Gallagher, M.J., Huang, H., Pritchett, D.B., and Lynch, D.R. (1996). Interactions between ifenprodil and the NR2B subunit of the N-methyl-D-aspartate receptor. J Biol Chem *271*, 9603-9611.

Gasic, G.P., and Hollmann, M. (1992). Molecular neurobiology of glutamate receptors. Annu Rev Physiol *54*, 507-536.

Gebhardt, C., and Cull-Candy, S.G. (2006). Influence of agonist concentration on AMPA and kainate channels in CA1 pyramidal cells in rat hippocampal slices. J Physiol *573*, 371-394.

Gibb, A.J., and Colquhoun, D. (1992). Activation of N-methyl-D-aspartate receptors by L-glutamate in cells dissociated from adult rat hippocampus. J Physiol *456*, 143-179.

Gielen, M., Le Goff, A., Stroebel, D., Johnson, J.W., Neyton, J., and Paoletti, P. (2008). Structural rearrangements of NR1/NR2A NMDA receptors during allosteric inhibition. Neuron *57*, 80-93.

Gielen, M., Siegler Retchless, B., Mony, L., Johnson, J.W., and Paoletti, P. (2009). Mechanism of differential control of NMDA receptor activity by NR2 subunits. Nature *459*, 703-707.

Goodsell, D.S., and Olson, A.J. (2000). Structural symmetry and protein function. Annu Rev Biophys Biomol Struct *29*, 105-153.

Gu, Y.P., and Huang, L.Y. (1991). Block of kainate receptor channels by Ca2+ in isolated spinal trigeminal neurons of rat. Neuron *6*, 777-784.

Gulbis, J.M., and Doyle, D.A. (2004). Potassium channel structures: do they conform? Curr Opin Struct Biol *14*, 440-446.

Heinemann, S.H., Terlau, H., Stuhmer, W., Imoto, K., and Numa, S. (1992). Calcium channel characteristics conferred on the sodium channel by single mutations. Nature *356*, 441-443.

Herin, G.A., and Aizenman, E. (2004). Amino terminal domain regulation of NMDA receptor function. Eur J Pharmacol *500*, 101-111.

Hidalgo, P., and MacKinnon, R. (1995). Revealing the architecture of a K+ channel pore through mutant cycles with a peptide inhibitor. Science *268*, 307-310.

Horning, M.S., and Mayer, M.L. (2004). Regulation of AMPA receptor gating by ligand binding core dimers. Neuron *41*, 379-388.

Ihle, E.C., and Patneau, D.K. (2000). Modulation of alpha-amino-3-hydroxy-5-methyl-4-isoxazolepropionic acid receptor desensitization by extracellular protons. Mol Pharmacol *58*, 1204-1212.

Iino, M., Ozawa, S., and Tsuzuki, K. (1990). Permeation of calcium through excitatory amino acid receptor channels in cultured rat hippocampal neurones. J Physiol *424*, 151-165.

Inanobe, A., Furukawa, H., and Gouaux, E. (2005). Mechanism of partial agonist action at the NR1 subunit of NMDA receptors. Neuron *47*, 71-84.

Ishii, T., Moriyoshi, K., Sugihara, H., Sakurada, K., Kadotani, H., Yokoi, M., Akazawa, C., Shigemoto, R., Mizuno, N., Masu, M., and et al. (1993). Molecular characterization of the family of the N-methyl-D-aspartate receptor subunits. J Biol Chem *268*, 2836-2843.

Jahr, C.E., and Stevens, C.F. (1990). A quantitative description of NMDA receptor-channel kinetic behavior. J Neurosci *10*, 1830-1837.

Jahr, C.E., and Stevens, C.F. (1993). Calcium permeability of the N-methyl-D-aspartate receptor channel in hippocampal neurons in culture. Proc Natl Acad Sci U S A *90*, 11573-11577.

Jan, L.Y., and Jan, Y.N. (1990). A superfamily of ion channels. Nature *345*, 672.

Jan, L.Y., and Jan, Y.N. (1992). Tracing the roots of ion channels. Cell *69*, 715-718.

Jatzke, C., Hernandez, M., and Wollmuth, L.P. (2003). Extracellular vestibule determinants of Ca2+ influx in Ca2+-permeable AMPA receptor channels. J Physiol *549*, 439-452.

Jatzke, C., Watanabe, J., and Wollmuth, L.P. (2002). Voltage and concentration dependence of Ca(2+) permeability in recombinant glutamate receptor subtypes. J Physiol *538*, 25-39.

Jiang, Y., Lee, A., Chen, J., Cadene, M., Chait, B.T., and MacKinnon, R. (2002). The open pore conformation of potassium channels. Nature *417*, 523-526.

Jin, L., Miyazaki, M., Mizuno, S., Takigawa, M., Hirose, T., Nishimura, K., Toida, T., Williams, K., Kashiwagi, K., and Igarashi, K. (2008). The pore region of N-methyl-D-aspartate receptors differentially influences stimulation and block by spermine. J Pharmacol Exp Ther *327*, 68-77.

Jin, L., Sugiyama, H., Takigawa, M., Katagiri, D., Tomitori, H., Nishimura, K., Kaur, N., Phanstiel, O.t., Kitajima, M., Takayama, H.*, et al.* (2007). Comparative studies of anthraquinone- and anthracene-tetraamines as blockers of N-methyl-D-aspartate receptors. J Pharmacol Exp Ther *320*, 47-55.

Jin, R., Banke, T.G., Mayer, M.L., Traynelis, S.F., and Gouaux, E. (2003). Structural basis for partial agonist action at ionotropic glutamate receptors. Nat Neurosci *6*, 803-810.

Jin, R., Clark, S., Weeks, A.M., Dudman, J.T., Gouaux, E., and Partin, K.M. (2005). Mechanism of positive allosteric modulators acting on AMPA receptors. J Neurosci *25*, 9027-9036.

Jin, R., Horning, M., Mayer, M.L., and Gouaux, E. (2002). Mechanism of activation and selectivity in a ligand-gated ion channel: structural and functional studies of GluR2 and quisqualate. Biochemistry *41*, 15635-15643.

Johnson, J.W., and Ascher, P. (1987). Glycine potentiates the NMDA response in cultured mouse brain neurons. Nature *325*, 529-531.

Johnson, J.W., and Ascher, P. (1990). Voltage-dependent block by intracellular Mg2+ of N-methyl-D-aspartate-activated channels. Biophys J *57*, 1085-1090.

Jones, K.S., VanDongen, H.M., and VanDongen, A.M. (2002). The NMDA receptor M3 segment is a conserved transduction element coupling ligand binding to channel opening. J Neurosci *22*, 2044-2053.

Kamboj, S.K., Swanson, G.T., and Cull-Candy, S.G. (1995). Intracellular spermine confers rectification on rat calcium-permeable AMPA and kainate receptors. J Physiol *486 (Pt 2)*, 297-303.

Karakas, E., Simorowski, N., and Furukawa, H. (2009). Structure of the zinc-bound amino-terminal domain of the NMDA receptor NR2B subunit. EMBO J *28*, 3910-3920.

Kashiwagi, K., Fukuchi, J., Chao, J., Igarashi, K., and Williams, K. (1996). An aspartate residue in the extracellular loop of the N-methyl-D-aspartate receptor controls sensitivity to spermine and protons. Mol Pharmacol *49*, 1131-1141.

Kashiwagi, K., Masuko, T., Nguyen, C.D., Kuno, T., Tanaka, I., Igarashi, K., and Williams, K. (2002). Channel blockers acting at N-methyl-D-aspartate receptors: differential effects of mutations in the vestibule and ion channel pore. Mol Pharmacol *61*, 533-545.

Kashiwagi, K., Pahk, A.J., Masuko, T., Igarashi, K., and Williams, K. (1997). Block and modulation of N-methyl-D-aspartate receptors by polyamines and protons: role of amino acid residues in the transmembrane and pore-forming regions of NR1 and NR2 subunits. Mol Pharmacol *52*, 701-713.

Kessels, H.W., and Malinow, R. (2009). Synaptic AMPA receptor plasticity and behavior. Neuron *61*, 340-350.

Kim, K.S., Yan, D., and Tomita, S. (2010). Assembly and stoichiometry of the AMPA receptor and transmembrane AMPA receptor regulatory protein complex. J Neurosci *30*, 1064-1072.

Kizelsztein, P., Eisenstein, M., Strutz, N., Hollmann, M., and Teichberg, V.I. (2000). Mutant cycle analysis of the active and desensitized states of an AMPA receptor induced by willardiines. Biochemistry *39*, 12819-12827.

Kleckner, N.W., and Dingledine, R. (1988). Requirement for glycine in activation of NMDA-receptors expressed in Xenopus oocytes. Science *241*, 835-837.

Kleckner, N.W., and Dingledine, R. (1991). Regulation of hippocampal NMDA receptors by magnesium and glycine during development. Brain Res Mol Brain Res *11*, 151-159.

Ko, S., Zhao, M.G., Toyoda, H., Qiu, C.S., and Zhuo, M. (2005). Altered behavioral responses to noxious stimuli and fear in glutamate receptor 5 (GluR5)- or GluR6-deficient mice. J Neurosci *25*, 977-984.

Kohler, M., Burnashev, N., Sakmann, B., and Seeburg, P.H. (1993). Determinants of Ca2+ permeability in both TM1 and TM2 of high affinity kainate receptor channels: diversity by RNA editing. Neuron *10*, 491-500.

Kotermanski, S.E., and Johnson, J.W. (2009). Mg2+ imparts NMDA receptor subtype selectivity to the Alzheimer's drug memantine. J Neurosci *29*, 2774-2779.

Krupp, J.J., Vissel, B., Heinemann, S.F., and Westbrook, G.L. (1998). N-terminal domains in the NR2 subunit control desensitization of NMDA receptors. Neuron *20*, 317-327.

Kumar, J., Schuck, P., Jin, R., and Mayer, M.L. (2009). The N-terminal domain of GluR6-subtype glutamate receptor ion channels. Nat Struct Mol Biol *16*, 631-638.

Kuner, T., and Schoepfer, R. (1996). Multiple structural elements determine subunit specificity of Mg2+ block in NMDA receptor channels. J Neurosci *16*, 3549-3558.

Kuner, T., Wollmuth, L.P., Karlin, A., Seeburg, P.H., and Sakmann, B. (1996). Structure of the NMDA receptor channel M2 segment inferred from the accessibility of substituted cysteines. Neuron *17*, 343-352.

Laube, B., Kuhse, J., and Betz, H. (1998). Evidence for a tetrameric structure of recombinant NMDA receptors. J Neurosci *18*, 2954-2961.

Lei, S., Orser, B.A., Thatcher, G.R., Reynolds, J.N., and MacDonald, J.F. (2001). Positive allosteric modulators of AMPA receptors reduce proton-induced receptor desensitization in rat hippocampal neurons. J Neurophysiol *85*, 2030-2038.

Lerma, J. (2006). Kainate receptor physiology. Curr Opin Pharmacol *6*, 89-97.

Lewis, C.A. (1979). Ion-concentration dependence of the reversal potential and the single channel conductance of ion channels at the frog neuromuscular junction. J Physiol *286*, 417-445.

Llansola, M., Sanchez-Perez, A., Cauli, O., and Felipo, V. (2005). Modulation of NMDA receptors in the cerebellum. 1. Properties of the NMDA receptor that modulate its function. Cerebellum *4*, 154-161.

Lockless, S.W., Zhou, M., and MacKinnon, R. (2007). Structural and thermodynamic properties of selective ion binding in a K+ channel. PLoS Biol *5*, e121.

Lohrke, S., and Friauf, E. (2002). Developmental distribution of the glutamate receptor subunits KA2, GluR6/7, and delta 1/2 in the rat medial nucleus of the trapezoid body. A quantitative image analysis. Cell Tissue Res *308*, 19-33.

Long, S.B., Campbell, E.B., and Mackinnon, R. (2005). Crystal structure of a mammalian voltage-dependent Shaker family K+ channel. Science *309*, 897-903.

Low, C.M., Lyuboslavsky, P., French, A., Le, P., Wyatte, K., Thiel, W.H., Marchan, E.M., Igarashi, K., Kashiwagi, K., Gernert, K.*, et al.* (2003). Molecular determinants of proton-sensitive N-methyl-D-aspartate receptor gating. Mol Pharmacol *63*, 1212-1222.

Lu, W., Shi, Y., Jackson, A.C., Bjorgan, K., During, M.J., Sprengel, R., Seeburg, P.H., and Nicoll, R.A. (2009). Subunit composition of synaptic AMPA receptors revealed by a single-cell genetic approach. Neuron *62*, 254-268.

Lynch, M.A. (2004). Long-term potentiation and memory. Physiol Rev *84*, 87-136.

Machado-Vieira, R., Salvadore, G., Ibrahim, L.A., Diaz-Granados, N., and Zarate, C.A., Jr. (2009). Targeting glutamatergic signaling for the development of novel therapeutics for mood disorders. Curr Pharm Des *15*, 1595-1611.

MacKinnon, R. (1995). Pore loops: an emerging theme in ion channel structure. Neuron *14*, 889-892.

Masuko, T., Kashiwagi, K., Kuno, T., Nguyen, N.D., Pahk, A.J., Fukuchi, J., Igarashi, K., and Williams, K. (1999). A regulatory domain (R1-R2) in the amino terminus of the N-methyl-D-aspartate receptor: effects of spermine, protons, and ifenprodil, and structural similarity to bacterial leucine/isoleucine/valine binding protein. Mol Pharmacol *55*, 957-969.

Mayer, M.L. (2005). Crystal structures of the GluR5 and GluR6 ligand binding cores: molecular mechanisms underlying kainate receptor selectivity. Neuron *45*, 539-552.

Mayer, M.L. (2006). Glutamate receptors at atomic resolution. Nature *440*, 456-462.

Mayer, M.L., and Armstrong, N. (2004). Structure and function of glutamate receptor ion channels. Annu Rev Physiol *66*, 161-181.

Mayer, M.L., Olson, R., and Gouaux, E. (2001). Mechanisms for ligand binding to GluR0 ion channels: crystal structures of the glutamate and serine complexes and a closed apo state. J Mol Biol *311*, 815-836.

Mayer, M.L., and Westbrook, G.L. (1985). The action of N-methyl-D-aspartic acid on mouse spinal neurones in culture. J Physiol *361*, 65-90.

Mayer, M.L., and Westbrook, G.L. (1987). Permeation and block of N-methyl-D-aspartic acid receptor channels by divalent cations in mouse cultured central neurones. J Physiol *394*, 501-527.

McGurk, J.F., Bennett, M.V., and Zukin, R.S. (1990). Polyamines potentiate responses of N-methyl-D-aspartate receptors expressed in xenopus oocytes. Proc Natl Acad Sci U S A *87*, 9971-9974.

Mishina, M., Mori, H., Araki, K., Kushiya, E., Meguro, H., Kutsuwada, T., Kashiwabuchi, N., Ikeda, K., Nagasawa, M., Yamazaki, M., and et al. (1993). Molecular and functional diversity of the NMDA receptor channel. Ann N Y Acad Sci *707*, 136-152.

Misra, C., Brickley, S.G., Wyllie, D.J., and Cull-Candy, S.G. (2000). Slow deactivation kinetics of NMDA receptors containing NR1 and NR2D subunits in rat cerebellar Purkinje cells. J Physiol *525 Pt 2*, 299-305.

Momiyama, A., Feldmeyer, D., and Cull-Candy, S.G. (1996). Identification of a native low-conductance NMDA channel with reduced sensitivity to Mg2+ in rat central neurones. J Physiol *494 (Pt 2)*, 479-492.

Monyer, H., Burnashev, N., Laurie, D.J., Sakmann, B., and Seeburg, P.H. (1994). Developmental and regional expression in the rat brain and functional properties of four NMDA receptors. Neuron *12*, 529-540.

Monyer, H., Sprengel, R., Schoepfer, R., Herb, A., Higuchi, M., Lomeli, H., Burnashev, N., Sakmann, B., and Seeburg, P.H. (1992). Heteromeric NMDA receptors: molecular and functional distinction of subtypes. Science *256*, 1217-1221.

Mori, H., Masaki, H., Yamakura, T., and Mishina, M. (1992). Identification by mutagenesis of a Mg(2+)-block site of the NMDA receptor channel. Nature *358*, 673-675.

Mott, D.D., Doherty, J.J., Zhang, S., Washburn, M.S., Fendley, M.J., Lyuboslavsky, P., Traynelis, S.F., and Dingledine, R. (1998). Phenylethanolamines inhibit NMDA receptors by enhancing proton inhibition. Nat Neurosci *1*, 659-667.

Mott, D.D., Washburn, M.S., Zhang, S., and Dingledine, R.J. (2003). Subunit-dependent modulation of kainate receptors by extracellular protons and polyamines. J Neurosci *23*, 1179-1188.

Muir, K.W. (2006). Glutamate-based therapeutic approaches: clinical trials with NMDA antagonists. Curr Opin Pharmacol *6*, 53-60.

Nanao, M.H., Green, T., Stern-Bach, Y., Heinemann, S.F., and Choe, S. (2005). Structure of the kainate receptor subunit GluR6 agonist-binding domain complexed with domoic acid. Proc Natl Acad Sci U S A *102*, 1708-1713.

Nishi, M., Hinds, H., Lu, H.P., Kawata, M., and Hayashi, Y. (2001). Motoneuron-specific expression of NR3B, a novel NMDA-type glutamate receptor subunit that works in a dominant-negative manner. J Neurosci *21*, RC185.

Nishida, M., Cadene, M., Chait, B.T., and MacKinnon, R. (2007). Crystal structure of a Kir3.1-prokaryotic Kir channel chimera. EMBO J *26*, 4005-4015.

Noskov, S.Y., and Roux, B. (2007). Importance of hydration and dynamics on the selectivity of the KcsA and NaK channels. J Gen Physiol *129*, 135-143.

O'Leary, T., and Wyllie, D.J. (2009). Single-channel properties of N-methyl-D-aspartate receptors containing chimaeric GluN2A/GluN2D subunits. Biochem Soc Trans *37*, 1347-1354.

Pahk, A.J., and Williams, K. (1997). Influence of extracellular pH on inhibition by ifenprodil at N-methyl-D-aspartate receptors in Xenopus oocytes. Neurosci Lett *225*, 29-32.

Panchenko, V.A., Glasser, C.R., and Mayer, M.L. (2001). Structural similarities between glutamate receptor channels and K(+) channels examined by scanning mutagenesis. J Gen Physiol *117*, 345-360.

Panchenko, V.A., Glasser, C.R., Partin, K.M., and Mayer, M.L. (1999). Amino acid substitutions in the pore of rat glutamate receptors at sites influencing block by polyamines. J Physiol *520 Pt 2*, 337-357.

Paoletti, P., Neyton, J., and Ascher, P. (1995). Glycine-independent and subunit-specific potentiation of NMDA responses by extracellular Mg2+. Neuron *15*, 1109-1120.

Paoletti, P., Perin-Dureau, F., Fayyazuddin, A., Le Goff, A., Callebaut, I., and Neyton, J. (2000). Molecular organization of a zinc binding n-terminal modulatory domain in a NMDA receptor subunit. Neuron *28*, 911-925.

Parsons, C.G., Stoffler, A., and Danysz, W. (2007). Memantine: a NMDA receptor antagonist that improves memory by restoration of homeostasis in the glutamatergic system--too little activation is bad, too much is even worse. Neuropharmacology *53*, 699-723.

Partin, K.M., Bowie, D., and Mayer, M.L. (1995). Structural determinants of allosteric regulation in alternatively spliced AMPA receptors. Neuron *14*, 833-843.

Perozo, E., Cortes, D.M., and Cuello, L.G. (1999). Structural rearrangements underlying K+-channel activation gating. Science *285*, 73-78.

Perrais, D., Coussen, F., and Mulle, C. (2009). Atypical functional properties of GluK3-containing kainate receptors. J Neurosci *29*, 15499-15510.

Perrais, D., Veran, J., and Mulle, C. (2010). Gating and permeation of kainate receptors: differences unveiled. Trends Pharmacol Sci.

Plested, A.J., and Mayer, M.L. (2007). Structure and mechanism of kainate receptor modulation by anions. Neuron *53*, 829-841.

Premkumar, L.S., and Auerbach, A. (1996). Identification of a high affinity divalent cation binding site near the entrance of the NMDA receptor channel. Neuron *16*, 869-880.

Premkumar, L.S., Qin, F., and Auerbach, A. (1997). Subconductance states of a mutant NMDA receptor channel kinetics, calcium, and voltage dependence. Journal of General Physiology *109*, 181-189.

Prieto, M.L., and Wollmuth, L.P. (2010). Gating modes in AMPA receptors. J Neurosci *30*, 4449-4459.

Puchalski, R.B., Louis, J.C., Brose, N., Traynelis, S.F., Egebjerg, J., Kukekov, V., Wenthold, R.J., Rogers, S.W., Lin, F., Moran, T., and et al. (1994). Selective RNA editing and subunit assembly of native glutamate receptors. Neuron *13*, 131-147.

Qian, A., Antonov, S.M., and Johnson, J.W. (2002). Modulation by permeant ions of Mg(2+) inhibition of NMDA-activated whole-cell currents in rat cortical neurons. J Physiol *538*, 65-77.

Qian, A., Buller, A.L., and Johnson, J.W. (2005). NR2 subunit-dependence of NMDA receptor channel block by external Mg2+. J Physiol *562*, 319-331.

Qian, A., and Johnson, J.W. (2006). Permeant ion effects on external Mg2+ block of NR1/2D NMDA receptors. J Neurosci *26*, 10899-10910.

Ranganathan, R., Lewis, J.H., and MacKinnon, R. (1996). Spatial localization of the K+ channel selectivity filter by mutant cycle-based structure analysis. Neuron *16*, 131-139.

Ransom, R.W., and Stec, N.L. (1988). Cooperative modulation of [3H]MK-801 binding to the N-methyl-D-aspartate receptor-ion channel complex by L-glutamate, glycine, and polyamines. J Neurochem *51*, 830-836.

Rosenmund, C., Stern-Bach, Y., and Stevens, C.F. (1998). The tetrameric structure of a glutamate receptor channel. Science *280*, 1596-1599.

Ryan, T.J., Emes, R.D., Grant, S.G., and Komiyama, N.H. (2008). Evolution of NMDA receptor cytoplasmic interaction domains: implications for organisation of synaptic signalling complexes. BMC Neurosci *9*, 6.

Sakurada, K., Masu, M., and Nakanishi, S. (1993). Alteration of Ca2+ permeability and sensitivity to Mg2+ and channel blockers by a single amino acid substitution in the N-methyl-D-aspartate receptor. J Biol Chem *268*, 410-415.

Savidge, J.R., and Bristow, D.R. (1998). Ca2+ permeability and joro spider toxin sensitivity of AMPA and kainate receptors on cerebellar granule cells. Eur J Pharmacol *351*, 131-138.

Schneggenburger, R. (1996). Simultaneous measurement of Ca2+ influx and reversal potentials in recombinant N-methyl-D-aspartate receptor channels. Biophys J *70*, 2165-2174.

Schneggenburger, R. (1998). Altered voltage dependence of fractional Ca2+ current in N-methyl-D-aspartate channel pore mutants with a decreased Ca2+ permeability. Biophys J *74*, 1790-1794.

Schneggenburger, R., and Ascher, P. (1997). Coupling of permeation and gating in an NMDA-channel pore mutant. Neuron *18*, 167-177.

Schoepfer, R., Monyer, H., Sommer, B., Wisden, W., Sprengel, R., Kuner, T., Lomeli, H., Herb, A., Kohler, M., Burnashev, N., and et al. (1994). Molecular biology of glutamate receptors. Prog Neurobiol *42*, 353-357.

Schorge, S., Elenes, S., and Colquhoun, D. (2005). Maximum likelihood fitting of single channel NMDA activity with a mechanism composed of independent dimers of subunits. J Physiol *569*, 395-418.

Sharma, G., and Stevens, C.F. (1996a). A mutation that alters magnesium block of N-methyl-D-aspartate receptor channels. Proc Natl Acad Sci U S A *93*, 9259-9263.

Sharma, G., and Stevens, C.F. (1996b). Interactions between two divalent ion binding sites in N-methyl-D-aspartate receptor channels. Proc Natl Acad Sci U S A *93*, 14170-14175.

Shi, N., Ye, S., Alam, A., Chen, L., and Jiang, Y. (2006). Atomic structure of a Na+- and K+-conducting channel. Nature *440*, 570-574.

Skeberdis, V.A., Chevaleyre, V., Lau, C.G., Goldberg, J.H., Pettit, D.L., Suadicani, S.O., Lin, Y., Bennett, M.V., Yuste, R., Castillo, P.E., and Zukin, R.S. (2006). Protein kinase A regulates calcium permeability of NMDA receptors. Nat Neurosci *9*, 501-510.

Smith, T.C., and Howe, J.R. (2000). Concentration-dependent substate behavior of native AMPA receptors. Nat Neurosci *3*, 992-997.

Sobczyk, A., Scheuss, V., and Svoboda, K. (2005). NMDA receptor subunit-dependent [Ca2+] signaling in individual hippocampal dendritic spines. J Neurosci *25*, 6037-6046.

Sobolevsky, A.I., Beck, C., and Wollmuth, L.P. (2002a). Molecular rearrangements of the extracellular vestibule in NMDAR channels during gating. Neuron *33*, 75-85.

Sobolevsky, A.I., Koshelev, S.G., and Khodorov, B.I. (1999). Probing of NMDA channels with fast blockers. J Neurosci *19*, 10611-10626.

Sobolevsky, A.I., Rooney, L., and Wollmuth, L.P. (2002b). Staggering of subunits in NMDAR channels. Biophys J *83*, 3304-3314.

Sobolevsky, A.I., Rosconi, M.P., and Gouaux, E. (2009). X-ray structure, symmetry and mechanism of an AMPA-subtype glutamate receptor. Nature *462*, 745-756.

Sobolevsky, A.I., Yelshansky, M.V., and Wollmuth, L.P. (2003). Different gating mechanisms in glutamate receptor and K+ channels. J Neurosci *23*, 7559-7568.

Sprengel, R., Aronoff, R., Volkner, M., Schmitt, B., Mosbach, R., and Kuner, T. (2001). Glutamate receptor channel signatures. Trends Pharmacol Sci *22*, 7-10.

Stern, P., Behe, P., Schoepfer, R., and Colquhoun, D. (1992). Single-channel conductances of NMDA receptors expressed from cloned cDNAs: comparison with native receptors. Proc Biol Sci *250*, 271-277.

Stern, P., Cik, M., Colquhoun, D., and Stephenson, F.A. (1994). Single channel properties of cloned NMDA receptors in a human cell line: comparison with results from Xenopus oocytes. J Physiol *476*, 391-397.

Stroebel, D., Carvalho, S., and Paoletti, P. (2010). Functional evidence for a twisted conformation of the NMDA receptor GluN2A subunit N-terminal domain. Neuropharmacology.

Sun, Y., Olson, R., Horning, M., Armstrong, N., Mayer, M., and Gouaux, E. (2002). Mechanism of glutamate receptor desensitization. Nature *417*, 245-253.

Swanson, G.T., Feldmeyer, D., Kaneda, M., and Cull-Candy, S.G. (1996). Effect of RNA editing and subunit co-assembly single-channel properties of recombinant kainate receptors. J Physiol *492 (Pt 1)*, 129-142.

Swanson, G.T., Green, T., Sakai, R., Contractor, A., Che, W., Kamiya, H., and Heinemann, S.F. (2002). Differential activation of individual subunits in heteromeric kainate receptors. Neuron *34*, 589-598.

Tikhonov, D.B. (2007). Ion channels of glutamate receptors: structural modeling. Mol Membr Biol *24*, 135-147.

Tikhonov, D.B., and Magazanik, L.G. (2009). Origin and molecular evolution of ionotropic glutamate receptors. Neurosci Behav Physiol *39*, 763-773.

Tikhonov, D.B., Mellor, J.R., Usherwood, P.N., and Magazanik, L.G. (2002). Modeling of the pore domain of the GLUR1 channel: homology with K+ channel and binding of channel blockers. Biophys J *82*, 1884-1893.

Tikhonov, D.B., Zhorov, B.S., and Magazanik, L.G. (1999). Intersegment hydrogen bonds as possible structural determinants of the N/Q/R site in glutamate receptors. Biophys J *77*, 1914-1926.

Tomita, S. (2010). Regulation of ionotropic glutamate receptors by their auxiliary subunits. Physiology (Bethesda) *25*, 41-49.

Tongiorgi, E., Ferrero, F., Cattaneo, A., and Domenici, L. (2003). Dark-rearing decreases NR2A N-methyl-D-aspartate receptor subunit in all visual cortical layers. Neuroscience *119*, 1013-1022.

Traynelis, S.F., and Cull-Candy, S.G. (1990). Proton inhibition of N-methyl-D-aspartate receptors in cerebellar neurons. Nature *345*, 347-350.

Traynelis, S.F., Hartley, M., and Heinemann, S.F. (1995). Control of proton sensitivity of the NMDA receptor by RNA splicing and polyamines. Science *268*, 873-876.

Traynelis, S.F., Wollmuth, L.P., McBain, C.J., Menniti, F.S., Vance, K.M., Ogden, K.K., Hansen, K.B., Yuan, H., Myers, S.J., Dingledine, R., and Sibley, D. (2010). Glutamate receptor ion channels: structure, regulation, and function. Pharmacol Rev *62*, 405-496.

Tsuzuki, K., Mochizuki, S., Iino, M., Mori, H., Mishina, M., and Ozawa, S. (1994). Ion permeation properties of the cloned mouse epsilon 2/zeta 1 NMDA receptor channel. Brain Res Mol Brain Res *26*, 37-46.

Vicini, S., and Rumbaugh, G. (2000). A slow NMDA channel: in search of a role. J Physiol *525 Pt 2*, 283.

Vijayan, R., Plested, A.J., Mayer, M.L., and Biggin, P.C. (2009). Selectivity and cooperativity of modulatory ions in a neurotransmitter receptor. Biophys J *96*, 1751-1760.

Villarroel, A., Burnashev, N., and Sakmann, B. (1995). Dimensions of the narrow portion of a recombinant NMDA receptor channel. Biophys J *68*, 866-875.

Washburn, M.S., and Dingledine, R. (1996). Block of alpha-amino-3-hydroxy-5-methyl-4-isoxazolepropionic acid (AMPA) receptors by polyamines and polyamine toxins. J Pharmacol Exp Ther *278*, 669-678.

Watanabe, J., Beck, C., Kuner, T., Premkumar, L.S., and Wollmuth, L.P. (2002). DRPEER: a motif in the extracellular vestibule conferring high Ca2+ flux rates in NMDA receptor channels. J Neurosci *22*, 10209-10216.

Weiss, J.H., and Sensi, S.L. (2000). Ca2+-Zn2+ permeable AMPA or kainate receptors: possible key factors in selective neurodegeneration. Trends Neurosci *23*, 365-371.

Weston, M.C., Gertler, C., Mayer, M.L., and Rosenmund, C. (2006a). Interdomain interactions in AMPA and kainate receptors regulate affinity for glutamate. J Neurosci *26*, 7650-7658.

Weston, M.C., Schuck, P., Ghosal, A., Rosenmund, C., and Mayer, M.L. (2006b). Conformational restriction blocks glutamate receptor desensitization. Nat Struct Mol Biol *13*, 1120-1127.

Williams, K. (1993). Ifenprodil discriminates subtypes of the N-methyl-D-aspartate receptor: selectivity and mechanisms at recombinant heteromeric receptors. Mol Pharmacol *44*, 851-859.

Williams, K. (1997). Modulation and block of ion channels: a new biology of polyamines. Cell Signal *9*, 1-13.

Williams, K., Pahk, A.J., Kashiwagi, K., Masuko, T., Nguyen, N.D., and Igarashi, K. (1998). The selectivity filter of the N-methyl-D-aspartate receptor: a tryptophan residue controls block and permeation of Mg2+. Mol Pharmacol *53*, 933-941.

Wollmuth, L.P., Kuner, T., Jatzke, C., Seeburg, P.H., Heintz, N., and Zuo, J. (2000). The Lurcher mutation identifies delta 2 as an AMPA/kainate receptor-like channel that is potentiated by Ca(2+). J Neurosci *20*, 5973-5980.

Wollmuth, L.P., Kuner, T., and Sakmann, B. (1998a). Adjacent asparagines in the NR2-subunit of the NMDA receptor channel control the voltage-dependent block by extracellular Mg2+. J Physiol *506 (Pt 1)*, 13-32.

Wollmuth, L.P., Kuner, T., and Sakmann, B. (1998b). Intracellular Mg2+ interacts with structural determinants of the narrow constriction contributed by the NR1-subunit in the NMDA receptor channel. J Physiol *506 (Pt 1)*, 33-52.

Wollmuth, L.P., Kuner, T., Seeburg, P.H., and Sakmann, B. (1996). Differential contribution of the NR1- and NR2A-subunits to the selectivity filter of recombinant NMDA receptor channels. J Physiol *491 (Pt 3)*, 779-797.

Wollmuth, L.P., and Sakmann, B. (1998). Different mechanisms of Ca2+ transport in NMDA and Ca2+-permeable AMPA glutamate receptor channels. J Gen Physiol *112*, 623-636.

Wollmuth, L.P., and Sobolevsky, A.I. (2004). Structure and gating of the glutamate receptor ion channel. Trends Neurosci *27*, 321-328.

Wood, M.W., VanDongen, H.M., and VanDongen, A.M. (1995). Structural conservation of ion conduction pathways in K channels and glutamate receptors. Proc Natl Acad Sci U S A *92*, 4882-4886.

Wrighton, D.C., Baker, E.J., Chen, P.E., and Wyllie, D.J. (2008). Mg2+ and memantine block of rat recombinant NMDA receptors containing chimeric NR2A/2D subunits expressed in Xenopus laevis oocytes. J Physiol *586*, 211-225.

Wyllie, D.J., Behe, P., and Colquhoun, D. (1998). Single-channel activations and concentration jumps: comparison of recombinant NR1a/NR2A and NR1a/NR2D NMDA receptors. J Physiol *510 (Pt 1)*, 1-18.

Wyllie, D.J., Behe, P., Nassar, M., Schoepfer, R., and Colquhoun, D. (1996). Single-channel currents from recombinant NMDA NR1a/NR2D receptors expressed in Xenopus oocytes. Proc Biol Sci *263*, 1079-1086.

Wyllie, D.J., Johnston, A.R., Lipscombe, D., and Chen, P.E. (2006). Single-channel analysis of a point mutation of a conserved serine residue in the S2 ligand-binding domain of the NR2A NMDA receptor subunit. J Physiol *574*, 477-489.

Yuan, H., Hansen, K.B., Vance, K.M., Ogden, K.K., and Traynelis, S.F. (2009). Control of NMDA receptor function by the NR2 subunit amino-terminal domain. J Neurosci *29*, 12045-12058.

Zarei, M.M., and Dani, J.A. (1994). Ionic permeability characteristics of the N-methyl-D-aspartate receptor channel. J Gen Physiol *103*, 231-248.

Zhang, L., Zheng, X., Paupard, M.C., Wang, A.P., Santchi, L., Friedman, L.K., Zukin, R.S., and Bennett, M.V. (1994). Spermine potentiation of recombinant N-methyl-D-aspartate receptors is affected by subunit composition. Proc Natl Acad Sci U S A *91*, 10883-10887.

Zhou, Y., Morais-Cabral, J.H., Kaufman, A., and MacKinnon, R. (2001). Chemistry of ion coordination and hydration revealed by a K+ channel-Fab complex at 2.0 A resolution. Nature *414*, 43-48.

Zhu, Y., and Auerbach, A. (2001a). K(+) occupancy of the N-methyl-d-aspartate receptor channel probed by Mg(2+) block. J Gen Physiol *117*, 287-298.

Zhu, Y., and Auerbach, A. (2001b). Na(+) occupancy and Mg(2+) block of the n-methyl-d-aspartate receptor channel. J Gen Physiol *117*, 275-286.